Numerical Weather Prediction

Normal Mode Analysis of the New Dynamics

Forecasting Research Technical Report No. 393

Elisabetta Cordero, Andrew Staniforth and Nigel Wood

email: nwp_publications@metoffice.com

©Crown Copyright

Normal Mode Analysis of the New Dynamics

Elisabetta Cordero, Andrew Staniforth, Nigel Wood

October 24, 2002

Contents

1 Introduction **1.1**

2 Matrix stability analysis of the coupled equation set **2.1**

2.1 Continuous governing equations 2.1

2.2 Temporal and vertical discretisation of the governing equations 2.1

2.2.1 Horizontal momentum at levels $k = 1/2, 3/2, ..., N - 1/2$ 2.2

2.2.2 Vertical momentum at levels $k = 0, 1, ..., N$ 2.2

2.2.3 Thermodynamic at levels $k = 0, 1, ..., N$ 2.2

2.2.4 Continuity at levels $k = 1/2, 3/2, ..., N - 1/2$ 2.3

2.2.5 Linearised gas law at levels $k = 1/2, 3/2, ..., N - 1/2$ 2.3

2.3 Basic state 2.4

2.3.1 Satisfaction of the discrete hydrostatic equation and equation of state 2.4

2.3.2 The isothermal (T_s = constant) basic state 2.5

2.3.3 The isentropic (θ_s = constant) basic state 2.6

2.4 Linearisation of the time-discretised equations. 2.8

2.4.1 Horizontal momentum at levels $k = 1/2, 3/2, ..., N - 1/2$ 2.8

2.4.2 Vertical momentum at levels $k = 0, 1, ..., N$ 2.8

2.4.3 Thermodynamic at levels $k = 0, 1, ..., N$ 2.9

2.4.4 Continuity at levels $k = 1/2, 3/2, ..., N - 1/2$ 2.9

2.4.5 Linearised gas law at levels $k = 1/2, 3/2, ..., N - 1/2$ 2.9

2.5 Rewriting the linearised time-discretised equations in operator form. 2.10

2.6 Rewriting the linearised discretisation in matrix form 2.12

2.7 Analysis of revised discretisations 2.19

2.7.1 A semi-Lagrangian discretisation of the continuity equation 2.19

2.7.2 θ active at the bottom 2.21

2.8 Eigen analysis and stability 2.22

3 Matrix stability analysis of a simple column-equations subset **3.1**

3.1 Continuous column equations 3.1

3.2 Column model equations 3.4

3.2.1 Vertical momentum at levels $k = 0, 1, ..., N$ 3.4

3.2.2 Thermodynamic at levels $k = 0, 1, ..., N$ . . . 3.4
3.2.3 Continuity at levels $k = 1/2, 3/2, ..., N - 1/2$ . . . 3.4
3.2.4 Linearised gas law at levels $k = 1/2, 3/2, ..., N - 1/2$ . . . 3.4
3.3 Column model equations rewritten . . . 3.5
3.3.1 Vertical momentum at levels $k = 0, 1, ..., N$ . . . 3.5
3.3.2 Thermodynamic at levels $k = 0, 1, ..., N$ . . . 3.5
3.3.3 Continuity at levels $k = 1/2, 3/2, ..., N - 1/2$ . . . 3.5
3.3.4 Linearised gas law at levels $k = 1/2, 3/2, ..., N - 1/2$ . . . 3.5
3.4 Special case where θ_s, Π_s and ρ_s are all constant and $\mathbf{I}_h \equiv 1$ . . . 3.6
3.4.1 Vertical momentum at levels $k = 0, 1, ..., N$ . . . 3.6
3.4.2 Thermodynamic at levels $k = 0, 1, ..., N$ . . . 3.6
3.4.3 Continuity at levels $k = 1/2, 3/2, ..., N - 1/2$ . . . 3.6
3.4.4 Linearised gas law at levels $k = 1/2, 3/2, ..., N - 1/2$ . . . 3.6
3.4.5 The equations rewritten in matrix form . . . 3.6
3.4.6 Eigen analysis when the grid is uniform . . . 3.8

4 Numerical solution of the column-equations model with constant θ_s, Π_s, and ρ_s 4.1

5 The eigenvalue problem for the 1D isothermal basic state case 5.1
5.1 The linearised continuous governing equations . . . 5.1
5.2 Linearised discrete equations and resulting matrices for the associated eigenvalue problem . . . 5.3
5.2.1 Horizontal momentum at levels $k = 1/2, ..., N - 1/2$ . . . 5.3
5.2.2 Vertical momentum at levels $k = 0, ..., N$ . . . 5.3
5.2.3 Thermodynamics at levels $k = 0, ..., N$ . . . 5.3
5.2.4 Continuity at levels $k = 1/2, ..., N - 1/2$ . . . 5.3
5.2.5 Linearised gas law at levels $k = 1/2, ..., N - 1/2$ . . . 5.4
5.2.6 Definition of the matrices defining the eigenvalue problem . . . 5.5
5.3 Top and bottom boundary conditions for the potential temperature . . . 5.5
5.3.1 Isothermal top layer . . . 5.6
5.3.2 Isentropic bottom layer . . . 5.7

6 Numerical normal modes of the 1D isothermal basic state column model 6.1

6.1 Numerical normal modes with θ active at the top and bottom 6.6

6.2 Numerical normal modes with non-active boundary conditions 6.16

6.3 Numerical normal modes with the isentropic boundary condition imposed within a thin bottom layer 6.22

7 Summary 7.1

A Eigen analysis of a "layer-by-layer" vertical discretisation A.1

A.1 Continuous equations A.1

A.1.1 Continuous vertical-slice equations A.1

A.1.2 Continuous column equations (with $F \equiv 0$) A.1

A.1.3 Linearised column equations ($F \equiv 0$) A.2

A.1.4 Linearised column equations ($F \equiv 0$, θ_s, ρ_s, Π_s constant) A.3

A.1.5 Analytic solution when $F \equiv 0$, θ_s, ρ_s, Π_s all constant A.3

A.2 Discrete equations A.4

A.2.1 Discretisation of linearised column model equations ($F \equiv 0$, θ_s, ρ_s, Π_s constant) A.4

A.2.2 The equations rewritten in matrix form A.5

A.3 Eigen analysis when the grid is uniform A.6

1 Introduction

A general 2D framework has been established to perform the normal mode analysis of the New Dynamics discretisation, which comprises the formulation of the eigenvalue problem associated with the New Dynamics, and the development of a suite of programs to compute numerically the eigenvalues and normal modes of the problem.

The purpose of the work is twofold: at present to analyse the numerical properties (accuracy and stability) of the 1D and 2D versions of the New Dynamics; in the future to use the normal mode model as a tool to test alternative improved discretisations before implementing them in the full model.

Issues of interest in the analysis include the behaviour of the normal modes in the presence of: the different top and bottom boundary conditions on the potential temperature employed in the New Dynamics; various vertical staggering of the variables; stretched grids, as opposed to uniform ones; the Eulerian or semi-Lagrangian discretisation of the continuity equation.

Up to now the normal mode analysis of the 1D version of the New Dynamics with an isentropic or an isothermal basic state at rest has been performed; in the isentropic basic state case the numerical normal modes have been compared with the analytic ones; in the isothermal basic state case the analysis has focussed on the sensitivity of the normal modes to the boundary conditions on the potential temperature. The present report documents the progress of the work to date.

In Section 2 the eigenvalue problem associated with the 2D $x - z$ version of the New Dynamics is derived for the dry set of equations written in Cartesian geometry and under suitable simplifying assumptions. In Section 3 the eigenvalue problem associated with the 1D version of the New Dynamics is derived and further simplified, under the assumption of an isentropic basic state. The normal modes of the 1D problem with an isentropic basic state are computed numerically in Section 4 and compared with the analytic ones. The normal modes of the 1D problem with an isothermal basic state, whose equations are summarised in Section 5, are computed and input as perturbations about the initial state of the 1D Dry Column Model (New Dynamics Formulation: 1-D Dry Column Model, M. Zerroukat, A. Staniforth, and T. Davies) in Section 6. The evolution of the modes computed using the 1D Column Model is compared with the linear evolution predicted by the normal mode analysis and the sensitivity of the numerical results to the top and bottom boundary conditions on

the potential temperature is investigated.

In the future it is planned to: incorporate into the normal mode analysis the effect of trajectory calculations, which amounts to extending the analysis to three-time-level schemes; and investigate the numerical properties of the normal modes associated with different vertical staggering of the variables.

2 Matrix stability analysis of the coupled equation set

2.1 Continuous governing equations

The continuous set of governing equations (2.71) - (2.84) of Staniforth, White, Wood, Thuburn, Zerroukat & Cordero (2002), henceforth referred to as UMDP15, written in Cartesian $x-z$ coordinates, in the absence of orography ($z=0$ defines the lower boundary) and forcing ($S^u = S^v = S^w = S^\theta \equiv 0$), for a dry atmosphere ($\theta_v = \theta$, $\rho_y = \rho$) on an F-plane (an $f-F$ plane located at the equator), and neglecting perturbations in the y direction ($\partial/\partial y \equiv 0$), is:

$$\frac{Du}{Dt} = -c_{pd}\theta\frac{\partial \Pi}{\partial x} - Fw, \tag{2.1}$$

$$\frac{Dv}{Dt} = 0, \tag{2.2}$$

$$\frac{Dw}{Dt} = -g - c_{pd}\theta\frac{\partial \Pi}{\partial z} + Fu, \tag{2.3}$$

$$\frac{D\theta}{Dt} = 0, \tag{2.4}$$

$$\frac{D\rho}{Dt} = -\rho\left(\frac{\partial u}{\partial x} + \frac{\partial w}{\partial z}\right), \tag{2.5}$$

$$\Pi^{\frac{\kappa_d - 1}{\kappa_d}}\rho\theta = \frac{p_0}{\kappa_d c_{pd}}, \tag{2.6}$$

where $D/Dt \equiv \partial/\partial t + u\partial/\partial x + w\partial/\partial z$, $\Pi \equiv (p/p_0)^{\kappa_d}$, $\kappa_d \equiv R_d/c_{pd}$, and $F \equiv (2\Omega\cos\phi)|_{\phi=0} = 2\Omega$.

2.2 Temporal and vertical discretisation of the governing equations

The temporally and vertically discretised forms of (2.1) - (2.6) are obtained from the corresponding discrete equations given in UMDP15, but rewritten using a spectral horizontal discretisation (i.e. no horizontal differencing or averaging). The discretisation is performed using a grid comprising $N+1$ vertical integer levels (including the surface and top levels, denoted by indices 0 and N respectively), and N half-integer levels. The Charney-Phillips grid staggering is used: θ and w are stored at integer model levels whereas Π, ρ, u, and v are evaluated at half-integer model levels.

2.2.1 Horizontal momentum at levels $k = 1/2,\ 3/2,\ ...,\ N - 1/2$

From (13.1) - (13.2) of UMDP15 and associated equations, the corresponding discretisation of (2.1) - (2.2) are

$$\frac{u^{n+1} - u_d^n}{\Delta t} = -\alpha_3 c_{pd} \overline{\theta^*}^z \frac{\partial \Pi^{n+1}}{\partial x} - \left(\alpha_4 F \overline{w}^z\right)^n - \left[\left(1-\alpha_3\right) c_{pd} \overline{\theta}^z \frac{\partial \Pi}{\partial x} + \left(1-\alpha_4\right) F \overline{w}^z\right]_d^n, \quad (2.7)$$

$$\frac{v^{n+1} - v_d^n}{\Delta t} = 0, \quad (2.8)$$

where θ^* is defined by (2.13) - (2.14).

2.2.2 Vertical momentum at levels $k = 0,\ 1,\ ...,\ N$

From (13.4) and associated equations of UMDP15, the corresponding discretisation of (2.3), at levels $k = 1,\ 2,\ ...,\ N-1$, is

$$\begin{aligned} \mathbf{I}_h \frac{w^{n+1} - w_d^n}{\Delta t} \;=\; & -g - \alpha_4 c_{pd} \theta^* \delta_z \Pi^{n+1} \\ & + \alpha_4 \left(F \overline{u}^z\right)^n + \left(1-\alpha_4\right) \left[F \overline{u}^z - c_{pd} \theta \delta_z \Pi\right]_d^n \\ & + c_{pd} \alpha_2 \alpha_4 \Delta t \delta_{2z} \theta^* \delta_z \Pi^n \left(w^{n+1} - w^n\right), \end{aligned} \quad (2.9)$$

where $\mathbf{I}_h$ is the hydrostatic switch ($\mathbf{I}_h = 0$ in the hydrostatic case, $\mathbf{I}_h = 1$ otherwise), and θ^* is defined by (2.13) - (2.14).

Since the lid is rigid, and using (6.45) and (6.51), w^{n+1} at levels $k = 0$ and $k = N$ are given by

$$w^{n+1}\Big|_{z_0 \equiv 0} = 0, \quad (2.10)$$

$$w^{n+1}\Big|_{z_N} = 0. \quad (2.11)$$

2.2.3 Thermodynamic at levels $k = 0,\ 1,\ ...,\ N$

From (13.14) and associated equations of UMDP15, the corresponding discretisation of (2.4), at levels $k = 1,\ 2,\ ...,\ N-1$, is

$$\frac{\theta^{n+1} - \theta^*}{\Delta t} = -\alpha_2 (w^{n+1} - w^n) \delta_{2z} \theta^*, \quad (2.12)$$

where

$$\theta^* \equiv \tilde{\theta}^{(2)} = \theta_{dl}^n - \alpha_2 \Delta t (w^n - w^*) \delta_{2z} \tilde{\theta}^{(1)} - (1-\alpha_2) \Delta t \left[(w - w^*) \delta_{2z} \theta\right]_{dl}^n, \quad (2.13)$$

$$\tilde{\theta}^{(1)} = \theta^n_{dl} - \alpha_2 \Delta t \left[(w - w^*)\delta_{2z}\theta\right]^n - (1-\alpha_2)\Delta t \left[(w - w^*)\delta_{2z}\theta\right]^n_{dl} . \tag{2.14}$$

and $w^* = (z_a - z_{dl})/\Delta t$, $z_{a/dl}$ are the vertical heights of the arrival and departure points.

From the bottom-layer isentropic assumption (see (9.42) of UMDP15), at the $k = 0$ level

$$\theta^{n+1}\Big|_{z_0 \equiv 0} = \theta^{n+1}\Big|_{z_1} , \tag{2.15}$$

and, at the top ($k = N$) level (see (9.48) of UMDP15)

$$\theta^{n+1}\Big|_{z_N} = (\theta^*)|_{z_N} = (\theta^n_{dl})|_{z_N} . \tag{2.16}$$

2.2.4 Continuity at levels $k = 1/2, 3/2, ..., N - 1/2$

From (13.8) and associated equations of UMDP15, the discretisation of (2.5), at levels $k = 3/2, 5/2, ..., N - 3/2$, is

$$\begin{aligned} \frac{\rho^{n+1} - \rho^n}{\Delta t} &= -\alpha_1 \frac{\partial}{\partial x}\left(\rho^n u^{n+1}\right) - (1-\alpha_1)\frac{\partial}{\partial x}\left(\rho^n u^n\right) \\ &\quad -\alpha_2 \delta_z \left(\overline{\rho^n}^z w^{n+1}\right) - (1-\alpha_2)\,\delta_z\left(\overline{\rho^n}^z w^n\right) . \end{aligned} \tag{2.17}$$

From (13.10) and (13.11) of UMDP15, the discretisation of (2.5) at levels $k = 1/2$ and $k = N - 1/2$ becomes

$$\begin{aligned} \left(\frac{\rho^{n+1} - \rho^n}{\Delta t}\right)\Big|_{z_{1/2}} &= -\left[\alpha_1 \frac{\partial}{\partial x}\left(\rho^n u^{n+1}\right) + (1-\alpha_1)\frac{\partial}{\partial x}\left(\rho^n u^n\right)\right]\Big|_{z_{1/2}} \\ &\quad - \left(\frac{1}{\Delta z}\right)\Big|_{z_{1/2}} \left[\alpha_2 \overline{\rho^n}^z w^{n+1} + (1-\alpha_2)\,\overline{\rho^n}^z w^n\right]\Big|_{z_1} , \end{aligned} \tag{2.18}$$

$$\begin{aligned} \left(\frac{\rho^{n+1} - \rho^n}{\Delta t}\right)\Big|_{z_{N-1/2}} &= -\left[\alpha_1 \frac{\partial}{\partial x}\left(\rho^n u^{n+1}\right) + (1-\alpha_1)\frac{\partial}{\partial x}\left(\rho^n u^n\right)\right]\Big|_{z_{N-1/2}} \\ &\quad + \left(\frac{1}{\Delta z}\right)\Big|_{z_{N-1/2}} \left[\alpha_2 \overline{\rho^n}^z w^{n+1} + (1-\alpha_2)\,\overline{\rho^n}^z w^n\right]\Big|_{z_{N-1}} . \end{aligned} \tag{2.19}$$

2.2.5 Linearised gas law at levels $k = 1/2, 3/2, ..., N - 1/2$

The rewritten time-discretised equation of state (13.18) of UMDP15 is

$$\frac{\rho^{n+1} - \rho^n}{\rho^n} + \left(1 - \frac{p^n}{\kappa_d R_d \Pi^n \rho^n \overline{\theta^n}^z}\right)\left(\frac{\Pi^{n+1} - \Pi^n}{\Pi^n}\right) + \frac{\overline{\theta^{n+1}}^z - \overline{\theta^n}^z}{\overline{\theta^n}^z} = \frac{p^n}{\kappa_d c_{pd} \Pi^n \rho^n \overline{\theta^n}^z} - 1. \tag{2.20}$$

Note that in the current New Dynamics implementation the semi-implicit weights α_i, $i = 1, ..., 4$ in (2.7), (2.9), (2.12) and (2.13) - (2.17) are assigned the following values: $\alpha_1 = \alpha_3 = 0.7$ and $\alpha_2 = \alpha_4 = 1$. Earlier versions were run with $\alpha_1 = \alpha_3 = 0.6$.

2.3 Basic state

To progress in the stability analysis, linear perturbations to the dependent variables are considered. Each dependent variable $G(x,z,t)$ is represented as the sum of a basic steady state (i.e. independent of time) part, $G_s(x,z)$, and a perturbation, $G'(x,z,t)$, under the assumptions that:

1. the basic state variables satisfy the governing equations, and

2. the perturbations are so small that terms involving their products can be neglected.

Let the basic steady state solution be

$$u_s = \text{constant},\ v_s = w_s \equiv 0,\ \theta_s = \theta_s(z),\ \rho_s = \rho_s(z),\ \Pi_s = \Pi_s(z), \tag{2.21}$$

(i.e. uniform wind in the $x-$direction, with potential temperature, density and Exner pressure all independent of x) , where

$$c_{pd}\theta_s\delta_z\Pi_s = -g, \tag{2.22}$$

$$\Pi_s^{\frac{\kappa_d-1}{\kappa_d}}\rho_s\overline{\theta_s}^z = \frac{p_0}{\kappa_d c_{pd}}. \tag{2.23}$$

Eqs. (2.22) and (2.23) (which mean that the basic state solution is in hydrostatic balance and satisfies the ideal gas law) are obtained from the model's discretisation of (2.3) and (2.6) respectively, the other governing equations being trivially satisfied.

2.3.1 Satisfaction of the discrete hydrostatic equation and equation of state

A basic state atmosphere that satisfies (2.22) and (2.23) by construction may be achieved as follows. Assume that θ_s is given at levels $k = 1, 2, ..., N$, that $(\theta_s)|_{z_1} = (\theta_s)|_{z_0\equiv 0}$ (i.e. the bottom-layer isentropic assumption of the model), and that Π_s is prescribed at the bottom level $z = z_0 \equiv 0$. Integration of the hydrostatic relation (2.22) over the bottom half-layer $\left[z_0, z_{1/2}\right]$ then gives

$$(\Pi_s)|_{z_{1/2}} = (\Pi_s)|_{z_0\equiv 0} - \frac{g\left(z_{1/2}-z_0\right)}{c_{pd}\,(\theta_s)|_{z_0\equiv 0}}, \tag{2.24}$$

where $(\Pi_s)|_{z_0\equiv 0}$ is known, and further integration of (2.22) over the layers $\left[z_{k-1/2}, z_{k+1/2}\right]$ gives

$$(\Pi_s)|_{z_{k+1/2}} = (\Pi_s)|_{z_{k-1/2}} - \frac{g\left(z_{k+1/2}-z_{k-1/2}\right)}{c_{pd}\,(\theta_s)|_{z_k}}, \tag{2.25}$$

for $k = 1, 2, ..., N-1$.

Having determined the discrete profile of Π_s, the discrete profile for ρ_s is determined by discrete evaluation of (2.23) to yield

$$(\rho_s)|_{z_{k+1/2}} = \frac{p_0}{\kappa_d c_{pd}} \left[\frac{(\Pi_s)^{\frac{1-\kappa_d}{\kappa_d}}}{\overline{\theta_s}^z} \right] \Bigg|_{z_{k+1/2}}, \tag{2.26}$$

for $k = 0, 1, ..., N-1$.

Note that the basic state profile for θ_s can be specified analytically (see following two subsections), e.g. for isothermal (T_s = constant) and isentropic (θ_s = constant) basic states, and discretely sampled at levels z_1, z_2,..., z_N (recall that $(\theta_s)|_{z_{0\equiv 0}}$ is then set equal to $(\theta_s)|_{z_1}$, to be consistent with the model).

2.3.2 The isothermal (T_s = constant) basic state

For an isothermal basic state, by expressing the potential temperature θ_s in terms of the (constant) temperature T_s as (cf. (1.44) of UMDP15)

$$\theta_s(z) = \frac{T_s}{\Pi_s(z)}, \tag{2.27}$$

and using (2.27) to eliminate θ_s in favour of the Exner pressure function Π_s in the hydrostatic relationship (2.22), the latter can be vertically integrated to give:

$$\Pi_s(z) = \exp\left(-\frac{\kappa_d}{H} z\right), \tag{2.28}$$

where

$$H \equiv \frac{R_d T_s}{g}, \tag{2.29}$$

is the scale height of the isothermal atmosphere, and $p_s(0)$ has been set to p_0.

Substituting for Π_s from (2.28) into (2.27) yields the following expression for the potential temperature θ_s:

$$\theta_s(z) = T_s \exp\left(\frac{\kappa_d}{H} z\right). \tag{2.30}$$

Eq. (2.30) should be used to determine $\theta_s|_{z_k}$, $k = 1, 2, ..., N$, for use in (2.24) - (2.26), which determine the discrete values for Π_s and ρ_s, rather than discretely evaluating (2.28) and (2.31). This then ensures the internal consistency of the discretised equations.

Using (2.28) and (2.30) to eliminate Π_s and θ_s from the ideal gas law (2.6), the latter can be solved for the density ρ_s to yield:

$$\rho_s(z) = \frac{p_0}{\kappa_d c_{pd} T_s} \exp\left(-\frac{z}{H}\right). \tag{2.31}$$

Furthermore, the following useful relations are introduced:

$$\frac{1}{H_\theta} \equiv \frac{1}{\theta_s}\frac{d\theta_s}{dz} = \frac{\kappa_d}{H}, \tag{2.32}$$

$$\frac{1}{H_\rho} \equiv -\frac{1}{\rho_s}\frac{d\rho_s}{dz} = \frac{1}{H}, \tag{2.33}$$

$$\frac{1}{\Pi_s}\frac{d\Pi_s}{dz} = -\frac{\kappa_d}{H}. \tag{2.34}$$

The expressions for the basic state buoyancy frequency and sound speed are:

$$N_s^2 \equiv \frac{g}{\theta_s}\frac{d\theta_s}{dz} = \frac{g}{H_\theta} = g\frac{\kappa_d}{H} = c_{pd}T\frac{\kappa_d^2}{H^2}, \tag{2.35}$$

$$c_s^2 \equiv \frac{\kappa_d}{1-\kappa_d} c_{pd} T_s = \frac{R_d T_s}{1-\kappa_d}, \tag{2.36}$$

and the square of the Froude number $F_k \equiv u_s k/N_s$ (where N_s is the square root of the buoyancy frequency) can be written as

$$F_k^2 = \frac{F_H^2 (kH)^2}{\kappa_d}, \tag{2.37}$$

where

$$F_H^2 \equiv \frac{u_s^2}{R_d T} \tag{2.38}$$

and kH are non-dimensional parameters.

2.3.3 The isentropic (θ_s = constant) basic state

For an isentropic basic state, vertically integrating the hydrostatic relationship (2.22) gives the following expression for the Exner pressure function Π_s:

$$\Pi_s(z) = \left[1 - \frac{\kappa_d}{H(0)} z\right], \tag{2.39}$$

where

$$H(0) \equiv \frac{R_d T_s(0)}{g}, \tag{2.40}$$

is the scale height of the isentropic atmosphere, $p_s\,(0)$ has been set to p_0, and the relationship (cf. (1.44) of UMDP15)

$$\theta_s = \frac{T_s(z)}{\Pi_s(z)}, \tag{2.41}$$

evaluated at $z = 0$, has been used to eliminate θ_s in favour of T_s.

Substituting for Π_s from (2.39) into (2.41) gives

$$T_s(z) = \theta_s \left[1 - \frac{\kappa_d}{H(0)} z\right], \tag{2.42}$$

and, substituting (2.39) into the ideal gas law (2.6) yields

$$\rho_s(z) = \frac{p_0}{\kappa_d c_{pd} \theta_s} \left[1 - \frac{\kappa_d}{H(0)} z\right]^{\frac{1-\kappa_d}{\kappa_d}} . \tag{2.43}$$

The specified (constant) value of θ_s should be replicated to obtain $\theta_s|_{z_k}$, $k = 1, 2, ..., N$, for use in (2.24) - (2.26), which then determine the discrete values for Π_s and ρ_s, rather than discretely evaluating (2.39) and (2.43). This then ensures the internal consistency of the discretised equations.

2.4 Linearisation of the time-discretised equations.

The time-discretised equations (2.7) - (2.20) are linearised about the steady state defined by (2.21) - (2.23). This is accomplished by writing each dependent variable as the sum of its basic state value (denoted by the subscript s and defined by (2.21)) and a perturbation (denoted by primes), i.e. :

$$u(x,z,t) = u_s + u'(x,z,t), \tag{2.44}$$

$$v(x,z,t) = v'(x,z,t), \tag{2.45}$$

$$w(x,z,t) = w'(x,z,t), \tag{2.46}$$

$$\theta(x,z,t) = \theta_s(z) + \theta'(x,z,t), \tag{2.47}$$

$$\rho(x,z,t) = \rho_s(z) + \rho'(x,z,t), \tag{2.48}$$

$$\Pi(x,z,t) = \Pi_s(z) + \Pi'(x,z,t). \tag{2.49}$$

Substituting (2.44) - (2.49) into the time-discretised equations (2.7) - (2.20), neglecting products of perturbations, and using (2.22) - (2.23) to simplify the resulting expressions, the following linearised time-discretised equations for the perturbed quantities, u, v, w, θ, ρ and Π are obtained, where primes have been dropped for convenience.

Note that since the basic state variables are independent of x and the basic state advection is only in the x-direction, terms of the form $[X_s(z)Y(x,z,t)]_d$ reduce to $X_s(z)[Y(x,z,t)]_d$, $[\ ]_{dl} \equiv [\ ]_d$, and $w^* \equiv 0$, since $z_a \equiv z_d \equiv z_{dl}$ (i.e. the heights of the arrival and departure points are the same, because the basic state advection is purely horizontal). Note also that (2.22) and (2.56) (solved for θ^{n+1}) are used to derive the $w-$momentum equation (2.53).

The equations are:

2.4.1 Horizontal momentum at levels $k = 1/2,\ 3/2,\ ...,\ N - 1/2$

$$\frac{u^{n+1} - u_d^n}{\Delta t} = -\alpha_3 c_{pd} \overline{\theta_s}^z \frac{\partial \Pi^{n+1}}{\partial x} - (1-\alpha_3)\, c_{pd} \overline{\theta_s}^z \left[\frac{\partial \Pi^n}{\partial x}\right]_d - \alpha_4 F \overline{w^n}^z - (1-\alpha_4)\, F\, [\overline{w^n}^z]_d\,, \tag{2.50}$$

$$\frac{v^{n+1} - v_d^n}{\Delta t} = 0, \tag{2.51}$$

2.4.2 Vertical momentum at levels $k = 0,\ 1,\ ...,\ N$

$$w^{n+1}\Big|_{z_0 \equiv 0} = 0, \tag{2.52}$$

$$\mathbf{I}_h \frac{w^{n+1} - w_d^n}{\Delta t} = -c_{pd}\theta_s \left\{ \alpha_4 \delta_z \Pi^{n+1} + (1-\alpha_4) \left[\delta_z \Pi^n \right]_d \right\} - c_{pd} \delta_z \Pi_s \left[\alpha_4 \theta^{n+1} + (1-\alpha_4)\, \theta_d^n \right] + F \left[\alpha_4 \overline{u^n}^z + (1-\alpha_4) \left(\overline{u}^z \right)_d^n \right], \tag{2.53}$$

at levels $k = 1,\ 2,\ ...,\ N-1$, and

$$w^{n+1}\Big|_{z_N} = 0. \tag{2.54}$$

2.4.3 Thermodynamic at levels $k = 0,\ 1,\ ...,\ N$

$$\theta^{n+1}\Big|_{z_0 \equiv 0} = \theta^{n+1}\Big|_{z_1}, \tag{2.55}$$

$$\frac{\theta^{n+1} - \theta_d^n}{\Delta t} = -\delta_{2z}\theta_s \left[\alpha_2 w^{n+1} + (1-\alpha_2) w_d^n \right], \tag{2.56}$$

at levels $k = 1,\ 2,\ ...,\ N-1$, and

$$\theta^{n+1}\Big|_{z_N} = \left(\theta_d^n\right)\Big|_{z_N}. \tag{2.57}$$

2.4.4 Continuity at levels $k = 1/2,\ 3/2,\ ...,\ N-1/2$

$$\left(\frac{\rho^{n+1} - \rho^n}{\Delta t} \right)\Big|_{z_{1/2}} = -\left\{ u_s \frac{\partial \rho^n}{\partial x} + \rho_s \left[\alpha_1 \frac{\partial u^{n+1}}{\partial x} + (1-\alpha_1) \frac{\partial u^n}{\partial x} \right] \right\}\Big|_{z_{1/2}} - \left(\frac{1}{\Delta z} \right)\Big|_{z_{1/2}} \left[\alpha_2 \overline{\rho_s}^z w^{n+1} + (1-\alpha_2) \overline{\rho_s}^z w^n \right]\Big|_{z_1}, \tag{2.58}$$

$$\frac{\rho^{n+1} - \rho^n}{\Delta t} = -u_s \frac{\partial \rho^n}{\partial x} - \rho_s \left[\alpha_1 \frac{\partial u^{n+1}}{\partial x} + (1-\alpha_1) \frac{\partial u^n}{\partial x} \right] - \left[\alpha_2 \delta_z \left(\overline{\rho_s}^z w^{n+1} \right) + (1-\alpha_2)\, \delta_z \left(\overline{\rho_s}^z w^n \right) \right], \tag{2.59}$$

at levels $k = 3/2,\ 5/2,\ ...,\ N-3/2$, and

$$\left(\frac{\rho^{n+1} - \rho^n}{\Delta t} \right)\Big|_{z_{N-1/2}} = -\left\{ u_s \frac{\partial \rho^n}{\partial x} + \rho_s \left[\alpha_1 \frac{\partial u^{n+1}}{\partial x} + (1-\alpha_1) \frac{\partial u^n}{\partial x} \right] \right\}\Big|_{z_{N-1/2}} + \left(\frac{1}{\Delta z} \right)\Big|_{z_{N-1/2}} \left[\alpha_2 \overline{\rho_s}^z w^{n+1} + (1-\alpha_2) \overline{\rho_s}^z w^n \right]\Big|_{z_{N-1}}. \tag{2.60}$$

2.4.5 Linearised gas law at levels $k = 1/2,\ 3/2,\ ...,\ N-1/2$

$$\left(\frac{1-\kappa_d}{\kappa_d} \right) \frac{\Pi^{n+1}}{\Pi_s} = \frac{\rho^{n+1}}{\rho_s} + \frac{\overline{\theta^{n+1}}^z}{\overline{\theta_s}^z}. \tag{2.61}$$

2.5 Rewriting the linearised time-discretised equations in operator form.

Following Gravel, Staniforth & Côté (1993) the linearised time-discretised equations (2.50) - (2.61) can be written in a way which preserves their continuous form by introducing a number of operators. This may, or may not, be useful for the purposes of the present stability study. A possible benefit of doing so is that it may allow us to significantly reduce (by algebraically eliminating variables in a manner analogous to the analytic elimination procedure used to derive continuous vertical normal modes) the rank of the stability matrices that arise. However, the downside of this is that if we then wish to modify the discretisation, e.g. the application of a vertical boundary condition, then the labour-intensive algebraic elimination procedure has to be redone, rather than simply modifying a few entries in a few matrices.

Let

$$\frac{D^L G}{Dt} \equiv \frac{G^{n+1} - G_d^n}{\Delta t}, \tag{2.62}$$

$$\frac{D^E G}{Dt} \equiv \frac{G^{n+1} - G^n}{\Delta t} + u_s \frac{\partial G^n}{\partial x}, \tag{2.63}$$

$$\overline{G}^{\alpha_i} \equiv (1-\alpha_i) G_d^n + \alpha_i G^{n+1}, \tag{2.64}$$

$$\overline{G}^{\tilde{\alpha}_i} \equiv (1-\alpha_i) G^n + \alpha_i G^{n+1}, \tag{2.65}$$

$$\overline{G}^{\hat{\alpha}_i} \equiv (1-\alpha_i) G_d^n + \alpha_i G^n. \tag{2.66}$$

Note that since all operators are linear and have constant coefficients (as u_s is independent of z) they, together with $\partial/\partial x$ and δ_z, all commute. (Note also that the analysis can be applied to the case of semi-Lagrangian treatment of the density equation by redefining $D^E G/Dt$ to be $D^L G/Dt$ and $\overline{G}^{\widetilde{\alpha}_i}$ to be $\overline{G}^{\alpha_i}$.)

By using the operators (2.62) - (2.66), the linearised time-discretised equations (2.50) - (2.61) can then be written as:

$$\frac{D^L u}{Dt} = -c_{pd} \overline{\theta_s}^z \frac{\partial \overline{\Pi}^{\alpha_3}}{\partial x} - F \overline{\overline{w}^z}^{\alpha_4}, \tag{2.67}$$

$$\frac{D^L v}{Dt} = 0, \tag{2.68}$$

$$w|_{z_0 \equiv 0} = 0, \tag{2.69}$$

$$\mathbf{I}_h \frac{D^L w}{Dt} = -c_{pd} \theta_s \delta_z \overline{\Pi}^{\alpha_4} - c_{pd} \delta_z \Pi_s \overline{\theta}^{\alpha_4} + F \overline{\overline{u}^z}^{\alpha_4}, \tag{2.70}$$

$$w|_{z_N} = 0, \tag{2.71}$$

$$\theta\big|_{z_0\equiv 0} = \theta\big|_{z_1}\,, \tag{2.72}$$

$$\frac{D^L\theta}{Dt} = -\delta_{2z}\theta_s\overline{w}^{\alpha_2}, \tag{2.73}$$

$$\left.\frac{D^L\theta}{Dt}\right|_{z_N} = 0, \tag{2.74}$$

$$\left.\frac{D^E\rho}{Dt}\right|_{z_{1/2}} = -\left(\rho_s\frac{\partial\overline{u}^{\tilde{\alpha}_1}}{\partial x}\right)\Big|_{z_{1/2}} - \left(\frac{1}{\Delta z}\right)\Big|_{z_{1/2}}\left(\overline{\rho_s}^z\overline{w}^{\tilde{\alpha}_2}\right)\Big|_{z_1}\,, \tag{2.75}$$

$$\frac{D^E\rho}{Dt} = -\rho_s\frac{\partial\overline{u}^{\tilde{\alpha}_1}}{\partial x} - \delta_z\left(\overline{\rho_s}^z\overline{w}^{\tilde{\alpha}_2}\right), \tag{2.76}$$

$$\left.\frac{D^E\rho}{Dt}\right|_{z_{N-1/2}} = -\left(\rho_s\frac{\partial\overline{u}^{\tilde{\alpha}_1}}{\partial x}\right)\Big|_{z_{N-1/2}} + \left(\frac{1}{\Delta z}\right)\Big|_{z_{N-1/2}}\left(\overline{\rho_s}^z\overline{w}^{\tilde{\alpha}_2}\right)\Big|_{z_{N-1}}\,, \tag{2.77}$$

$$\left(\frac{1-\kappa_d}{\kappa_d}\right)\frac{\Pi}{\Pi_s} = \frac{\rho}{\rho_s} + \frac{\overline{\theta}^z}{\overline{\theta_s}^z}. \tag{2.78}$$

2.6 Rewriting the linearised discretisation in matrix form

Eqs. (2.50) - (2.61) are a set of $6N+2$ linear equations for the $6N+2$ unknowns $\Pi_{1/2}$,..., $\Pi_{N-1/2}$, θ_0, θ_1,..., θ_N, w_0, w_1,..., w_N, $\rho_{1/2}$,..., $\rho_{N-1/2}$, $u_{1/2}$,..., $u_{N-1/2}$, $v_{1/2}$,..., $v_{N-1/2}$, all evaluated at $(n+1)\,\Delta t$. Following Côté, Béland & Staniforth (1983), this set may be written in the form

$$A\underline{x}^{n+1} = B\underline{x}^{n}, \tag{2.79}$$

where

$$A\underline{x}^{n+1} = \begin{bmatrix} A_{\Pi,\Pi} & A_{\Pi,\theta} & A_{\Pi,w} & A_{\Pi,\rho} & A_{\Pi,u} & A_{\Pi,v} \\ A_{\theta,\Pi} & A_{\theta,\theta} & A_{\theta,w} & A_{\theta,\rho} & A_{\theta,u} & A_{\theta,v} \\ A_{w,\Pi} & A_{w,\theta} & A_{w,w} & A_{w,\rho} & A_{w,u} & A_{w,v} \\ A_{\rho,\Pi} & A_{\rho,\theta} & A_{\rho,w} & A_{\rho,\rho} & A_{\rho,u} & A_{\rho,v} \\ A_{u,\Pi} & A_{u,\theta} & A_{u,w} & A_{u,\rho} & A_{u,u} & A_{u,v} \\ A_{v,\Pi} & A_{v,\theta} & A_{v,w} & A_{v,\rho} & A_{v,u} & A_{v,v} \end{bmatrix} \begin{bmatrix} \underline{\Pi}^{n+1} \\ \underline{\theta}^{n+1} \\ \underline{w}^{n+1} \\ \underline{\rho}^{n+1} \\ \underline{u}^{n+1} \\ \underline{v}^{n+1} \end{bmatrix}, \tag{2.80}$$

$$B\underline{x}^{n} = \begin{bmatrix} B_{\Pi,\Pi} & B_{\Pi,\theta} & B_{\Pi,w} & B_{\Pi,\rho} & B_{\Pi,u} & B_{\Pi,v} \\ B_{\theta,\Pi} & B_{\theta,\theta} & B_{\theta,w} & B_{\theta,\rho} & B_{\theta,u} & B_{\theta,v} \\ B_{w,\Pi} & B_{w,\theta} & B_{w,w} & B_{w,\rho} & B_{w,u} & B_{w,v} \\ B_{\rho,\Pi} & B_{\rho,\theta} & B_{\rho,w} & B_{\rho,\rho} & B_{\rho,u} & B_{\rho,v} \\ B_{u,\Pi} & B_{u,\theta} & B_{u,w} & B_{u,\rho} & B_{u,u} & B_{u,v} \\ B_{v,\Pi} & B_{v,\theta} & B_{v,w} & B_{v,\rho} & B_{v,u} & B_{v,v} \end{bmatrix} \begin{bmatrix} \underline{\Pi}^{n} \\ \underline{\theta}^{n} \\ \underline{w}^{n} \\ \underline{\rho}^{n} \\ \underline{u}^{n} \\ \underline{v}^{n} \end{bmatrix}, \tag{2.81}$$

$$\underline{\Pi} = \begin{bmatrix} \Pi_{1/2} \\ \Pi_{3/2} \\ . \\ . \\ . \\ \Pi_{N-1/2} \end{bmatrix}, \underline{\rho} = \begin{bmatrix} \rho_{1/2} \\ \rho_{3/2} \\ . \\ . \\ . \\ \rho_{N-1/2} \end{bmatrix}, \underline{u} = \begin{bmatrix} u_{1/2} \\ u_{3/2} \\ . \\ . \\ . \\ u_{N-1/2} \end{bmatrix}, \underline{v} = \begin{bmatrix} v_{1/2} \\ v_{3/2} \\ . \\ . \\ . \\ v_{N-1/2} \end{bmatrix}, \tag{2.82}$$

$$\underline{\theta} = \begin{bmatrix} \theta_0 \\ \theta_1 \\ . \\ . \\ . \\ \theta_N \end{bmatrix}, \underline{w} = \begin{bmatrix} w_0 \\ w_1 \\ . \\ . \\ . \\ w_N \end{bmatrix}. \tag{2.83}$$

The sub-matrices of A and B are of dimension $N \times N$, $(N+1) \times (N+1)$, $(N+1) \times N$ or $N \times (N+1)$. The dimension structure of A and B may be obtained from the tensor product $(N, N+1, N+1, N, N, N)^T \otimes (N, N+1, N+1, N, N, N)$, leading to the matrix structure

$$\begin{bmatrix} N \times N & N \times (N+1) & N \times (N+1) & N \times N & N \times N & N \times N \\ (N+1) \times N & (N+1) \times (N+1) & (N+1) \times (N+1) & (N+1) \times N & (N+1) \times N & (N+1) \times N \\ (N+1) \times N & (N+1) \times (N+1) & (N+1) \times (N+1) & (N+1) \times N & (N+1) \times N & (N+1) \times N \\ N \times N & N \times (N+1) & N \times (N+1) & N \times N & N \times N & N \times N \\ N \times N & N \times (N+1) & N \times (N+1) & N \times N & N \times N & N \times N \\ N \times N & N \times (N+1) & N \times (N+1) & N \times N & N \times N & N \times N \end{bmatrix}. \tag{2.84}$$

Introducing a horizontal spectral representation $G = \widehat{G} \exp(i\ell x)$ into (2.50) - (2.61), normalising and dropping the carets for convenience, leads to the matrix definitions:

$$A = \begin{bmatrix} I & A_{\Pi,\theta} & 0 & A_{\Pi,\rho} & 0 & 0 \\ 0 & I & A_{\theta,w} & 0 & 0 & 0 \\ A_{w,\Pi} & A_{w,\theta} & \mathbf{I}_h I & 0 & 0 & 0 \\ 0 & 0 & A_{\rho,w} & I & A_{\rho,u} & 0 \\ A_{u,\Pi} & 0 & 0 & 0 & I & 0 \\ 0 & 0 & 0 & 0 & 0 & I \end{bmatrix}, \tag{2.85}$$

$$B = e^{-i\ell u_s \Delta t} \begin{bmatrix} 0 & 0 & 0 & 0 & 0 & 0 \\ 0 & I & B'_{\theta,w} & 0 & 0 & 0 \\ B'_{w,\Pi} & B'_{w,\theta} & \mathbf{I}_h I_0 & 0 & B'_{w,u} & 0 \\ 0 & 0 & B'_{\rho,w} & (1 - i\ell u_s \Delta t)\, e^{i\ell u_s \Delta t} I & B'_{\rho,u} & 0 \\ B'_{u,\Pi} & 0 & B'_{u,w} & 0 & I & 0 \\ 0 & 0 & 0 & 0 & 0 & I \end{bmatrix}, \tag{2.86}$$

$$I = \begin{bmatrix} 1 & 0 & \cdot & 0 & 0 \\ 0 & 1 & 0 & \cdot & 0 \\ \cdot & \cdot & \ddots & \cdot & \cdot \\ 0 & \cdot & 0 & 1 & 0 \\ 0 & 0 & \cdot & 0 & 1 \end{bmatrix}, \tag{2.87}$$

$$I_0 = \begin{bmatrix} 0 & 0 & 0 & \cdot & \cdot & 0 \\ 0 & 1 & 0 & \cdot & \cdot & 0 \\ 0 & 0 & 1 & 0 & \cdot & 0 \\ \cdot & \cdot & \cdot & \ddots & \cdot & \cdot \\ 0 & \cdot & \cdot & 0 & 1 & 0 \\ 0 & \cdot & \cdot & 0 & 0 & 0 \end{bmatrix}, \tag{2.88}$$

$$A_{\Pi,\theta} = -\frac{\kappa_d}{1-\kappa_d} \begin{bmatrix} \left(a\frac{\Pi_s}{\theta_s z}\right)\Big|_{z_{\frac{1}{2}}} & \left(b\frac{\Pi_s}{\theta_s z}\right)\Big|_{z_{\frac{1}{2}}} & 0 & 0 & 0 & 0 \\ 0 & \cdot & \cdot & 0 & 0 & 0 \\ 0 & 0 & \left(a\frac{\Pi_s}{\theta_s z}\right)\Big|_{z_{k-\frac{1}{2}}} & \left(b\frac{\Pi_s}{\theta_s z}\right)\Big|_{z_{k-\frac{1}{2}}} & 0 & 0 \\ 0 & 0 & 0 & \cdot & \cdot & 0 \\ 0 & 0 & 0 & 0 & \left(a\frac{\Pi_s}{\theta_s z}\right)\Big|_{z_{N-\frac{1}{2}}} & \left(b\frac{\Pi_s}{\theta_s z}\right)\Big|_{z_{N-\frac{1}{2}}} \end{bmatrix}, \tag{2.89}$$

$$A_{\Pi,\rho} = -\frac{\kappa_d}{1-\kappa_d} \begin{bmatrix} \frac{\Pi_s}{\rho_s}\Big|_{z_{\frac{1}{2}}} & 0 & 0 & 0 & 0 \\ 0 & \cdot & 0 & 0 & 0 \\ 0 & 0 & \frac{\Pi_s}{\rho_s}\Big|_{z_{\frac{1}{2}}} & 0 & 0 \\ 0 & 0 & 0 & \cdot & 0 \\ 0 & 0 & 0 & 0 & \frac{\Pi_s}{\rho_s}\Big|_{z_{\frac{1}{2}}} \end{bmatrix}, \tag{2.90}$$

$$A_{\theta,w} = \alpha_2 \Delta t \begin{bmatrix} 0 & (\delta_{2z}\theta_s)\big|_{z_1} & 0 & 0 & 0 & 0 \\ 0 & (\delta_{2z}\theta_s)\big|_{z_1} & 0 & 0 & 0 & 0 \\ 0 & 0 & \cdot & 0 & 0 & 0 \\ 0 & 0 & 0 & (\delta_{2z}\theta_s)\big|_{z_k} & 0 & 0 \\ 0 & 0 & 0 & 0 & \cdot & 0 \\ 0 & 0 & 0 & 0 & 0 & 0 \end{bmatrix}, \tag{2.91}$$

$$B'_{\theta,w} = -\left(1-\alpha_2\right)\Delta t \begin{bmatrix} 0 & \left(\delta_{2z}\theta_s\right)\big|_{z_1} & 0 & 0 & 0 & 0 \\ 0 & \left(\delta_{2z}\theta_s\right)\big|_{z_1} & 0 & 0 & 0 & 0 \\ 0 & 0 & \cdot & 0 & 0 & 0 \\ 0 & 0 & 0 & \left(\delta_{2z}\theta_s\right)\big|_{z_k} & 0 & 0 \\ 0 & 0 & 0 & 0 & \cdot & 0 \\ 0 & 0 & 0 & 0 & 0 & 0 \end{bmatrix}, \tag{2.92}$$

$$A_{w,\Pi} = \alpha_4 \Delta t c_{pd} \begin{bmatrix} 0 & 0 & 0 & 0 & 0 \\ -\frac{1}{\Delta z_1}\left(\theta_s\right)\big|_{z_1} & \frac{1}{\Delta z_1}\left(\theta_s\right)\big|_{z_1} & 0 & 0 & 0 \\ 0 & \cdot & \cdot & 0 & 0 \\ 0 & 0 & -\frac{1}{\Delta z_k}\left(\theta_s\right)\big|_{z_k} & \frac{1}{\Delta z_k}\left(\theta_s\right)\big|_{z_k} & 0 \\ 0 & 0 & 0 & \cdot & \cdot \\ 0 & 0 & 0 & 0 & 0 \end{bmatrix}, \tag{2.93}$$

$$A_{w,\theta} = \alpha_4 \Delta t c_{pd} \begin{bmatrix} 0 & 0 & 0 & 0 & 0 & 0 \\ 0 & \left(\delta_z \Pi_s\right)\big|_{z_1} & 0 & 0 & 0 & 0 \\ 0 & 0 & \cdot & 0 & 0 & 0 \\ 0 & 0 & 0 & \left(\delta_z \Pi_s\right)\big|_{z_k} & 0 & 0 \\ 0 & 0 & 0 & 0 & \cdot & 0 \\ 0 & 0 & 0 & 0 & 0 & 0 \end{bmatrix}, \tag{2.94}$$

$$B'_{w,\Pi} = -\left(1-\alpha_4\right)\Delta t c_{pd} \begin{bmatrix} 0 & 0 & 0 & 0 & 0 \\ -\frac{1}{\Delta z_1}\left(\theta_s\right)\big|_{z_1} & \frac{1}{\Delta z_1}\left(\theta_s\right)\big|_{z_1} & 0 & 0 & 0 \\ 0 & \cdot & \cdot & 0 & 0 \\ 0 & 0 & -\frac{1}{\Delta z_k}\left(\theta_s\right)\big|_{z_k} & \frac{1}{\Delta z_k}\left(\theta_s\right)\big|_{z_k} & 0 \\ 0 & 0 & 0 & \cdot & \cdot \\ 0 & 0 & 0 & 0 & 0 \end{bmatrix}, \tag{2.95}$$

$$B'_{w,\theta} = -\left(1-\alpha_4\right)\Delta t c_{pd} \begin{bmatrix} 0 & 0 & 0 & 0 & 0 & 0 \\ 0 & \left(\delta_z \Pi_s\right)\big|_{z_1} & 0 & 0 & 0 & 0 \\ 0 & 0 & \cdot & 0 & 0 & 0 \\ 0 & 0 & 0 & \left(\delta_z \Pi_s\right)\big|_{z_k} & 0 & 0 \\ 0 & 0 & 0 & 0 & \cdot & 0 \\ 0 & 0 & 0 & 0 & 0 & 0 \end{bmatrix}, \tag{2.96}$$

$$B'_{w,u} = F\Delta t\left[\alpha_4 e^{i\ell u_s \Delta t} + (1-\alpha_4)\right]\begin{bmatrix} 0 & 0 & 0 & 0 & 0 \\ a\big|_{z_1} & b\big|_{z_1} & 0 & 0 & 0 \\ 0 & \cdot & \cdot & 0 & 0 \\ 0 & 0 & a\big|_{z_k} & b\big|_{z_k} & 0 \\ 0 & 0 & 0 & \cdot & \cdot \\ 0 & 0 & 0 & 0 & 0 \end{bmatrix}, \tag{2.97}$$

$$A_{\rho,w} = \alpha_2\Delta t\begin{bmatrix} 0 & \frac{(\overline{\rho_s}^z)|_{z_1}}{\Delta z_{\frac{1}{2}}} & 0 & 0 & 0 & 0 \\ 0 & \cdot & \cdot & 0 & 0 & 0 \\ 0 & 0 & -\frac{(\overline{\rho_s}^z)|_{z_{k-1}}}{\Delta z_{k-\frac{1}{2}}} & \frac{(\overline{\rho_s}^z)|_{z_k}}{\Delta z_{k-\frac{1}{2}}} & 0 & 0 \\ 0 & 0 & 0 & \cdot & \cdot & 0 \\ 0 & 0 & 0 & 0 & -\frac{(\overline{\rho_s}^z)|_{z_{N-1}}}{\Delta z_{N-\frac{1}{2}}} & 0 \end{bmatrix}, \tag{2.98}$$

$$A_{\rho,u} = i\ell\alpha_1\Delta t\begin{bmatrix} (\rho_s)\big|_{z_{\frac{1}{2}}} & 0 & 0 & 0 & 0 \\ 0 & \cdot & 0 & 0 & 0 \\ 0 & 0 & (\rho_s)\big|_{z_{k-\frac{1}{2}}} & 0 & 0 \\ 0 & 0 & 0 & \cdot & 0 \\ 0 & 0 & 0 & 0 & (\rho_s)\big|_{z_{N-\frac{1}{2}}} \end{bmatrix}, \tag{2.99}$$

$$B'_{\rho,w} = -\left(1-\alpha_2\right)\Delta t e^{i\ell u_s \Delta t}\begin{bmatrix} 0 & \frac{(\overline{\rho_s}^z)|_{z_1}}{\Delta z_{\frac{1}{2}}} & 0 & 0 & 0 & 0 \\ 0 & \cdot & \cdot & 0 & 0 & 0 \\ 0 & 0 & -\frac{(\overline{\rho_s}^z)|_{z_{k-1}}}{\Delta z_{k-\frac{1}{2}}} & \frac{(\overline{\rho_s}^z)|_{z_k}}{\Delta z_{k-\frac{1}{2}}} & 0 & 0 \\ 0 & 0 & 0 & \cdot & \cdot & 0 \\ 0 & 0 & 0 & 0 & -\frac{(\overline{\rho_s}^z)|_{z_{N-1}}}{\Delta z_{N-\frac{1}{2}}} & 0 \end{bmatrix}, \tag{2.100}$$

$$B'_{\rho,u} = -i\ell\left(1-\alpha_1\right)\Delta t e^{i\ell u_s \Delta t}\begin{bmatrix} (\rho_s)\big|_{z_{\frac{1}{2}}} & 0 & 0 & 0 & 0 \\ 0 & \cdot & 0 & 0 & 0 \\ 0 & 0 & (\rho_s)\big|_{z_{k-\frac{1}{2}}} & 0 & 0 \\ 0 & 0 & 0 & \cdot & 0 \\ 0 & 0 & 0 & 0 & (\rho_s)\big|_{z_{N-\frac{1}{2}}} \end{bmatrix}, \tag{2.101}$$

$$A_{u,\Pi} = i\ell\alpha_3\Delta t c_{pd}\begin{bmatrix} \left(\overline{\theta_s}^z\right)\Big|_{z_{\frac{1}{2}}} & 0 & 0 & 0 & 0 \\ 0 & \cdot & 0 & 0 & 0 \\ 0 & 0 & \left(\overline{\theta_s}^z\right)\Big|_{z_{k-\frac{1}{2}}} & 0 & 0 \\ 0 & 0 & 0 & \cdot & 0 \\ 0 & 0 & 0 & 0 & \left(\overline{\theta_s}^z\right)\Big|_{z_{N-\frac{1}{2}}} \end{bmatrix}, \tag{2.102}$$

$$B'_{u,\Pi} = -i\ell\left(1-\alpha_3\right)\Delta t c_{pd}\begin{bmatrix} \left(\overline{\theta_s}^z\right)\Big|_{z_{\frac{1}{2}}} & 0 & 0 & 0 & 0 \\ 0 & \cdot & 0 & 0 & 0 \\ 0 & 0 & \left(\overline{\theta_s}^z\right)\Big|_{z_{k-\frac{1}{2}}} & 0 & 0 \\ 0 & 0 & 0 & \cdot & 0 \\ 0 & 0 & 0 & 0 & \left(\overline{\theta_s}^z\right)\Big|_{z_{N-\frac{1}{2}}} \end{bmatrix}, \tag{2.103}$$

$$B'_{u,w} = -F\Delta t\left[\alpha_4 e^{i\ell u_s\Delta t} + (1-\alpha_4)\right]\begin{bmatrix} a\big|_{z_{\frac{1}{2}}} & b\big|_{z_{\frac{1}{2}}} & 0 & 0 & 0 & 0 \\ 0 & \cdot & \cdot & 0 & 0 & 0 \\ 0 & 0 & a\big|_{z_{k-\frac{1}{2}}} & b\big|_{z_{k-\frac{1}{2}}} & 0 & 0 \\ 0 & 0 & 0 & \cdot & \cdot & 0 \\ 0 & 0 & 0 & 0 & a\big|_{z_{N-\frac{1}{2}}} & b\big|_{z_{N-\frac{1}{2}}} \end{bmatrix}, \tag{2.104}$$

where

$$a\big|_{z_{k-\frac{1}{2}}} \equiv \left(\frac{z_k - z_{k-\frac{1}{2}}}{z_k - z_{k-1}}\right) = \frac{z_k - z_{k-\frac{1}{2}}}{\Delta z_{k-\frac{1}{2}}}, b\big|_{z_{k-\frac{1}{2}}} \equiv \left(\frac{z_{k-\frac{1}{2}} - z_{k-1}}{z_k - z_{k-1}}\right) = \frac{z_{k-\frac{1}{2}} - z_{k-1}}{\Delta z_{k-\frac{1}{2}}}, \tag{2.105}$$

$$a\big|_{z_k} \equiv \left(\frac{z_{k+\frac{1}{2}} - z_k}{z_{k+\frac{1}{2}} - z_{k-\frac{1}{2}}}\right) = \frac{z_{k+\frac{1}{2}} - z_k}{\Delta z_k}, b\big|_{z_k} \equiv \left(\frac{z_k - z_{k-\frac{1}{2}}}{z_{k+\frac{1}{2}} - z_{k-\frac{1}{2}}}\right) = \frac{z_k - z_{k-\frac{1}{2}}}{\Delta z_k}, \tag{2.106}$$

are the weights of the vertical averaging operators $\overline{(\,)}^z\Big|_{z_{k-\frac{1}{2}}}$ and $\overline{(\,)}^z\Big|_{z_k}$.

Note that the $B'_{x,y}$ sub-matrices are related to the $B_{x,y}$ ones via the definitions

$$B_{x,y} \equiv e^{-i\ell u_s\Delta t}B'_{x,y}. \tag{2.107}$$

The factor $\exp\left(-i\ell u_s\Delta t\right)$ represents the phase shift due to the upstream evaluations of a semi-Lagrangian discretisation. It is convenient to take it out as a factor since its modulus is unity, which means that it will not contribute to the stability relation. As written, it is implicitly assumed that there is no smoothing due to (horizontal) interpolation. To include

this effect, a multiplicative factor (the response function for the interpolator of interest) would have to be introduced here.

To apply the boundary conditions (2.52) and (2.54) on w, the matrix I_0 has been introduced into the definition (2.86) of B. This matrix is simply the identity matrix, but with the unit entries on the first and last rows replaced by zeros. If this were not done (i.e. if the identity matrix I appeared instead of I_0), then the weaker conditions

$$w^{n+1}\Big|_{z_0\equiv 0} = w_d^n|_{z_0\equiv 0}\,, \tag{2.108}$$

$$w^{n+1}\Big|_{z_N} = w_d^n|_{z_N}\,, \tag{2.109}$$

would be applied instead of the stronger ones (2.52) and (2.54).

To get the thermodynamic equations (2.55) - (2.57) into the form $I\underline{\theta}^{n+1} + A_{\theta,w}\underline{w}^{n+1} = e^{-il u_s \Delta t}\left(I\underline{\theta}^n + B'_{\theta,w}\underline{w}^n\right)$, (2.55) has been replaced, noting that $\theta^n|_{z_0\equiv 0} = \theta^n|_{z_1}$, by the weighted sum of (2.55) and (2.56) evaluated at level $k = 1$ (if this is not done, then the matrix on the left-hand side is no longer the identity matrix I, but I with the first row modified to have elements $(1, -1, 0, 0, ..., 0)$).

2.7 Analysis of revised discretisations

By modifying the definition of the A and B matrices. and their sub-matrices, it is possible to modify the analysis to examine the expected impact on the stability of the model of a possible change of discretisation.

2.7.1 A semi-Lagrangian discretisation of the continuity equation

Consider changing the present Eulerian discretisation of the continuity equation to a semi-Lagrangian one. One (good) way of doing this is to modify (2.17) - (2.19) to

$$\begin{aligned}\frac{\ln\rho^{n+1}-(\ln\rho)_d^n}{\Delta t} &= -\alpha_1\frac{\partial u^{n+1}}{\partial x}-(1-\alpha_1)\left(\frac{\partial u}{\partial x}\right)_d^n \\ &\quad -\alpha_2\delta_z w^{n+1}-(1-\alpha_2)\left(\delta_z w\right)_d^n, \end{aligned} \tag{2.110}$$

$$\begin{aligned}\left[\frac{\ln\rho^{n+1}-(\ln\rho)_d^n}{\Delta t}\right]\Big|_{z_{1/2}} &= -\left[\alpha_1\frac{\partial u^{n+1}}{\partial x}+(1-\alpha_1)\left(\frac{\partial u}{\partial x}\right)_d^n\right]\Big|_{z_{1/2}} \\ &\quad -\alpha_2\left(\frac{1}{\Delta z}\right)\Big|_{z_{1/2}}\left(w^{n+1}\right)\Big|_{z_1}-(1-\alpha_2)\left[(\delta_z w)_d^n\right]\Big|_{z_{1/2}}, \end{aligned} \tag{2.111}$$

$$\begin{aligned}\left[\frac{\ln\rho^{n+1}-(\ln\rho)_d^n}{\Delta t}\right]\Big|_{z_{N-1/2}} &= -\left[\alpha_1\frac{\partial u^{n+1}}{\partial x}+(1-\alpha_1)\left(\frac{\partial u}{\partial x}\right)_d^n\right]\Big|_{z_{N-1/2}} \\ &\quad +\alpha_2\left(\frac{1}{\Delta z}\right)\Big|_{z_{N-1/2}}\left(w^{n+1}\right)\Big|_{z_{N-1}}-(1-\alpha_2)\left[(\delta_z w)_d^n\right]\Big|_{z_{N-1/2}} \end{aligned} \tag{2.112}$$

leading to the following linearised equations, corresponding to (2.58) - (2.60):

$$\begin{aligned}\left(\frac{\rho^{n+1}-\rho_d^n}{\Delta t}\right)\Big|_{z_{1/2}} &= -\left\{\rho_s\left[\alpha_1\frac{\partial u^{n+1}}{\partial x}+(1-\alpha_1)\left(\frac{\partial u}{\partial x}\right)_d^n\right]\right\}\Big|_{z_{1/2}} \\ &\quad -\left(\frac{\rho_s}{\Delta z}\right)\Big|_{z_{1/2}}\left[\alpha_2 w^{n+1}+(1-\alpha_2)\,w_d^n\right]\Big|_{z_1}, \end{aligned} \tag{2.113}$$

$$\begin{aligned}\frac{\rho^{n+1}-\rho_d^n}{\Delta t} &= -\rho_s\left[\alpha_1\frac{\partial u^{n+1}}{\partial x}+(1-\alpha_1)\left(\frac{\partial u}{\partial x}\right)_d^n\right] \\ &\quad -\rho_s\left[\alpha_2\delta_z w^{n+1}+(1-\alpha_2)\left(\delta_z w\right)_d^n\right], \end{aligned} \tag{2.114}$$

at levels $k = 3/2,\ 5/2,\ ...,\ N-3/2$, and

$$\begin{aligned}\left(\frac{\rho^{n+1}-\rho_d^n}{\Delta t}\right)\Big|_{z_{N-1/2}} &= -\left\{\rho_s\left[\alpha_1\frac{\partial u^{n+1}}{\partial x}+(1-\alpha_1)\left(\frac{\partial u}{\partial x}\right)_d^n\right]\right\}\Big|_{z_{N-1/2}} \\ &\quad +\left(\frac{\rho_s}{\Delta z}\right)\Big|_{z_{N-1/2}}\left[\alpha_2 w^{n+1}+(1-\alpha_2)\,w_d^n\right]\Big|_{z_{N-1}}. \end{aligned} \tag{2.115}$$

Another (not so good, because of its adverse impact on both accuracy and stability) way of discretising the continuity equation in a semi-Lagrangian manner is to modify (2.17) - (2.19) to

$$\begin{aligned}\frac{\rho^{n+1}-\rho_d^n}{\Delta t} &= -\left[\alpha_1\rho^n\frac{\partial u^{n+1}}{\partial x}+(1-\alpha_1)\left(\rho\frac{\partial u}{\partial x}\right)_d^n\right]\\ &\quad -\left[\alpha_2\rho^n\delta_z w^{n+1}+(1-\alpha_2)\left(\rho\delta_z w\right)_d^n\right], \end{aligned}\tag{2.116}$$

$$\begin{aligned}\left[\frac{\rho^{n+1}-\rho_d^n}{\Delta t}\right]\Big|_{z_{1/2}} &= -\left[\alpha_1\rho^n\frac{\partial u^{n+1}}{\partial x}+(1-\alpha_1)\left(\rho\frac{\partial u}{\partial x}\right)_d^n\right]\Big|_{z_{1/2}}\\ &\quad -\alpha_2\left(\frac{\rho}{\Delta z}\right)\Big|_{z_{1/2}}\left(w^{n+1}\right)\Big|_{z_1}-(1-\alpha_2)\left[(\rho\delta_z w)_d^n\right]|_{z_{1/2}}, \end{aligned}\tag{2.117}$$

$$\begin{aligned}\left[\frac{\rho^{n+1}-\rho_d^n}{\Delta t}\right]\Big|_{z_{N-1/2}} &= -\left[\alpha_1\frac{\partial u^{n+1}}{\partial x}+(1-\alpha_1)\left(\frac{\partial u}{\partial x}\right)_d^n\right]\Big|_{z_{N-1/2}}\\ &\quad +\alpha_2\left(\frac{\rho}{\Delta z}\right)\Big|_{z_{N-1/2}}\left(w^{n+1}\right)\Big|_{z_{N-1}}-(1-\alpha_2)\left[(\rho\delta_z w)_d^n\right]|_{z_{N-1/2}}, \end{aligned}\tag{2.118}$$

The linearised form of these equations is identical to (2.113) - (2.115). Thus (2.113) - (2.115) can be used to analyse, to linear order, the impact on the discretised system of equations of adopting either of these two alternative semi-Lagrangian discretisations of the continuity equation.

To analyse either of these two changes to the discretisation, it suffices to change the matrix definitions as follows:

- in the definition (2.86) of the matrix B, replace the sub-matrix "$(1-i\ell u_s\Delta t)\,e^{i\ell u_s\Delta t}I$" by the identity matrix "I";
- in the definition (2.98) of the matrix $A_{\rho,w}$, replace the elements $(\overline{\rho_s}^z)|_{z_1}/\Delta z_{1/2}$, $-(\overline{\rho_s}^z)|_{z_{k-1}}/\Delta z_{k-1/2}$, $(\overline{\rho_s}^z)|_{z_k}/\Delta z_{k-1/2}$ and $-(\overline{\rho_s}^z)|_{z_N}/\Delta z_{N-1/2}$ respectively by $(\rho_s/\Delta z)|_{z_{1/2}}$, $-(\rho_s/\Delta z)|_{z_{k-1/2}}$, $(\rho_s/\Delta z)|_{z_{k-1/2}}$ and $-(\rho_s/\Delta z)|_{z_{N-1/2}}$;
- in the definition (2.100) of the matrix $B'_{\rho,w}$, delete the multiplicative factor "$e^{i\ell u_s\Delta t}$" ;
- in the definition (2.100) of the matrix $B'_{\rho,w}$, replace the elements $(\overline{\rho_s}^z)|_{z_1}/\Delta z_{1/2}$, $-(\overline{\rho_s}^z)|_{z_{k-1}}/\Delta z_{k-1/2}$, $(\overline{\rho_s}^z)|_{z_k}/\Delta z_{k-1/2}$ and $-(\overline{\rho_s}^z)|_{z_N}/\Delta z_{N-1/2}$ respectively by $(\rho_s/\Delta z)|_{z_{1/2}}$, $-(\rho_s/\Delta z)|_{z_{k-1/2}}$, $(\rho_s/\Delta z)|_{z_{k-1/2}}$ and $-(\rho_s/\Delta z)|_{z_{N-1/2}}$;
- in the definition (2.101) of the matrix $B'_{\rho,u}$, delete the multiplicative factor "$e^{i\ell u_s\Delta t}$" .

2.7.2 θ active at the bottom

Consider removing the present assumption that the bottom layer is isentropic (i.e. $\theta\big|_{z_0\equiv 0} = \theta\big|_{z_1}$), and replacing this by discretising the prognostic thermodynamic equation at the bottom boundary $z = 0$ subject to the no-normal flow condition $w\big|_{z_0\equiv 0} = 0$. Thus, using (2.13) (where $w = w^* = 0$), (2.15) and (2.55) would be modified to

$$\theta^{n+1}\Big|_{z_0\equiv 0} = (\theta^*)|_{z_0\equiv 0} = (\theta^n_{dl})|_{z_0\equiv 0}\,, \tag{2.119}$$

$$\theta^{n+1}\Big|_{z_0\equiv 0} = (\theta^n_{d})|_{z_0\equiv 0}\,. \tag{2.120}$$

To analyse this change to the discretisation, it suffices to change the matrix definitions as follows:

- in the definition (2.91) of the matrix $A_{\theta,w}$, replace the first row by a row of all zeros;
- in the definition (2.92) of the matrix $B'_{\theta,w}$, replace the first row by a row of all zeros.

2.8 Eigen analysis and stability

To determine the stability of the model summarised by the linear equation set (2.79) amounts to analysing the generalised eigenvalue problem

$$B\underline{x} = \lambda A\underline{x}, \tag{2.121}$$

or, if A is non-singular, the conceptually-simpler equivalent problem

$$A^{-1}B\underline{x} = \lambda\underline{x}. \tag{2.122}$$

The eigenvalue or generalised eigenvalue problems are derived from the matrix problem (2.79) via the definition of the eigenvalues:

$$\underline{x}^{n+1} = \lambda\underline{x}^{n}. \tag{2.123}$$

The normal modes of the problem,

$$\underline{x} = \left[\begin{array}{cccccc} \underline{\Pi}, & \underline{\theta}, & \underline{w}, & \underline{\rho}, & \underline{u}, & \underline{v} \end{array} \right]^T, \tag{2.124}$$

are composed of arrays of dimensions $N+1$ ($\underline{\theta}$ and $\underline{w}$) and N ($\underline{\Pi}$, $\underline{\rho}$, $\underline{u}$, and $\underline{v}$), which store the values of the corresponding variables evaluated at integer or half-integer model levels respectively. Throughout this report the underlined notation for each of the variable denotes the associated array storing the values of the variable at the appropriate integer or half-integer model levels, whilst the variables themselves are left not underlined.

In general, A is not expected to be singular, but if it is then this means that A has a null space (with an associated zero eigenvalue), corresponding to the existence of a computational mode or modes. It is quite possible for B to be singular - this is typically a consequence of applying homogeneous boundary conditions.

To gain further insight into the methodology, it is instructive to examine simple column-equations subsets. The simplest such subset is obtained by assuming that θ_s, ρ_s, and Π_s are all constants. It has an analytic solution and is examined in some detail. Another simple subset is obtained by assuming an isothermal basic state. It again has an analytic solution, and it would be of interest to use this case to examine the impact the bottom-layer isentropic assumption has on the discretisation. Further including uniform advection in the x direction would allow comparison of the impact of the semi-Lagrangian and Eulerian discretisations of the continuity equation.

Looking at the limits that Δt and Δz tend to zero permits verification that the discrete linear solution converges to the corresponding analytic one, including dispersion relations and associated eigenvectors. The analytic solutions then provide useful controls for evaluating the numerical results.

3 Matrix stability analysis of a simple column-equations subset

It is instructive to examine the procedure in the context of a simpler problem, the equations for a column model.

3.1 Continuous column equations

Setting $F \equiv 0$ and neglecting variations in the x direction ($\partial/\partial x \equiv 0$) the continuous set of governing equations (2.1) - (2.6) reduce to

$$\frac{Du}{Dt} = 0, \tag{3.1}$$

$$\frac{Dv}{Dt} = 0, \tag{3.2}$$

$$\frac{Dw}{Dt} = -g - c_{pd}\theta\frac{\partial \Pi}{\partial z}, \tag{3.3}$$

$$\frac{D\theta}{Dt} = 0, \tag{3.4}$$

$$\frac{D\rho}{Dt} = -\rho\frac{\partial w}{\partial z}, \tag{3.5}$$

$$\Pi^{\frac{\kappa_d - 1}{\kappa_d}}\rho\theta = \frac{p_0}{\kappa_d c_{pd}}, \tag{3.6}$$

subject to

$$w\big|_{z=z_0\equiv 0} = w\big|_{z=z_N} = 0, \tag{3.7}$$

where $D/Dt \equiv \partial/\partial t + w\partial/\partial z$, $\Pi \equiv (p/p_0)^{\kappa_d}$, and $\kappa_d \equiv R_d/c_{pd}$.

Linearising these equations about a basic state atmosphere defined by

$$c_{pd}\theta_s\frac{\partial \Pi_s}{\partial z} = -g, \tag{3.8}$$

$$\Pi_s^{\frac{\kappa_d - 1}{\kappa_d}}\rho_s\theta_s = \frac{p_0}{\kappa_d c_{pd}}, \tag{3.9}$$

and expanding variables as

$$u(z,t) = u'(z,t), \tag{3.10}$$

$$v(z,t) = v'(z,t), \tag{3.11}$$

$$w(z,t) = w'(z,t), \tag{3.12}$$

$$\theta(z,t) = \theta_s(z) + \theta'(z,t), \tag{3.13}$$

$$\rho(z,t) = \rho_s(z) + \rho'(z,t), \tag{3.14}$$

$$\Pi(z,t) = \Pi_s(z) + \Pi'(z,t), \tag{3.15}$$

leads to the linearised equation set

$$\frac{\partial w}{\partial t} = -c_{pd}\theta_s \frac{\partial \Pi}{\partial z} - c_{pd}\frac{d\Pi_s}{dz}\theta, \tag{3.16}$$

$$\frac{\partial \theta}{\partial t} = -\frac{d\theta_s}{dz}w, \tag{3.17}$$

$$\frac{\partial \rho}{\partial t} = -\frac{\partial(\rho_s w)}{\partial z}, \tag{3.18}$$

$$\left(\frac{1-\kappa_d}{\kappa_d}\right)\frac{\Pi}{\Pi_s} = \frac{\rho}{\rho_s} + \frac{\theta}{\theta_s}, \tag{3.19}$$

where primes have been dropped for convenience.

For an isothermal basic-state atmosphere, the linear equation set (3.16) - (3.19), subject to (3.7), can be solved analytically. This might be a useful case to examine at some point, particularly regarding the bottom-layer isentropic assumption.

Assume however an isentropic basic state (i.e. $\theta_s = constant$). Assume also a very shallow atmosphere such that $z_T/H(0) \ll 1$, where the atmospheric scale height $H(0)$ is given by (2.40). Then from (2.39) and (2.43), not only is θ_s constant, but ρ_s and Π_s are also approximately constant. Thus the linear equation set (3.16) - (3.19) can be further simplified to

$$\frac{\partial w}{\partial t} = -c_{pd}\theta_s \frac{\partial \Pi}{\partial z}, \tag{3.20}$$

$$\frac{\partial \theta}{\partial t} = 0, \tag{3.21}$$

$$\frac{\partial \rho}{\partial t} = -\rho_s \frac{\partial w}{\partial z}, \tag{3.22}$$

$$\left(\frac{1-\kappa_d}{\kappa_d}\right)\frac{\Pi}{\Pi_s} = \frac{\rho}{\rho_s} + \frac{\theta}{\theta_s}. \tag{3.23}$$

This constant-coefficient equation set is particularly simple since it is analytically equivalent to $\theta = \theta(z)$ ($\theta(z)$ can be arbitrarily set to zero without loss of generality since it only appears in the analysis when differentiated with respect to t), and the two simple harmonic problems

$$\frac{\partial^2 w}{\partial t^2} = c_{pd}\left(\frac{\kappa_d}{1-\kappa_d}\right)\theta_s \Pi_s \frac{\partial^2 w}{\partial z^2} = c_s^2 \frac{\partial^2 w}{\partial z^2}, \tag{3.24}$$

subject to (3.7), and

$$\frac{\partial^2 \Pi}{\partial t^2} = c_{pd}\left(\frac{\kappa_d}{1-\kappa_d}\right)\theta_s \Pi_s \frac{\partial^2 \Pi}{\partial z^2} = c_s^2 \frac{\partial^2 \Pi}{\partial z^2}, \tag{3.25}$$

subject to

$$\left.\frac{\partial \Pi}{\partial z}\right|_{z=z_0 \equiv 0} = \left.\frac{\partial \Pi}{\partial z}\right|_{z=z_T} = 0, \tag{3.26}$$

where

$$c_s^2 \equiv \frac{R_d T_s}{1-\kappa_d}, \tag{3.27}$$

is the adiabatic sound speed.

The solutions of (3.24) - (3.25) subject to (3.26) - (3.27) are

$$w = \sum_{m=1}^{\infty} \sin\left(\frac{m\pi z}{z_T}\right)\left[w_m^0 \cos\left(\frac{m\pi c_s t}{z_T}\right) + \frac{c_{pd}\theta_s}{c_s}\Pi_m^0 \sin\left(\frac{m\pi c_s t}{z_T}\right)\right], \tag{3.28}$$

$$\Pi = \sum_{m=0}^{\infty} \cos\left(\frac{m\pi z}{z_T}\right)\left[\Pi_m^0 \cos\left(\frac{m\pi c_s t}{z_T}\right) - \frac{c_s}{c_{pd}\theta_s} w_m^0 \sin\left(\frac{m\pi c_s t}{z_T}\right)\right], \tag{3.29}$$

where w_m^0 and Π_m^0 are the Fourier components of the initial conditions, where it is assumed that both w and Π are specified functions at $t = 0$.

3.2 Column model equations

The linearised equations for the column model reduce to:

3.2.1 Vertical momentum at levels $k = 0, 1, ..., N$

$$w^{n+1}\Big|_{z_0 \equiv 0} = 0, \tag{3.30}$$

$$\begin{aligned} \mathbf{I}_h \frac{w^{n+1} - w^n}{\Delta t} &= -c_{pd}\theta_s \left[\alpha_4 \delta_z \Pi^{n+1} + (1-\alpha_4)\,\delta_z \Pi^n\right] \\ &\quad -c_{pd}\delta_z \Pi_s \left[\alpha_4 \theta^{n+1} + (1-\alpha_4)\,\theta^n\right], \end{aligned} \tag{3.31}$$

at levels $k = 1, 2, ..., N-1$, and

$$w^{n+1}\Big|_{z_N} = 0. \tag{3.32}$$

3.2.2 Thermodynamic at levels $k = 0, 1, ..., N$

$$\theta^{n+1}\Big|_{z_0 \equiv 0} = \theta^{n+1}\Big|_{z_1}, \tag{3.33}$$

$$\frac{\theta^{n+1} - \theta^n}{\Delta t} = -\delta_{2z}\theta_s \left[\alpha_2 w^{n+1} + (1-\alpha_2) w^n\right], \tag{3.34}$$

at levels $k = 1, 2, ..., N-1$, and

$$\theta^{n+1}\Big|_{z_N} = \theta^n|_{z_N}. \tag{3.35}$$

3.2.3 Continuity at levels $k = 1/2, 3/2, ..., N-1/2$

$$\left(\frac{\rho^{n+1} - \rho^n}{\Delta t}\right)\Big|_{z_{1/2}} = -\left(\frac{1}{\Delta z}\right)\Big|_{z_{1/2}} \left[\alpha_2 \overline{\rho_s}^z w^{n+1} + (1-\alpha_2)\,\overline{\rho_s}^z w^n\right]\Big|_{z_1}, \tag{3.36}$$

$$\frac{\rho^{n+1} - \rho^n}{\Delta t} = -\left[\alpha_2 \delta_z \left(\overline{\rho_s}^z w^{n+1}\right) + (1-\alpha_2)\,\delta_z \left(\overline{\rho_s}^z w^n\right)\right], \tag{3.37}$$

at levels $k = 3/2, 5/2, ..., N-3/2$, and

$$\left(\frac{\rho^{n+1} - \rho^n}{\Delta t}\right)\Big|_{z_{N-1/2}} = \left(\frac{1}{\Delta z}\right)\Big|_{z_{N-1/2}} \left[\alpha_2 \overline{\rho_s}^z w^{n+1} + (1-\alpha_2)\,\overline{\rho_s}^z w^n\right]\Big|_{z_{N-1}}. \tag{3.38}$$

3.2.4 Linearised gas law at levels $k = 1/2, 3/2, ..., N-1/2$

$$\left(\frac{1-\kappa_d}{\kappa_d}\right)\frac{\Pi^{n+1}}{\Pi_s} = \frac{\rho^{n+1}}{\rho_s} + \frac{\overline{\theta^{n+1}}^z}{\overline{\theta_s}^z}. \tag{3.39}$$

3.3 Column model equations rewritten

The linearised equations for the column model can be rewritten as:

3.3.1 Vertical momentum at levels $k = 0,\ 1,\ ...,\ N$

$$w^{n+1}\Big|_{z_0 \equiv 0} = 0, \tag{3.40}$$

$$\begin{aligned} \mathbf{I}_h w^{n+1} + \alpha_4 c_{pd} \Delta t \theta_s \delta_z \Pi^{n+1} + \alpha_4 c_{pd} \Delta t \left(\delta_z \Pi_s\right) \theta^{n+1} \quad &= \quad \mathbf{I}_h w^n - \left(1 - \alpha_4\right) c_{pd} \Delta t \theta_s \delta_z \Pi^n \\ &\quad - \left(1 - \alpha_4\right) c_{pd} \Delta t \left(\delta_z \Pi_s\right) \theta^n, \end{aligned} \tag{3.41}$$

at levels $k = 1,\ 2,\ ...,\ N-1$, and

$$w^{n+1}\Big|_{z_N} = 0. \tag{3.42}$$

3.3.2 Thermodynamic at levels $k = 0,\ 1,\ ...,\ N$

$$\theta^{n+1}\Big|_{z_0 \equiv 0} - \theta^{n+1}\Big|_{z_1} = 0, \tag{3.43}$$

$$\theta^{n+1} + \alpha_2 \Delta t \delta_{2z} \theta_s w^{n+1} \quad = \quad \theta^n - \left(1 - \alpha_2\right) \Delta t \delta_{2z} \theta_s w^n, \tag{3.44}$$

at levels $k = 1,\ 2,\ ...,\ N-1$, and

$$\theta^{n+1}\Big|_{z_N} = \theta^n|_{z_N}. \tag{3.45}$$

3.3.3 Continuity at levels $k = 1/2,\ 3/2,\ ...,\ N - 1/2$

$$\rho^{n+1}\Big|_{z_{1/2}} + \alpha_2 \left(\frac{\Delta t}{\Delta z}\right)\Big|_{z_{1/2}} \left(\overline{\rho_s}^z w^{n+1}\right)\Big|_{z_1} = \rho^n|_{z_{1/2}} - \left(1 - \alpha_2\right) \left(\frac{\Delta t}{\Delta z}\right)\Big|_{z_{1/2}} \left(\overline{\rho_s}^z w^n\right)|_{z_1}, \tag{3.46}$$

$$\rho^{n+1} + \alpha_2 \Delta t \delta_z \left(\overline{\rho_s}^z w^{n+1}\right) = \rho^n - \left(1 - \alpha_2\right) \Delta t \delta_z \left(\overline{\rho_s}^z w^n\right), \tag{3.47}$$

at levels $k = 3/2,\ 5/2,\ ...,\ N - 3/2$, and

$$\rho^{n+1}\Big|_{z_{N-1/2}} - \alpha_2 \left(\frac{\Delta t}{\Delta z}\right)\Big|_{z_{N-1/2}} \left(\overline{\rho_s}^z w^{n+1}\right)\Big|_{z_{N-1}} = \rho^n|_{z_{N-1/2}} + \left(1 - \alpha_2\right) \left(\frac{\Delta t}{\Delta z}\right)\Big|_{z_{N-1/2}} \left(\overline{\rho_s}^z w^n\right)|_{z_{N-1}}. \tag{3.48}$$

3.3.4 Linearised gas law at levels $k = 1/2,\ 3/2,\ ...,\ N - 1/2$

$$\left(\frac{1 - \kappa_d}{\kappa_d}\right) \frac{\Pi^{n+1}}{\Pi_s} \quad - \quad \frac{\rho^{n+1}}{\rho_s} - \frac{\overline{\theta^{n+1}}^z}{\overline{\theta_s}^z} = 0. \tag{3.49}$$

3.4 Special case where θ_s, Π_s and ρ_s are all constant and $\mathbf{I}_h \equiv 1$

When θ_s, Π_s and ρ_s are all constant and $\mathbf{I}_h \equiv 1$, (3.30) - (3.49) reduce to

3.4.1 Vertical momentum at levels $k = 0, 1, ..., N$

$$w^{n+1}\Big|_{z_0 \equiv 0} = 0, \tag{3.50}$$

$$w^{n+1} + \alpha_4 c_{pd} \Delta t \theta_s \delta_z \Pi^{n+1} = w^n - (1 - \alpha_4)\, c_{pd} \Delta t \theta_s \delta_z \Pi^n, \tag{3.51}$$

at levels $k = 1, 2, ..., N-1$, and

$$w^{n+1}\Big|_{z_N} = 0. \tag{3.52}$$

3.4.2 Thermodynamic at levels $k = 0, 1, ..., N$

$$\theta^{n+1} \;=\; \theta^n = 0. \tag{3.53}$$

3.4.3 Continuity at levels $k = 1/2, 3/2, ..., N - 1/2$

$$\rho^{n+1}\Big|_{z_{1/2}} + \alpha_2 \Delta t \rho_s \left(\frac{1}{\Delta z}\right)\Big|_{z_{1/2}} w^{n+1}\Big|_{z_1} = \rho^n|_{z_{1/2}} - (1 - \alpha_2)\, \Delta t \rho_s \left(\frac{1}{\Delta z}\right)\Big|_{z_{1/2}} w^n|_{z_1}\,, \tag{3.54}$$

$$\rho^{n+1} + \alpha_2 \Delta t \rho_s \delta_z \left(w^{n+1}\right) = \rho^n - (1 - \alpha_2)\, \Delta t \rho_s \delta_z \left(w^n\right), \tag{3.55}$$

at levels $k = 3/2, 5/2, ..., N - 3/2$, and

$$\rho^{n+1}\Big|_{z_{N-1/2}} - \alpha_2 \Delta t \rho_s \left(\frac{1}{\Delta z}\right)\Big|_{z_{N-1/2}} w^{n+1}\Big|_{z_{N-1}} = \rho^n|_{z_{N-1/2}} + (1 - \alpha_2)\, \Delta t \rho_s \left(\frac{1}{\Delta z}\right)\Big|_{z_{N-1/2}} w^n|_{z_{N-1}}\,. \tag{3.56}$$

3.4.4 Linearised gas law at levels $k = 1/2, 3/2, ..., N - 1/2$

$$\left(\frac{1 - \kappa_d}{\kappa_d}\right) \frac{\Pi^{n+1}}{\Pi_s} \;-\; \frac{\rho^{n+1}}{\rho_s} = 0. \tag{3.57}$$

3.4.5 The equations rewritten in matrix form

Using (3.57) to eliminate ρ in favour of Π in (3.50) - (3.56) leads to

$$A \begin{bmatrix} \underline{\Pi}^{n+1} \\ \underline{w}^{n+1} \end{bmatrix} = B \begin{bmatrix} \underline{\Pi}^{n} \\ \underline{w}^{n} \end{bmatrix}, \tag{3.58}$$

where

$$A = \begin{bmatrix} I & \alpha_2 \Delta t \left(\frac{\kappa_d}{1-\kappa_d}\right) \Pi_s D \\ \alpha_4 \Delta t c_{pd} \theta_s E & I \end{bmatrix}, \tag{3.59}$$

$$B = \begin{bmatrix} I & -(1-\alpha_2)\,\Delta t \left(\frac{\kappa_d}{1-\kappa_d}\right) \Pi_s D \\ -(1-\alpha_4)\,\Delta t c_{pd} \theta_s E & I_0 \end{bmatrix}, \tag{3.60}$$

$$I = \begin{bmatrix} 1 & 0 & \cdot & 0 & 0 \\ 0 & 1 & 0 & \cdot & 0 \\ \cdot & \cdot & \ddots & \cdot & \cdot \\ 0 & \cdot & 0 & 1 & 0 \\ 0 & 0 & \cdot & 0 & 1 \end{bmatrix}, \tag{3.61}$$

$$I_0 = \begin{bmatrix} 0 & 0 & 0 & \cdot & \cdot & 0 \\ 0 & 1 & 0 & \cdot & \cdot & 0 \\ 0 & 0 & 1 & 0 & \cdot & 0 \\ \cdot & \cdot & \cdot & \ddots & \cdot & \cdot \\ 0 & \cdot & \cdot & 0 & 1 & 0 \\ 0 & \cdot & \cdot & 0 & 0 & 0 \end{bmatrix}, \tag{3.62}$$

$$D = \begin{bmatrix} -\left(\frac{1}{\Delta z}\right)\Big|_{z_{\frac{1}{2}}} & \left(\frac{1}{\Delta z}\right)\Big|_{z_{\frac{1}{2}}} & 0 & 0 & 0 & 0 \\ 0 & \cdot & \cdot & 0 & 0 & 0 \\ 0 & 0 & -\left(\frac{1}{\Delta z}\right)\Big|_{z_{k-\frac{1}{2}}} & \left(\frac{1}{\Delta z}\right)\Big|_{z_{k-\frac{1}{2}}} & 0 & 0 \\ 0 & 0 & 0 & \cdot & \cdot & 0 \\ 0 & 0 & 0 & 0 & -\left(\frac{1}{\Delta z}\right)\Big|_{z_{N-\frac{1}{2}}} & \left(\frac{1}{\Delta z}\right)\Big|_{z_{N-\frac{1}{2}}} \end{bmatrix}, \tag{3.63}$$

$$E = \begin{bmatrix} 0 & 0 & 0 & 0 & 0 \\ -\left(\frac{1}{\Delta z}\right)\Big|_{z_1} & \left(\frac{1}{\Delta z}\right)\Big|_{z_1} & 0 & 0 & 0 \\ 0 & \cdot & \cdot & 0 & 0 \\ 0 & 0 & -\left(\frac{1}{\Delta z}\right)\Big|_{z_k} & \left(\frac{1}{\Delta z}\right)\Big|_{z_k} & 0 \\ 0 & 0 & 0 & \cdot & \cdot \\ 0 & 0 & 0 & 0 & 0 \end{bmatrix}. \tag{3.64}$$

3.4.6 Eigen analysis when the grid is uniform

In general, one would now proceed to perform a discrete eigen analysis of $A^{-1}B\underline{x} = \lambda\underline{x}$ using standard eigen-analysis software. However, when the grid is uniform, i.e. when

$$\Delta z_{1/2} = \Delta z_1 = ... = \Delta z_{N-1} = \Delta z_{N-1/2} = \Delta z = z_T/N, \tag{3.65}$$

it is relatively straightforward to perform the analysis analytically. This is now done.

By inspection it is seen that the eigenfunctions (all but two, more on this later) can be obtained by expanding Π and w respectively as half-wave discrete Fourier cosine and sine series. Thus the m'th pair of eigenfunctions have the form

$$\begin{aligned}\underline{x}_m &= [\Pi_m, w_m]^T \\ &= \left[\Pi_m^{\pm}\left(\cos\frac{m\pi}{2N}, \cos\frac{3m\pi}{2N}, \cdots, \cos\frac{(2N-1)\,m\pi}{2N}\right), w_m^{\pm}\left(0, \sin\frac{m\pi}{N}, \cdots, \sin\frac{(N-1)\,m\pi}{N}, 0\right)\right]^T, \\ & \quad m = 0, 1, \cdots, N-1.\end{aligned} \tag{3.66}$$

where $\Pi_m^{\pm}$ and $w_m^{\pm}$ are constant coefficients to be determined (the two signs anticipate downward and upward propagating modes). Note however that the $m = 0$ "pair" is degenerate and is actually a single mode such that Π is everywhere constant and w is identically zero everywhere.

Now using (3.58) - (3.64) yields

$$A\underline{x}_m = \begin{bmatrix} \left(\Pi_m^{\pm} + \alpha_2\beta_m\frac{c_s^2}{c_{pd}\theta_s}w_m^{\pm}\right)\left(\cos\frac{m\pi}{2N}, \cos\frac{3m\pi}{2N}, \cdots, \cos\frac{(2N-1)m\pi}{2N}\right)^T \\ \left(w_m^{\pm} - \alpha_4\beta_m c_{pd}\theta_s\Pi_m^{\pm}\right)\left(0, \sin\frac{m\pi}{N}, \cdots, \sin\frac{(N-1)m\pi}{N}, 0\right)^T \end{bmatrix}, \tag{3.67}$$

and

$$B\underline{x}_m = \begin{bmatrix} \left(\Pi_m^{\pm} - (1-\alpha_2)\,\beta_m\frac{c_s^2}{c_{pd}\theta_s}w_m^{\pm}\right)\left(\cos\frac{m\pi}{2N}, \cos\frac{3m\pi}{2N}, \cdots, \cos\frac{(2N-1)m\pi}{2N}\right)^T \\ \left(w_m^{\pm} + (1-\alpha_4)\,\beta_m c_{pd}\theta_s\Pi_m^{\pm}\right)\left(0, \sin\frac{m\pi}{N}, \cdots, \sin\frac{(N-1)m\pi}{N}, 0\right)^T \end{bmatrix}, \tag{3.68}$$

where

$$\beta_m = \frac{\sin\frac{m\pi}{2N}}{\Delta z/2}\Delta t, \tag{3.69}$$

and

$$c_s^2 = \frac{R_d T_s}{1-\kappa_d}, \tag{3.70}$$

is the adiabatic sound speed.

So

$$
\begin{aligned}
0 &= \lambda_m A\underline{x}_m - B\underline{x}_m \\
&= \left[\lambda_m\left(\Pi_m^{\pm} + \alpha_2\beta_m\frac{c_s^2}{c_{pd}\theta_s}w_m^{\pm}\right) - \left(\Pi_m^{\pm} - (1-\alpha_2)\,\beta_m\frac{c_s^2}{c_{pd}\theta_s}w_m^{\pm}\right)\right]\begin{bmatrix}\cos\frac{m\pi}{2N}\\ \cos\frac{3m\pi}{2N}\\ \vdots\\ \cos\frac{(2N-3)m\pi}{2N}\\ \cos\frac{(2N-1)m\pi}{2N}\end{bmatrix} \\
&\quad + \left[\lambda_m\left(w_m^{\pm} - \alpha_4\beta_m c_{pd}\theta_s\Pi_m^{\pm}\right) - \left(w_m^{\pm} + (1-\alpha_4)\,\beta_m c_{pd}\theta_s\Pi_m^{\pm}\right)\right]\begin{bmatrix}0\\ \sin\frac{m\pi}{N}\\ \vdots\\ \sin\frac{(N-1)m\pi}{N}\\ 0\end{bmatrix}.
\end{aligned}
\tag{3.71}
$$

Thus

$$(\lambda_m - 1)\,\Pi_m^{\pm} + [\alpha_2\lambda_m + (1-\alpha_2)]\,\beta_m\frac{c_s^2}{c_{pd}\theta_s}w_m^{\pm} = 0, \tag{3.72}$$

$$-[\alpha_4\lambda_m + (1-\alpha_4)]\,\beta_m c_{pd}\theta_s\Pi_m^{\pm} + (\lambda_m - 1)\,w_m^{\pm} = 0. \tag{3.73}$$

For (3.72) - (3.73) to have non-trivial solutions for $\Pi_m^{\pm}$ and $w_m^{\pm}$ requires the determinant to be zero, i.e.

$$(\lambda_m - 1)^2 = -[\alpha_2\lambda_m + (1-\alpha_2)]\,[\alpha_4\lambda_m + (1-\alpha_4)]\,\beta_m^2 c_s^2. \tag{3.74}$$

Solving (3.74) for λ_m with general values of α_2 and α_4 is a job for the computer. However if $\alpha_2 = \alpha_4 = \alpha$ (traditionally this has been so with α set to unity) then (3.74) has solutions

$$\lambda_m = \frac{1 \pm i\,(1-\alpha)\,\beta_m c_s}{1 \mp i\alpha\beta_m c_s} = \frac{1 - \alpha\,(1-\alpha)\,\beta_m^2 c_s^2 \pm i\beta_m c_s}{1 + \alpha^2\beta_m^2 c_s^2}. \tag{3.75}$$

Thus

$$|\lambda_m|^2 = \frac{1 + (1-\alpha)^2\,\beta_m^2 c_s^2}{1 + \alpha^2\beta_m^2 c_s^2}, \tag{3.76}$$

and the scheme will be stable (i.e. $|\lambda_m|^2 \leq 1$) provided $\alpha \geq 1/2$, with neutral stability ($|\lambda_m| = 1$) obtaining when $\alpha = 1/2$.

Setting $\lambda_m \equiv \exp(i\omega\Delta t) \equiv \exp[i\,(\omega_R + i\omega_I)\,\Delta t] = \exp(-\omega_I\Delta t)\exp(i\omega_R\Delta t)$ in (3.75) and using (3.69) and (3.76) yields

$$\tan(\omega_R\Delta t) = \pm\frac{\beta_m c_s}{1 - \alpha\,(1-\alpha)\,\beta_m^2 c_s^2} = \pm\frac{\left(\sin\frac{m\pi}{2N}\right)c_s\Delta t}{1 - \alpha\,(1-\alpha)\left(\sin\frac{m\pi}{2N}\right)^2 c_s^2\Delta t^2}, \tag{3.77}$$

$$|\lambda_m|^2 = \exp\left(-2\omega_I \Delta t\right) = \frac{1 + \left(1-\alpha\right)^2 \beta_m^2 c_s^2}{1 + \alpha^2 \beta_m^2 c_s^2}. \tag{3.78}$$

Dividing (3.77) by Δt and taking the limits $\Delta t \to 0$ and $\Delta z \to 0$ in both the resulting equation and in (3.78) then gives

$$\lim_{\Delta t, \Delta z \to 0} \omega_R \;\; \to \;\; \frac{m \pi c_s}{z_T}, \tag{3.79}$$

$$\lim_{\Delta t, \Delta z \to 0} \omega_I \;\; \to \;\; 0, \tag{3.80}$$

and so

$$\lim_{\Delta t, \Delta z \to 0} \omega \equiv \lim_{\Delta t, \Delta z \to 0} \left(\omega_R + i\omega_I\right) \to \frac{m \pi c_s}{z_T}, \tag{3.81}$$

i.e. ω converges to the exact result - cf. (3.28) - (3.29).

Substituting (3.75) into (3.72) or (3.73) yields the relationship (when $\alpha_2 = \alpha_4 = \alpha$) between the coefficients:

$$\Pi_m^{\pm} = \pm i \frac{c_s}{c_{pd} \theta_s} w_m^{\pm}. \tag{3.82}$$

Thus far $2N-1$ independent eigenmodes have been identified. Since A and B are square matrices of dimension $2N+1$, two further modes are expected.

These are both in the null space of B, i.e. they both have $\lambda = 0$ as their eigenvalue. For the special case $\alpha_2 = \alpha_4 = \alpha = 1$, they both have $\underline{\Pi} = 0$ and they both satisfy $I_0 \underline{w} = 0$: thus their eigenstructures are $\left[(0,0,...,0,0),(1,0,0,...,0,0)\right]^T$ and $\left[(0,0,...,0,0),(0,0,...,0,0,1)\right]^T$. More generally, their eigenstructures can be obtained by arbitrarily setting $\Pi|_{z_0} = 1$ and $w|_{z_0} = \pm 1$ and solving $B\left[\Pi, w\right]^T = 0$. These modes are associated with the boundary conditions $w = 0$ at $z = 0, z_T$, and are a consequence of having explicitly included these in the definition of the eigen problem, even though they could have been decoupled from it (this would then have reduced the dimension of the A and B matrices from $2N+1$ to $2N-1$ and led to the $2N-1$ eigenmodes defined by (3.66)).

4 Numerical solution of the column-equations model with constant θ_s, Π_s, and ρ_s

The generalised eigenvalue problem obtained for the simplified column model with constant basic state variables θ_s, Π_s and ρ_s, derived in Section 3.4 has been solved numerically. The problem is defined by

$$B \begin{bmatrix} \underline{\Pi} \\ \underline{w} \end{bmatrix} = \lambda A \begin{bmatrix} \underline{\Pi} \\ \underline{w} \end{bmatrix}, \tag{4.1}$$

where A and B are defined as in (3.59) and (3.60).

The eigenvalues and the associated normal modes have been computed using the *Fortran*77 *NAG* (Numerical Algorithm Group) library routine $F02BJF$, called by a *Fortran*90 code.

The matrices have dimension $(2N+1)$ times $(2N+1)$, where N is the model level associated with the top boundary, and the arrays have $2N+1$ components: the first N correspond to the Exner pressure function, Π, which is evaluated at half-integer model levels, the remaining $N+1$ correspond to the vertical velocity, w, which is evaluated at integer model levels, including the top and bottom boundaries.

Since the matrices A and B defining the problem are real, the eigenvalues (and their associated normal modes) are either real or complex conjugate pairs.

Specifically, three of the eigenvalues are real: two of them are zeros (i.e. they lie in the null space of matrix B), and are associated with the boundary conditions ($w = 0$ at the top and bottom of the domain); the third is non-zero and the normal mode associated with it yields $\underline{w} = \underline{0}$ (i.e. a trivial solution of the system for the vertical velocity) and $\underline{\Pi} = constant$, which corresponds to the external mode (i.e. the one with the greatest equivalent depth) for the Exner pressure function.

The remaining $2N-2$ normal modes are complex conjugate pairs, from which $N-1$ real modes, one for each of the internal model levels, are derived, as is explained later.

Thus, alongside the two boundary condition modes, N non-trivial normal modes are determined for the Exner pressure function, consistent with the fact that it is evaluated at half-integer model levels, so that $\underline{\Pi}$ has N components; whereas $N-1$ non-trivial normal modes associated with interior model levels are determined for the vertical velocity, which is evaluated at integer model levels, so that $\underline{w}$ has $N-1$ components corresponding to interior model levels (the remaining two are associated with the boundary conditions).

In the simple case of a constant basic state the analytic solution of the linearised continuous equation set (3.3) - (3.6) underlying the eigenvalue problem is given by (3.28) - (3.29)), and it can be rewritten as the real part of a more general solution, i.e:

$$w = \sum_{m=1}^{\infty} \Re \left[\sin\left(\frac{m\pi z}{z_T}\right) \left(w_m^0 - i\frac{c_{pd}\theta_s}{c_s}\Pi_m^0 \right) \exp\left(i\frac{m\pi c_s t}{z_T} \right) \right], \tag{4.2}$$

$$\Pi = \sum_{m=1}^{\infty} \Re \left[\cos\left(\frac{m\pi z}{z_T}\right) \left(\Pi_m^0 + i\frac{c_s}{c_{pd}\theta_s}w_m^0 \right) \exp\left(i\frac{m\pi c_s t}{z_T} \right) \right], \tag{4.3}$$

where $\Re$ denotes the real part. The complex normal modes obtained by solving the eigenvalue problem represent the more general numerical discrete solution approximating the expression in brackets in (4.2) and (4.3).

Further, in the case of constant basic state variables θ_s, Π_s, and ρ_s, and for a uniform grid, the analytic expression for the normal modes of the discrete problem (3.58) is given by (3.66), with coefficients related via (3.82)).

Comparing (3.82) and (4.2) - (4.3), where:

$$w_m^{\pm} = w_m^0 - i\frac{c_{pd}\theta_s}{c_s}\Pi_m^0, \tag{4.4}$$

$$\Pi_m^{\pm} = \Pi_m^0 + i\frac{c_s}{c_{pd}\theta_s}w_m^0, \tag{4.5}$$

shows that the definition of the analytic discrete normal modes coincides with that of the $z-$dependent part of the complex definition of the analytic continuous ones (i.e. (4.2) - (4.3), omitting $\Re$) evaluated at integer and half-integer (for $\underline{w}$ and $\underline{\Pi}$ respectively) model levels.

As to the numerical normal modes, the $N-1$ complex conjugate pairs are found to have purely real $\underline{w}-$components and purely imaginary $\underline{\Pi}-$components. This is consistent with the analytic discrete definition (3.66) with $w^{\pm}$ real and $\Pi^{\pm}$ defined by (3.82) and therefore purely imaginary, which is obtained for $\Pi_m^0 = 0$ or purely imaginary.

For the purposes of our analysis, in which the $\underline{w}-$ and the $\underline{\Pi}-$components are considered separately, each pair of complex conjugate modes yields a single normal mode, since the $\underline{w}-$components are the same, and the $\underline{\Pi}-$components differs only in sign (thus they represent the same normal mode to within a multiplicative constant).

For the parameters appearing in the problem the following values have been used: $\theta_s = 270\,\mathrm{K}$, $\Pi_s = 1$, $\rho_s = 1.2\,\mathrm{kg\,m^{-3}}$, $\alpha_2 = \alpha_4 = 0.6$, $\Delta t = 600\,\mathrm{s}$, $z_0 = 0$, $z_T = 10000\,\mathrm{m}$ and N has been set to either 4 or 5, yielding $\Delta z = 2500\,\mathrm{m}$ and $\Delta z = 2000\,\mathrm{m}$ respectively in the case of a uniform grid.

It is found that the numerical normal modes other than those associated with the boundary conditions (i.e. those associated with the interior model levels) agree well with the corresponding analytic ones (both continuous and discrete), after normalising them.

In the case of a uniform grid the analytic expression for the discrete eigenvalues is given by (3.75)), where β_m is defined by (3.69).

It is verified that the eigenvalues computed numerically, for $N = 4$, $N = 5$, and $N = 19$, agree with their analytic definition (3.75): the maximum absolute error is $O\left(10^{-11}\right)$.

As an example of the numerical results, the $\underline{\Pi}$ (purely imaginary) and $\underline{w}$ (purely real) components of the normal modes associated with the interior model levels obtained for $N = 4$ are plotted separately (although the normal modes of the problem are the vectors composed of both the $\underline{\Pi}-$ and $\underline{w}-$ components) in frames (a) - (d) of Figs. 1 and 2.

As to the normal modes associated with the boundary conditions, they lie in the null space of the matrix B, so they can also be obtained by solving directly the system

$$B \begin{bmatrix} \underline{\Pi} \\ \underline{w} \end{bmatrix} = 0. \tag{4.6}$$

In the latter case, since the matrix B has two zero rows (which account for the null space having dimension two), there are: one undetermined component for each of the modes and a normalisation constant (since normal modes are only defined to within an arbitrary multiplicative constant). Provided these are set so that the first component of each of the normal modes is the same as that of the normal modes associated with the two zero eigenvalues computed by the NAG routine, the same normal modes are found - this is used to verify the correctness of the results. The boundary condition modes for the case $N = 4$ are plotted in Figs. 1 and 2 (e) and (f).

The boundary condition $\underline{\Pi}-$modes shown in Fig. 1 (e) and (f) appear to be very close to each other (apart from a scaling factor): they are (numerically) almost linearly dependent, and therefore unsuitable for spanning the null space of the matrix B. However it is worth remembering that the normal modes of B are given by the vector $\begin{bmatrix} \underline{\Pi} & \underline{w} \end{bmatrix}^T$, and not by its $\underline{\Pi}-$ and $\underline{w}-$ components separately. For this reason the complete $\begin{bmatrix} \underline{\Pi} & \underline{w} \end{bmatrix}^T$ boundary condition modes have been considered and plotted in Fig. 3, which reveals that they are indeed very close to each other. More distinct boundary condition modes can be obtained by choosing different normalisation constants when solving the system (4.6).

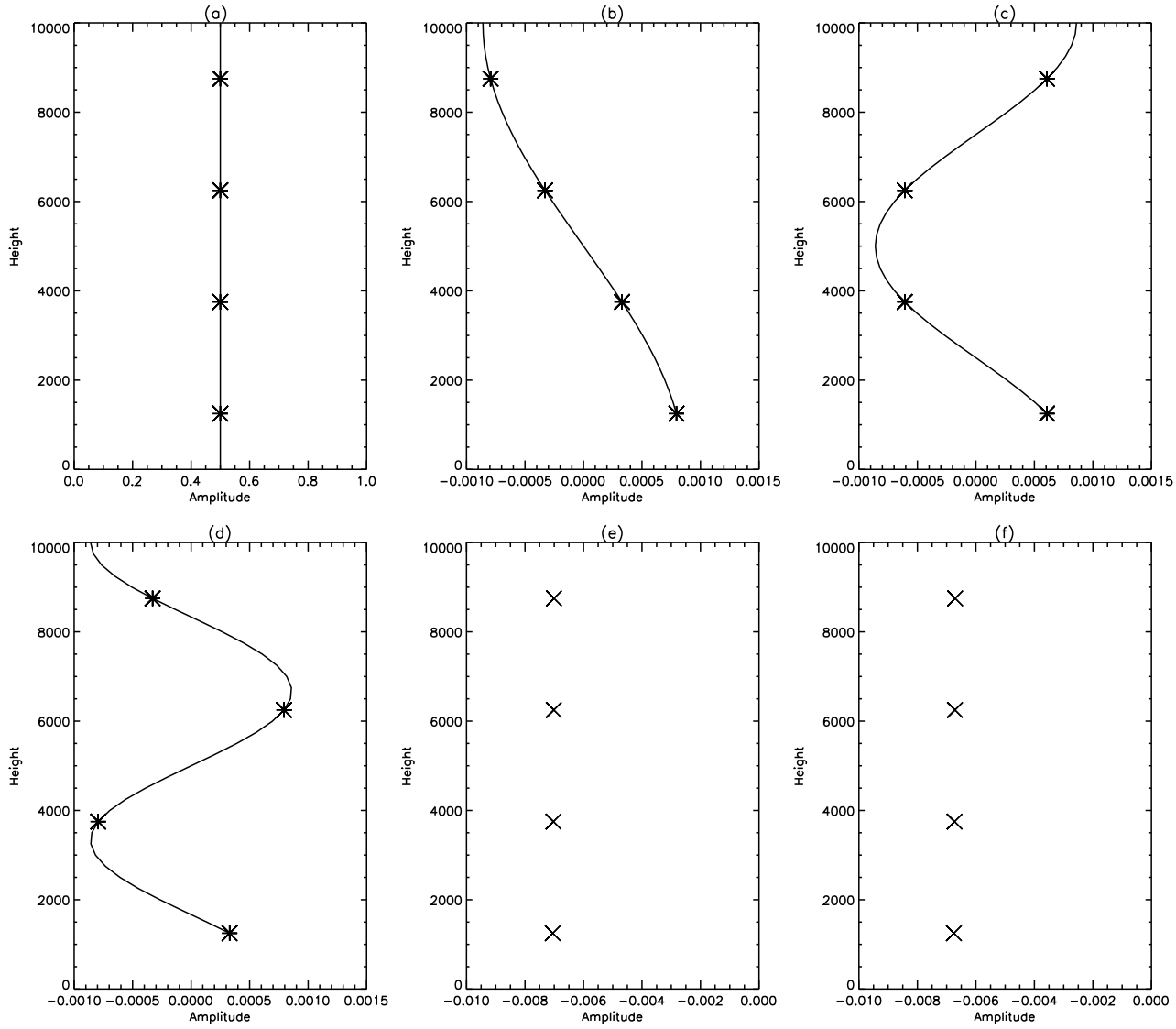

Figure 1: $\underline{\Pi}-$modes obtained with a uniform grid and $N = 4$ plotted against height. In frames (a) - (d) the analytic continuous (solid line), analytic discrete (asterisks), and numerical (crosses) modes associated with the interior model levels are shown. The numerical normal modes associated with the boundary conditions are plotted in frames (e) and (f).

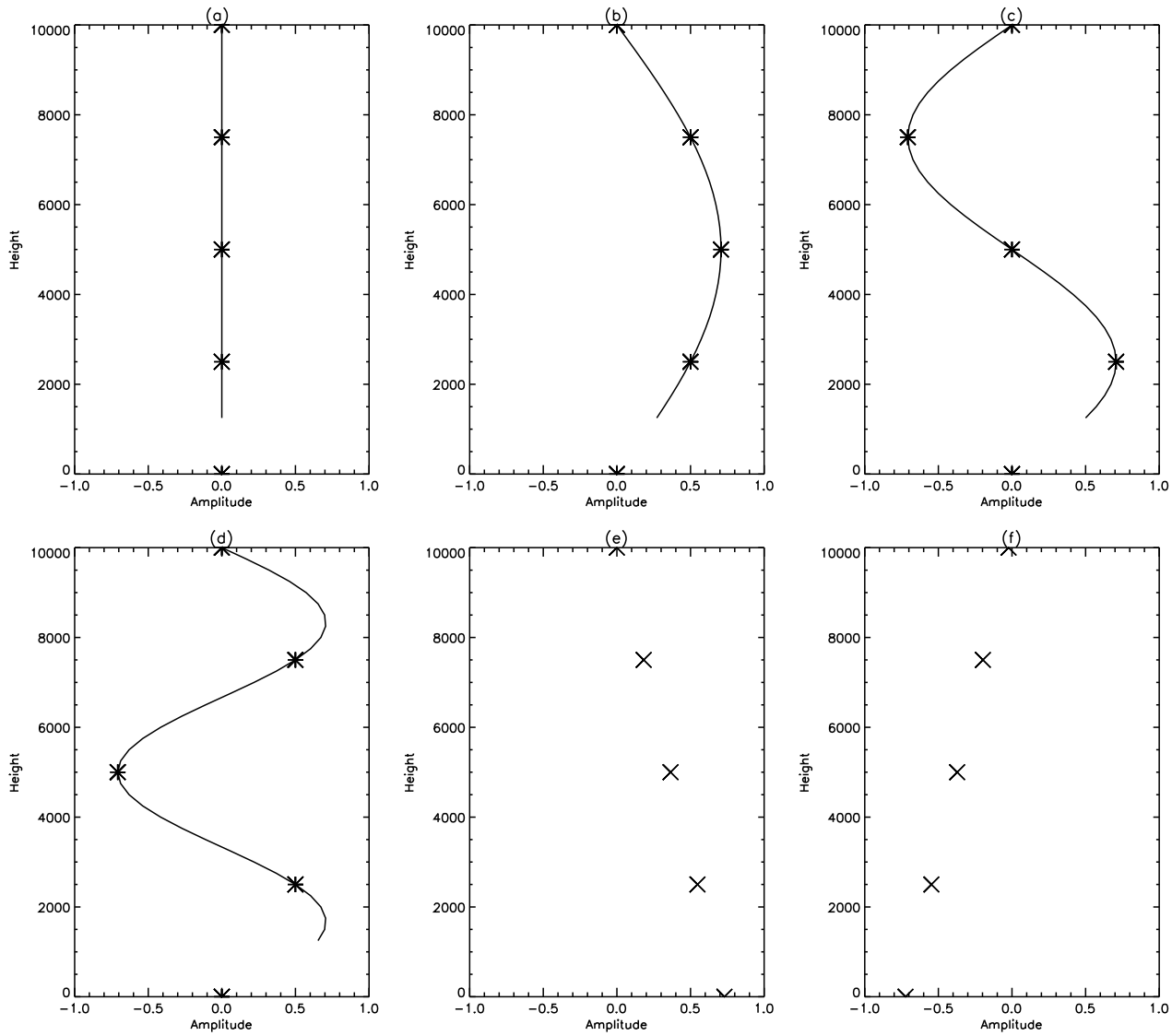

Figure 2: Same as in Fig. 1, but for the $\underline{w}-$modes.

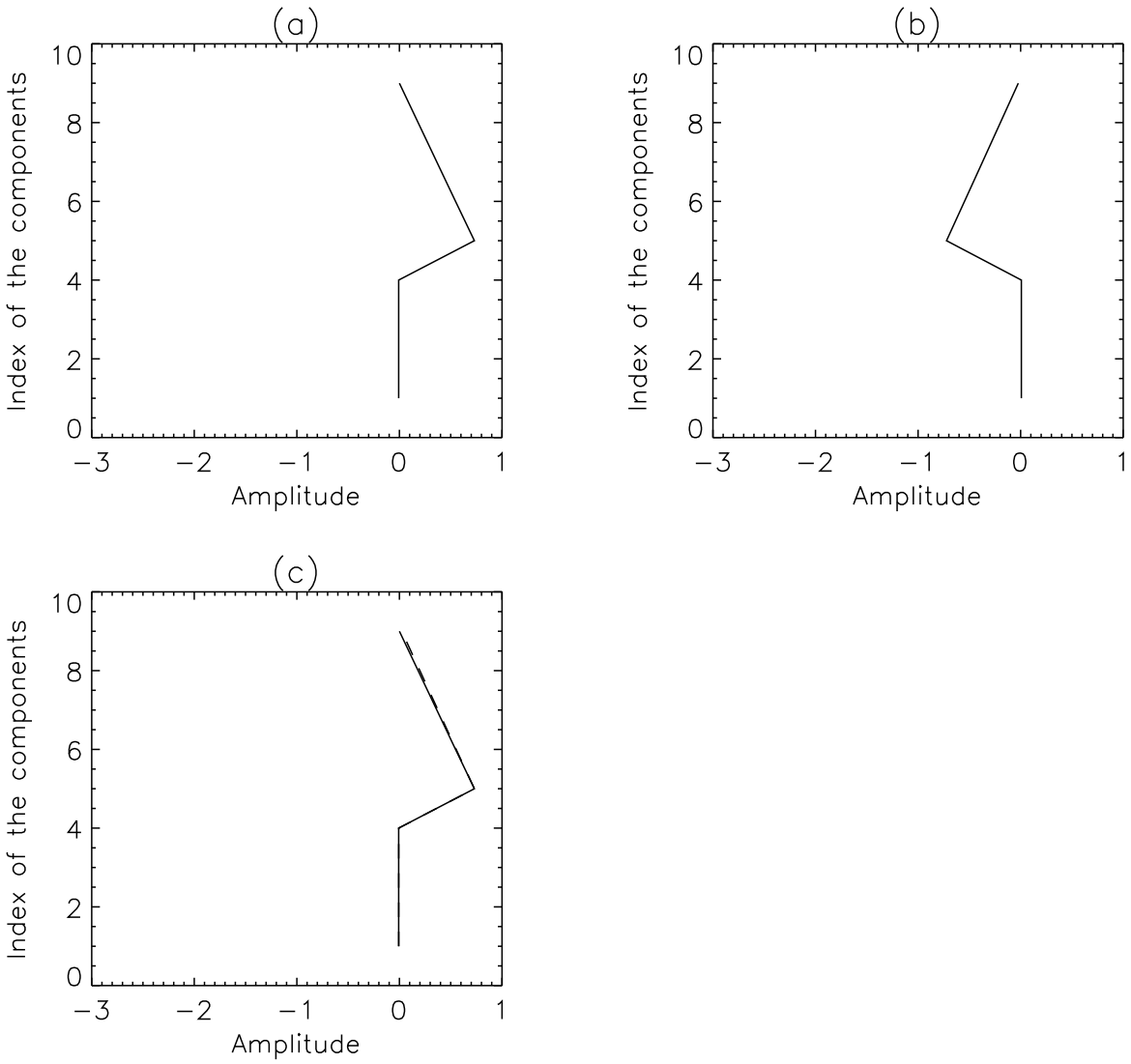

Figure 3: Complete $\left[\begin{array}{cc} \underline{\Pi} & \underline{w} \end{array} \right]^T$ boundary condition modes for the unscaled problem.

A possible choice is: let Π_1 be arbitrary; set $w_1 = c_1 \cdot \Pi_1$ for the first normal mode, $w_1 = c_2 \cdot \Pi_1$ for the second one; use the $2N-1$ non-trivial equations of the system to write the remaining components of each of the normal modes in terms of Π_1 and w_1; determine c_1 and c_2 so that the scalar product of the two normal modes is zero (i.e. the two modes are orthogonal); and finally determine Π_1 so that the modes are unitary (for consistency with the normal modes associated with the interior model levels).

However, since this procedure can be applied to the boundary modes computed via (4.6) only, whereas the normalisation of those computed by the *NAG* routine is built into the routine itself and cannot be changed, a better solution to the problem is to re-scale the entries of the matrices A and B, in order to make them more balanced.

The scaling has been introduced through the variable $\underline{\tilde{\Pi}} = S\underline{\Pi}$, in terms of which the eigenvalue problem (4.1) is rewritten as

$$\tilde{B} \begin{bmatrix} \underline{\tilde{\Pi}} \\ \underline{w} \end{bmatrix} = \lambda \tilde{A} \begin{bmatrix} \underline{\tilde{\Pi}} \\ \underline{w} \end{bmatrix}, \tag{4.7}$$

where

$$\tilde{A} = \begin{bmatrix} I & \alpha_2 \Delta t \left(\frac{\kappa_d}{1-\kappa_d}\right) \Pi_s S D \\ \alpha_4 \Delta t c_{pd} \theta_s \frac{E}{S} & I_0 \end{bmatrix}, \tag{4.8}$$

$$\tilde{B} = \begin{bmatrix} I & -(1-\alpha_2)\, \Delta t \left(\frac{\kappa_d}{1-\kappa_d}\right) \Pi_s S D \\ -(1-\alpha_4)\, \Delta t c_{pd} \theta_s \frac{E}{S} & I_0 \end{bmatrix}, \tag{4.9}$$

and D and E are defined as in (3.63) and (3.64).

Three different scaling factors (as explained below) have been tested, and the resulting boundary conditions modes are plotted in the following figures, for the case $N = 4$.

First a scaling factor $S = O(10^3)$ is chosen, by setting $S = c_{pd} = 1003.67\,\mathrm{J\,kg^{-1}\,K}$: this aims at generally balancing all the entries of the matrices, by multiplying by 10^3 those depending on D (of order 10^{-2}) and by 10^{-3} those depending on E (of order 10^4), so that all the entries of the rescaled matrix are of order one (I and I_0) or ten. The resulting boundary condition modes are shown in Fig. 4.

A different solution is that of balancing the terms appearing in the $\underline{\tilde{\Pi}}-$equations (i.e. the upper block) of the matrices, by multiplying those depending on D by a scaling factor $S = O(10^2)$, to make them order one. This is achieved by setting $S = \kappa_d \cdot \theta_s / (1-\kappa_d) = 108.15$ K, which however makes the terms depending on E order 10^2, so that the $\underline{w}-$equations (i.e. the

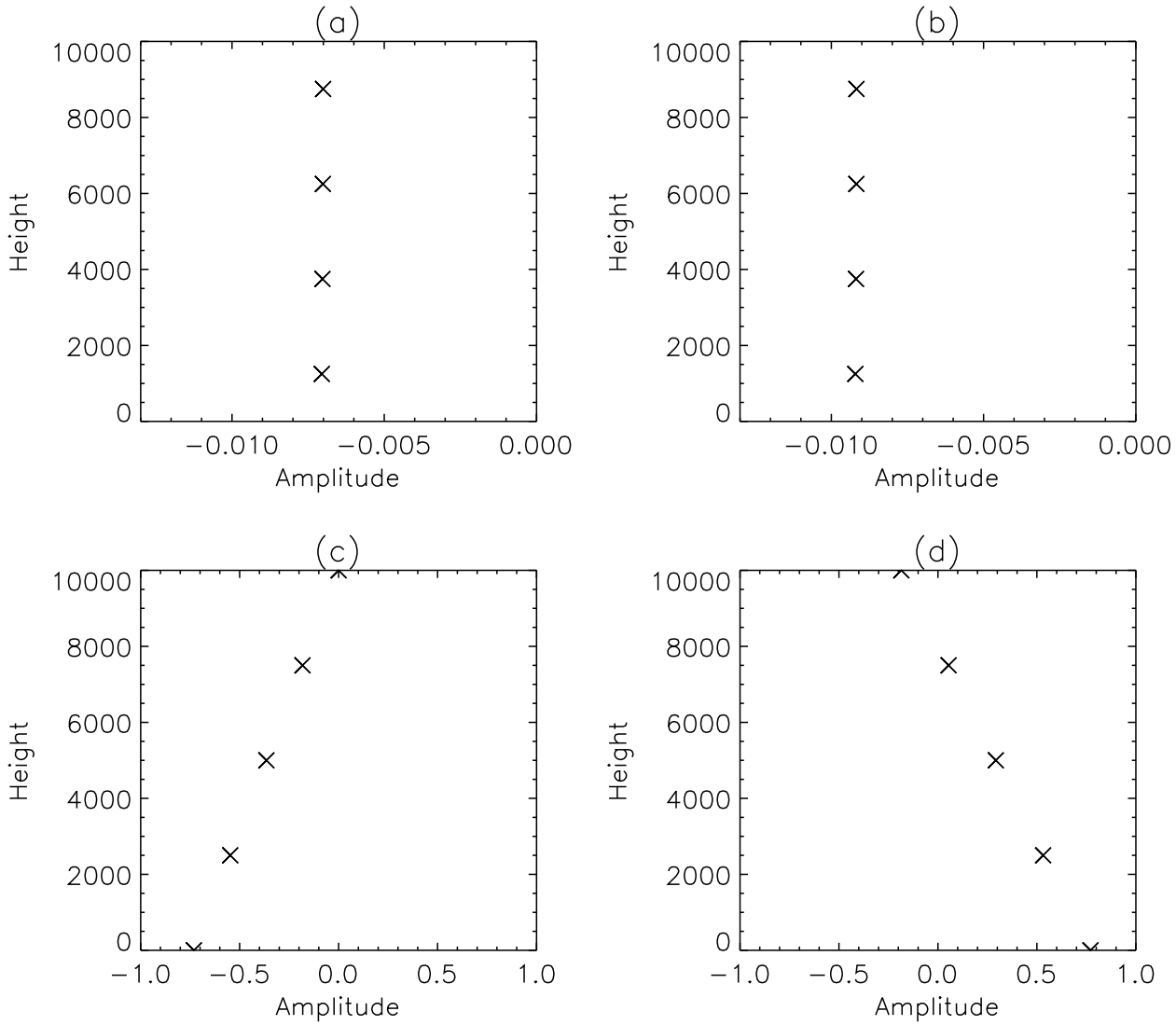

Figure 4: Boundary condition modes for the eigenvalue problem with $N = 4$, after scaling by $S = c_{pd}$, plotted against height. The $\underline{\Pi}-$modes are shown in (a) and (b) ; the $\underline{w}-$modes in (c) and (d).

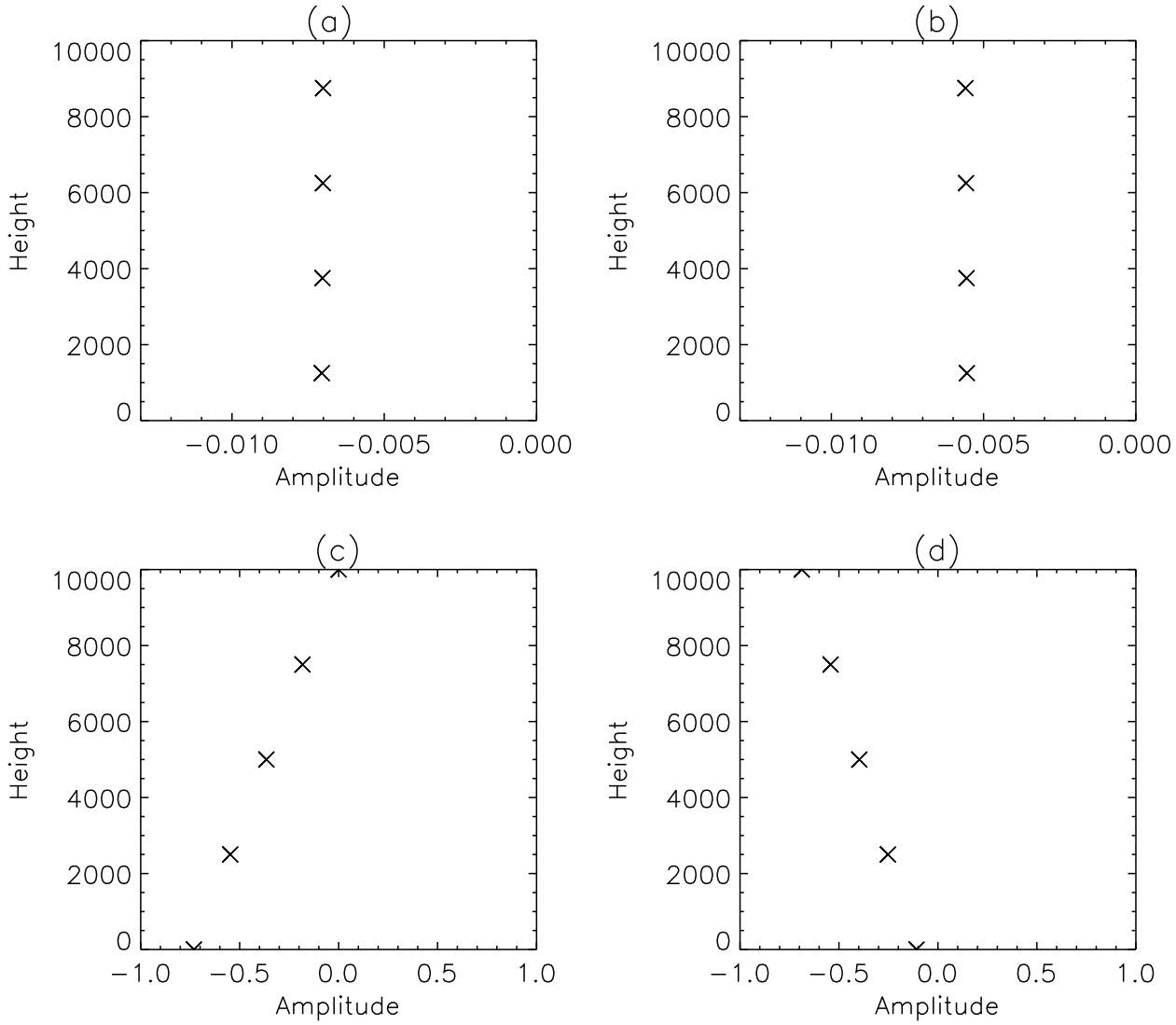

Figure 5: Same as in Fig. 4, but for a scaling factor $S = \kappa_d \cdot \theta_s / (1 - \kappa_d)$.

lower block of the matrices) become less balanced. The corresponding boundary condition modes are plotted in Fig. 5.

Alternatively the terms appearing in the $\underline{w}$−equations of the matrices can be balanced, by choosing a scaling factor $S = O(10^4)$, such as $S = c_{pd} \cdot (\Delta z / \Delta t) \cdot (1 - \kappa_d)/\kappa_d = 1.044 \times 10^4\,\mathrm{m^3\,s^{-3}\,K^{-1}}$. The resulting boundary condition modes are plotted in Fig. 6.

The boundary condition modes plotted in Figs. 4 - 6 are obtained by: first solving the eigenvalue problem (4.7), which yields the normal modes $\left[\begin{array}{cc} \underline{\tilde{\Pi}} & \underline{w} \end{array} \right]^T$; rescaling $\underline{\tilde{\Pi}}$ to retrieve $\underline{\Pi} = S^{-1}\tilde{\Pi}$; and normalise the resulting $\left[\begin{array}{cc} \underline{\Pi} & \underline{w} \end{array} \right]^T$ normal modes to make them unitary (for consistency with the results produced by the NAG routine and plotted in previous plots).

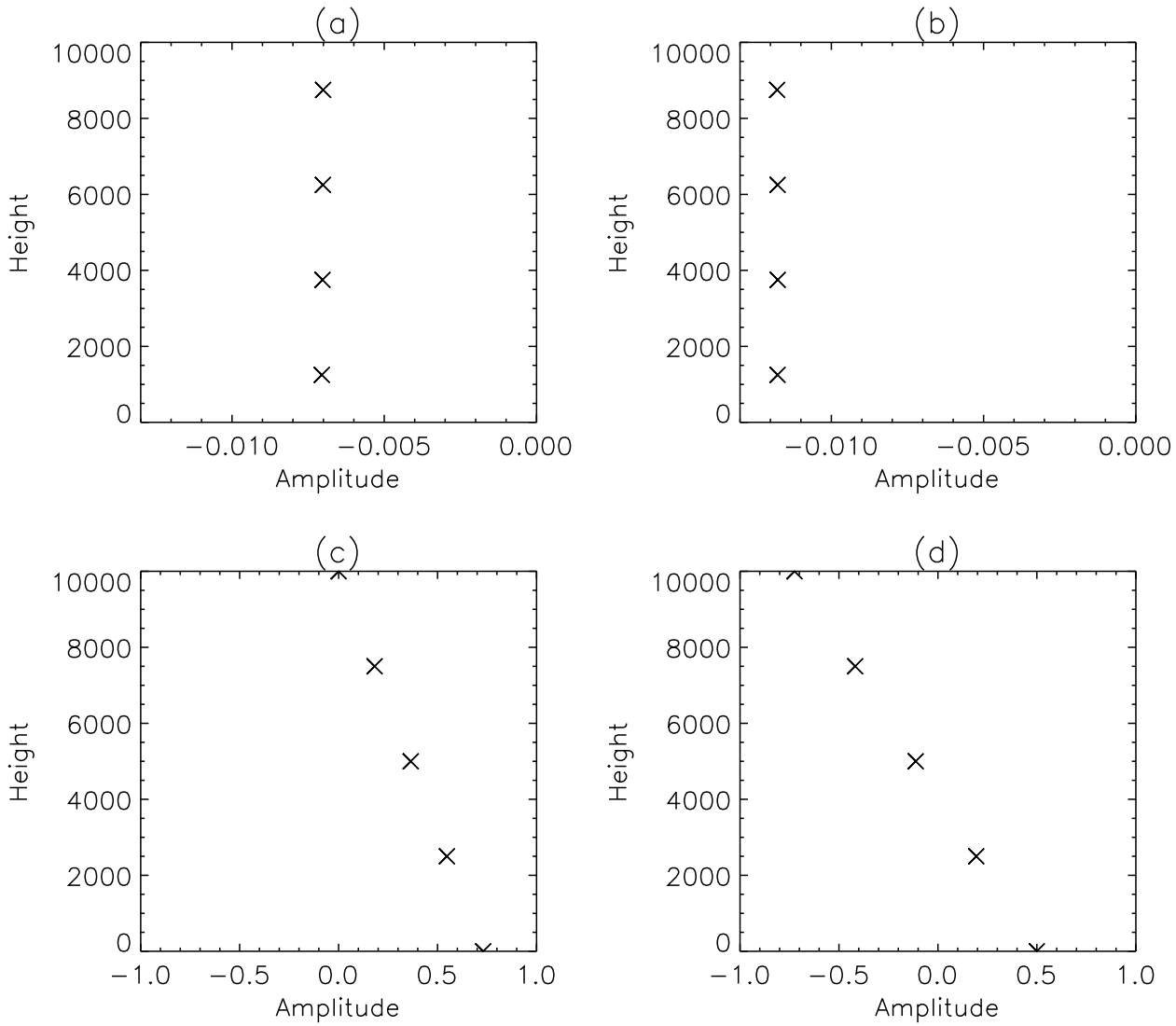

Figure 6: Same as in Figs. 4 and 5, but for a scaling factor $S = c_{pd} \cdot (\Delta z/\Delta t) \cdot (1 - \kappa_d)\,/\kappa_d$.

The same procedure is also applied to the normal modes associated with the interior model levels, and it is checked that they are indeed the same as those computed without rescaling the matrices and plotted in Figs. 1 and 2.

Also, in order to compare more clearly how close or distinct the boundary condition modes are, the complete $\left[\begin{array}{cc} \underline{\Pi} & \underline{w} \end{array} \right]^T$ boundary condition modes whose $\underline{\Pi}-$ and $\underline{w}-$ components are shown separately in Figs. 4 - 6 are plotted against the index of the components in frames (a) and (b) of Figs. 7 - 9. The same boundary condition modes obtained for the original (unscaled) problem (4.1) in the case $N = 4$ have been plotted before in Fig. 3. In order to make the comparison easier, in frame (c) of the same figures the second of the boundary condition modes is renormalised so that the first of its $\underline{w}-$components coincides with that of the first one.

As the figures show, the most effective scaling of the problem seems to be the second one, with a scaling factor of order $S = O(10^2)$. This may indicate that in order to get more distinct boundary condition modes it is important to balance the terms in the equations in the upper part of the matrices (the $\underline{\Pi}-$equations). A possible explanation for this, is that, although there are $N + 1$ $\underline{w}-$equations, two of them are trivial, so that the N $\underline{\Pi}-$equations in the upper part of the matrices have a larger impact on the solution.

Also it is found that the above results are sensitive to (even small) variations in the scaling factor. In fact, before scaling the problem by the physical parameters as described above, the scaling factor was set to $S = 10^3$, 10^2, and 10^4 respectively and the resulting normal modes differ from those obtained above for the physical parameters of the corresponding order of magnitude, although similar conclusions can be drawn: the scaling of order 10^2 appears to be the most effective, that of order 10^3 the least effective. It is also interesting to note that the scaling $S = O(10^2)$ appears to be the most robust: the results obtained with $S = O(10^2)$ are indeed very similar to those with $S = \kappa_d \cdot \theta_s / (1 - \kappa_d) = 108.15\,\mathrm{K}$.

Finally, comparing Figs. 7 - 9 shows that the $\left[\begin{array}{cc} \underline{\Pi} & \underline{w} \end{array} \right]^T$ boundary condition modes obtained for the scaled problem (4.7) with any of the scaling examined in this study are more distinct than those obtained for the original problem (4.1).

The discussion and numerical results for the boundary condition modes reported above demonstrate that it is possible to correctly represent the null space of the matrix B with which these modes are associated. This is important since one of the aims of the analysis is

to examine the response of the model to different boundary conditions (otherwise they could have simply been removed from the problem by eliminating algebraically the corresponding equations from the system).

However, once this issue has been clarified, it is important to extend the analysis to the case of nonuniform grids, in which case the analytic discrete normal modes are not known, although the analytic continuous solution defined by (3.28) - (3.29) still holds.

Quadratic and fully quadratic stretched grids have been considered and their definition is given below. They are chosen because they are among the options used in the Unified Model (cf. UMDP15).

For the quadratic grid: the integer model levels are uniformly quadratically stretched, whilst the half-integer levels are placed half-way between them, so their vertical height is defined as:

$$\begin{aligned} z_k &= (k \cdot \Delta\eta)^2 \cdot z_N, \quad k = 0, ..., N \\ z_{k-1/2} &= \frac{z_k + z_{k-1}}{2}, \quad k = 1, ..., N \end{aligned} \tag{4.10}$$

where $\Delta\eta = 1/N$, z_k, $k = 0, ..., N$ denotes integer model levels (z_0 and z_N correspond to the bottom and top boundaries respectively); $k - 1/2$ for $k = 1, ...N$ denotes half-integer model levels and the height increments are computed varying the $\eta-$coordinate quadratically in order to mimic as closely as possible the full model which uses

$$\eta = \frac{z - z_0}{z_N - z_0} \tag{4.11}$$

as a vertical coordinate (cf. UMDP15).

For the fully quadratic grid: both integer and half-integer model levels are uniformly quadratically stretched, so their vertical height is defined as:

$$\begin{aligned} z_k &= (k \cdot \Delta\eta)^2 \cdot z_N, \quad k = 0, ..., N \\ z_{k-1/2} &= \left(\frac{2 \cdot k - 1}{2} \cdot \Delta\eta\right)^2 \cdot z_N, \quad k = 1, ..., N, \end{aligned} \tag{4.12}$$

and the notation is the same as in (4.10).

As an example of the numerical results, the $\underline{\Pi}-$ and $\underline{w}-$modes computed for the quadratic grid in the case $N = 4$ are shown in Figs. 10 and 11 respectively. Similar results (not shown) are obtained for $N = 5$, and for the fully quadratic grid with $N = 4$ or $N = 5$.

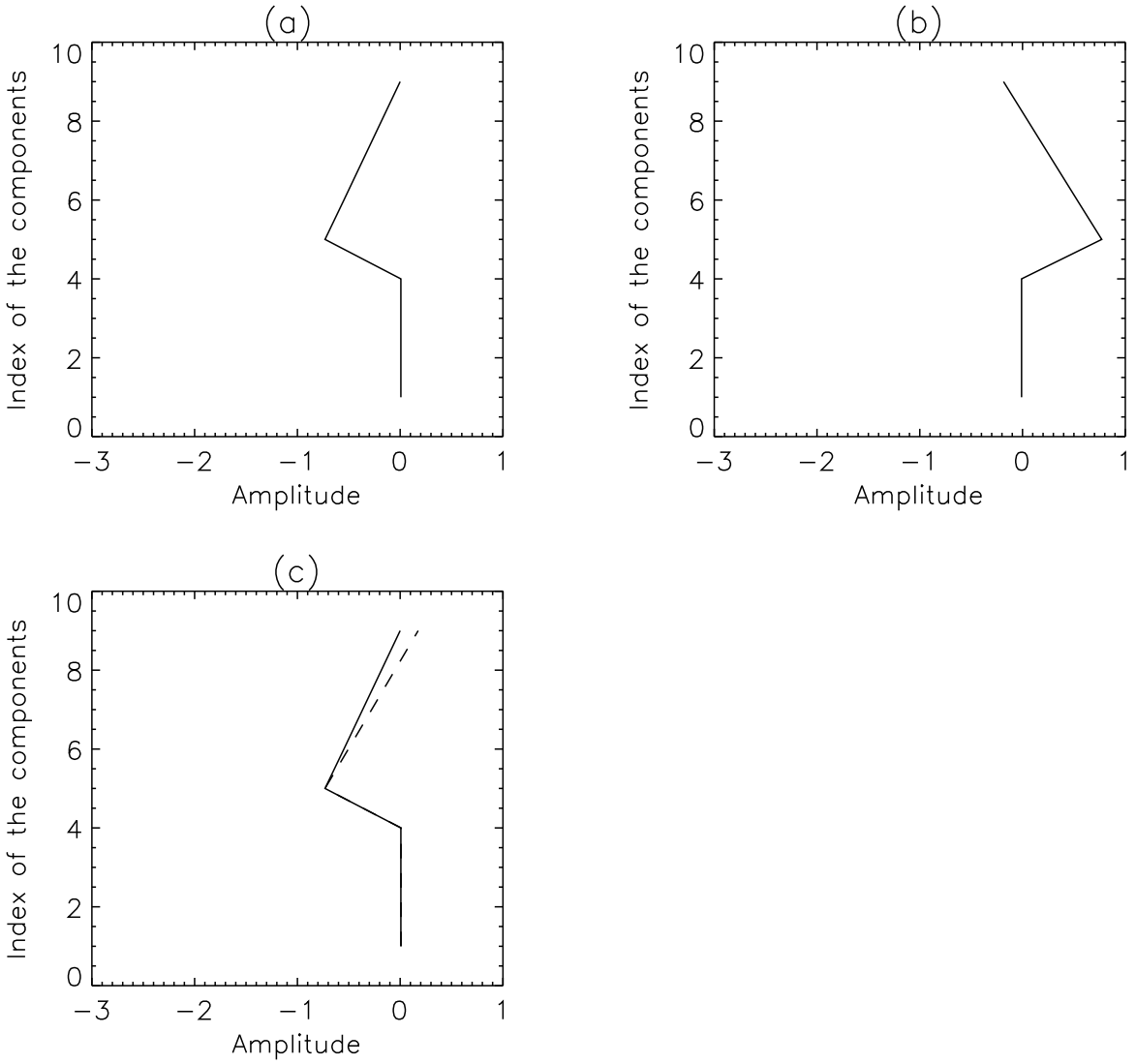

Figure 7: Complete $\left[\begin{array}{cc} \underline{\Pi} & \underline{w} \end{array} \right]$ boundary condition modes obtained for the problem rescaled by $S = c_{pd}$.

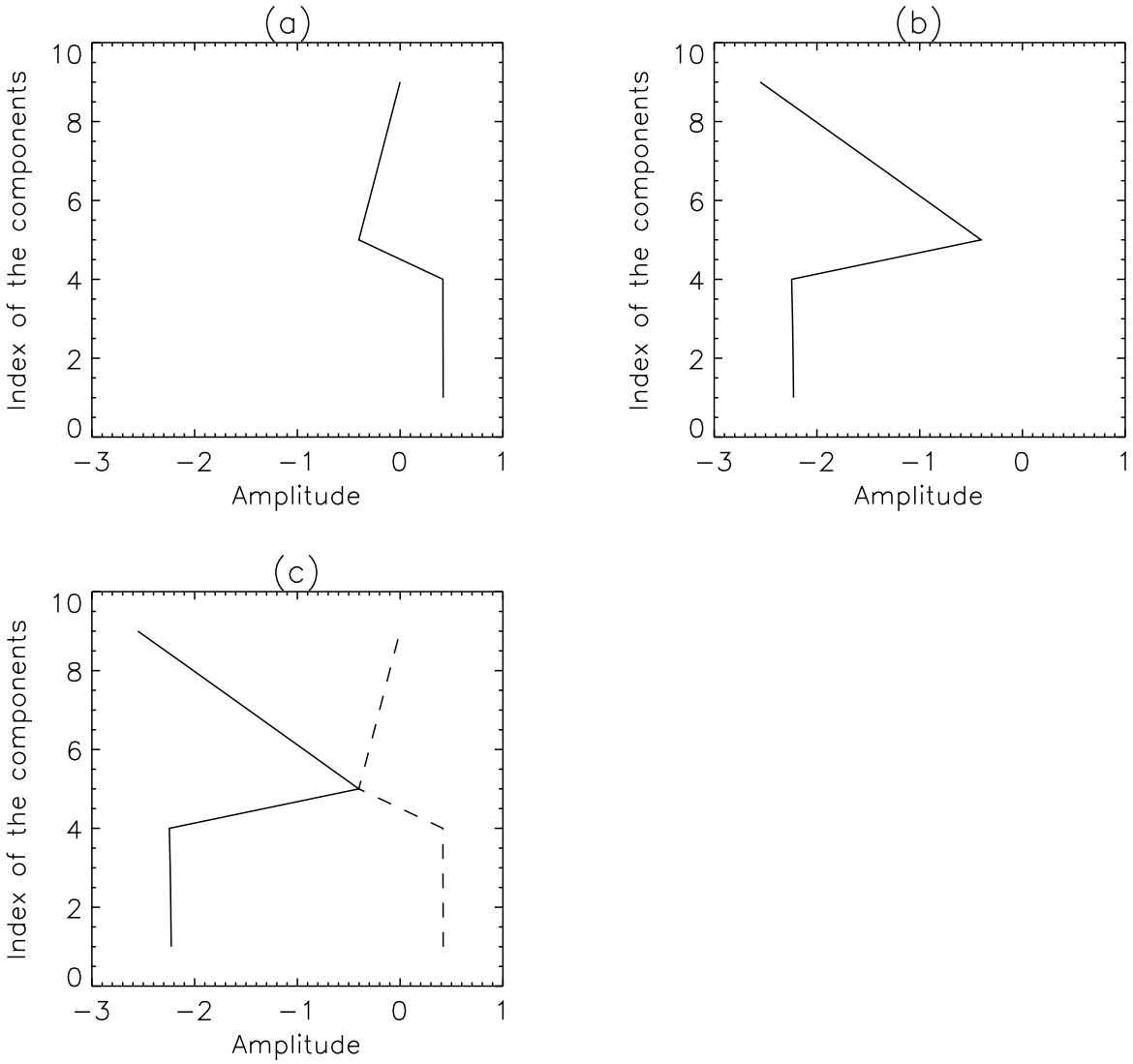

Figure 8: Same as in Fig. 7, but for $S = \kappa_d \cdot \theta_s / (1 - \kappa_d)$.

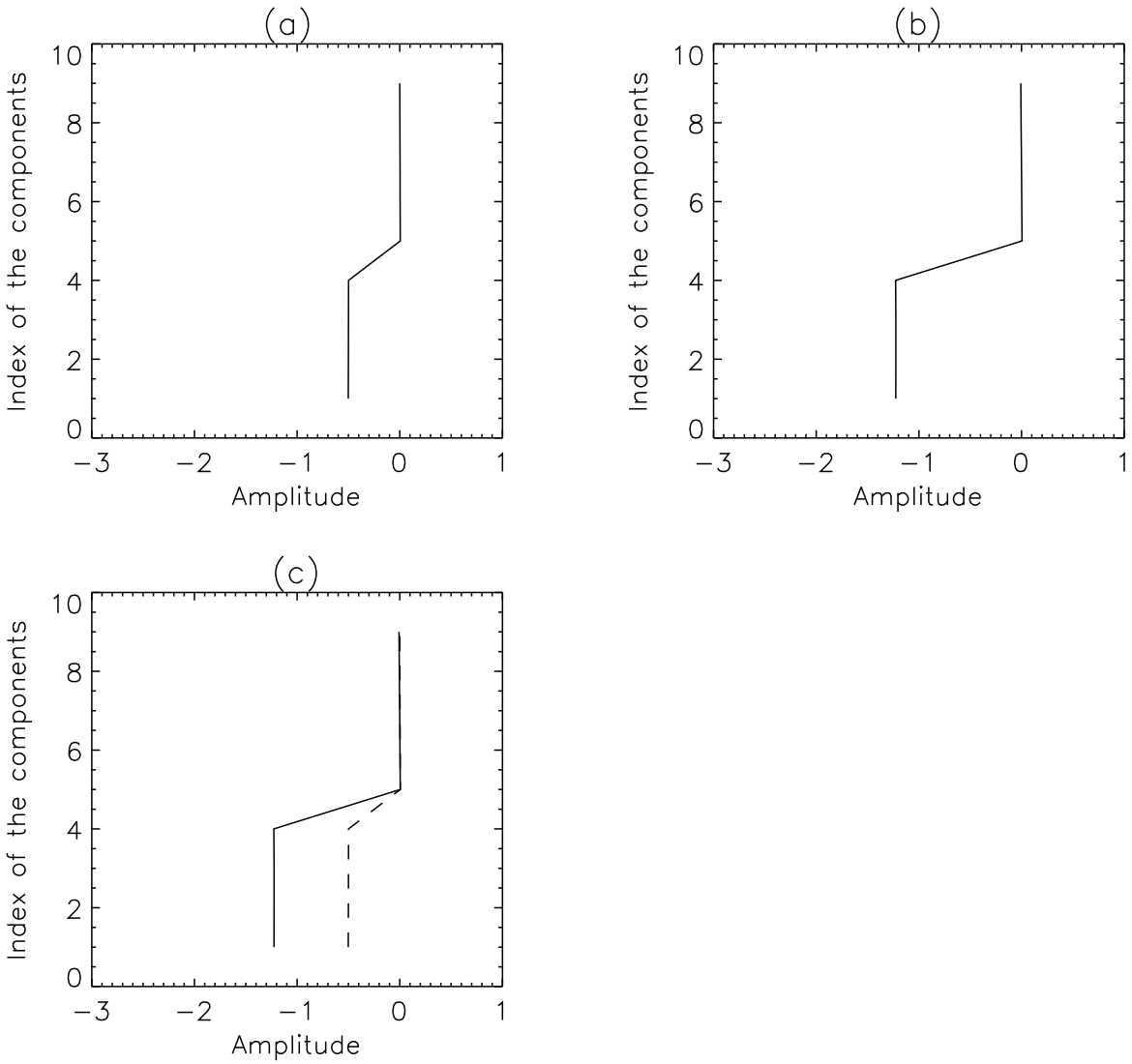

Figure 9: Same as in Figs. 7 and 8 but for $S = c_{pd} \cdot (\Delta z/\Delta t) \cdot (1 - \kappa_d)/\kappa_d$.

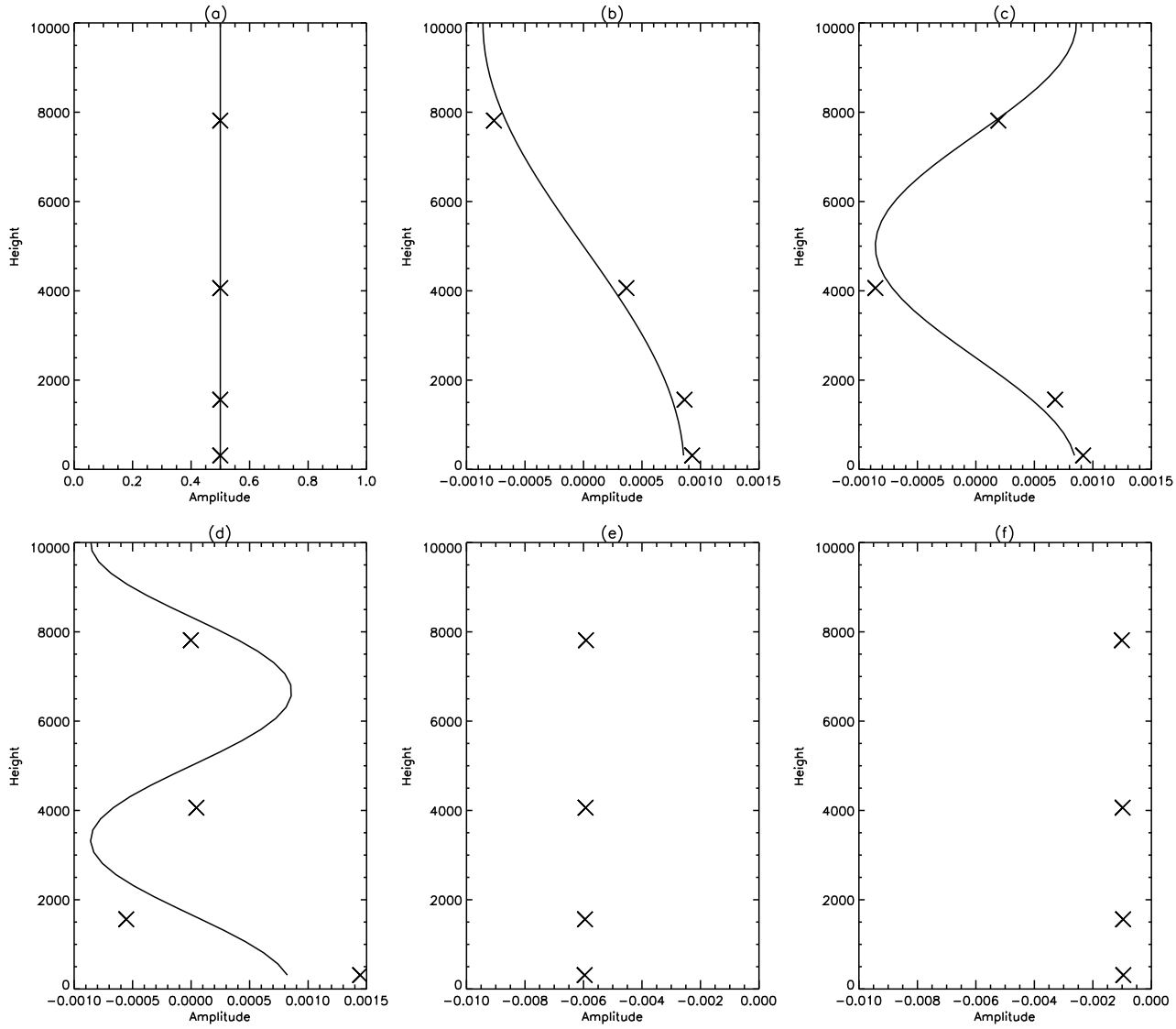

Figure 10: $\underline{\Pi}-$modes obtained with a quadratic grid and $N = 4$ plotted against height. In frames (a) - (d) the analytic continuous (solid line), and numerical (crosses) modes associated with the interior model levels are shown. The numerical modes associated with the boundary conditions are plotted in frames (e) and (f).

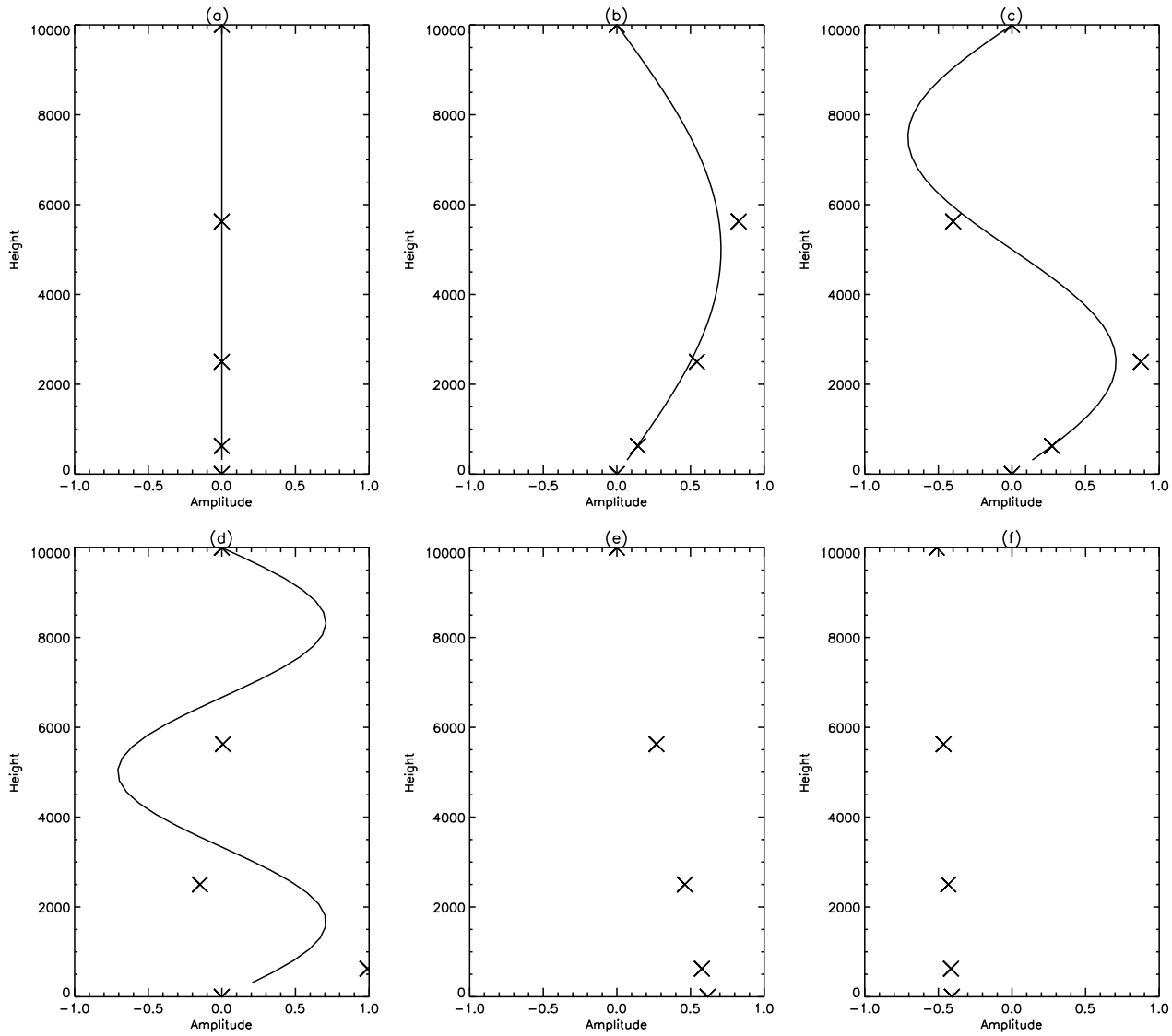

Figure 11: Same as in Fig. 10 but for the $\underline{w}-$modes.

As expected the results appear to be less accurate than those obtained with a uniform grid. The reason for this is that the order of accuracy of the discretisation is formally only first order for the stretched grids, as opposed to the second order accuracy of the uniform one. For low index normal modes (frames (a)-(c)) the results appear to be still close to the continuous curve depicting the analytical modes, although no longer on it, whereas for higher index ones, they appear to be less accurate, because the resolution is not high enough to resolve them well.

It is worth noting that in general the results shown in Figs. 10 and 11 do not appear to be more accurate at lower model levels, as would be expected, since lower levels correspond to higher resolution (Δz is smaller), and therefore greater accuracy. A possible explanation for this is thought to be the poor resolution given by either $N = 4$ or $N = 5$: the number of model levels is too small for the expected greater accuracy at lower model levels to be observed. This feature becomes however visible in the results obtained for the more practically relevant case of $N = 19$, which are shown in Figs. 12 - 15.

The results obtained for $N = 5$ appear to be slightly more accurate than those for $N = 4$, although the differences between them are small (in both cases the resolution is too low, particularly for the highest mode indices).

The more practically relevant case of $N = 19$ model levels is then considered in Figs. 12 - 15 for the case of the quadratic grid. These results are more accurate, as expected, because of the higher resolution - in particular the low index normal modes are much better resolved - and are consistent with those obtained for $N = 4$ and $N = 5$. They are more accurate at lower model levels, and for lower index normal modes, but the highest index normal modes appear to be still not well resolved: this is an indication that the number of model levels is still insufficient to resolve the shortest wavelengths.

It may be worth making a final comment about the ordering of the normal modes. The analytic ones, which are of the form (cf. (3.28) - (3.29)):

$$w = w^{\pm} \sin\left(\frac{m\pi z}{z_T}\right), \tag{4.13}$$

$$\Pi = \Pi^{\pm} \cos\left(\frac{m\pi z}{z_T}\right), \tag{4.14}$$

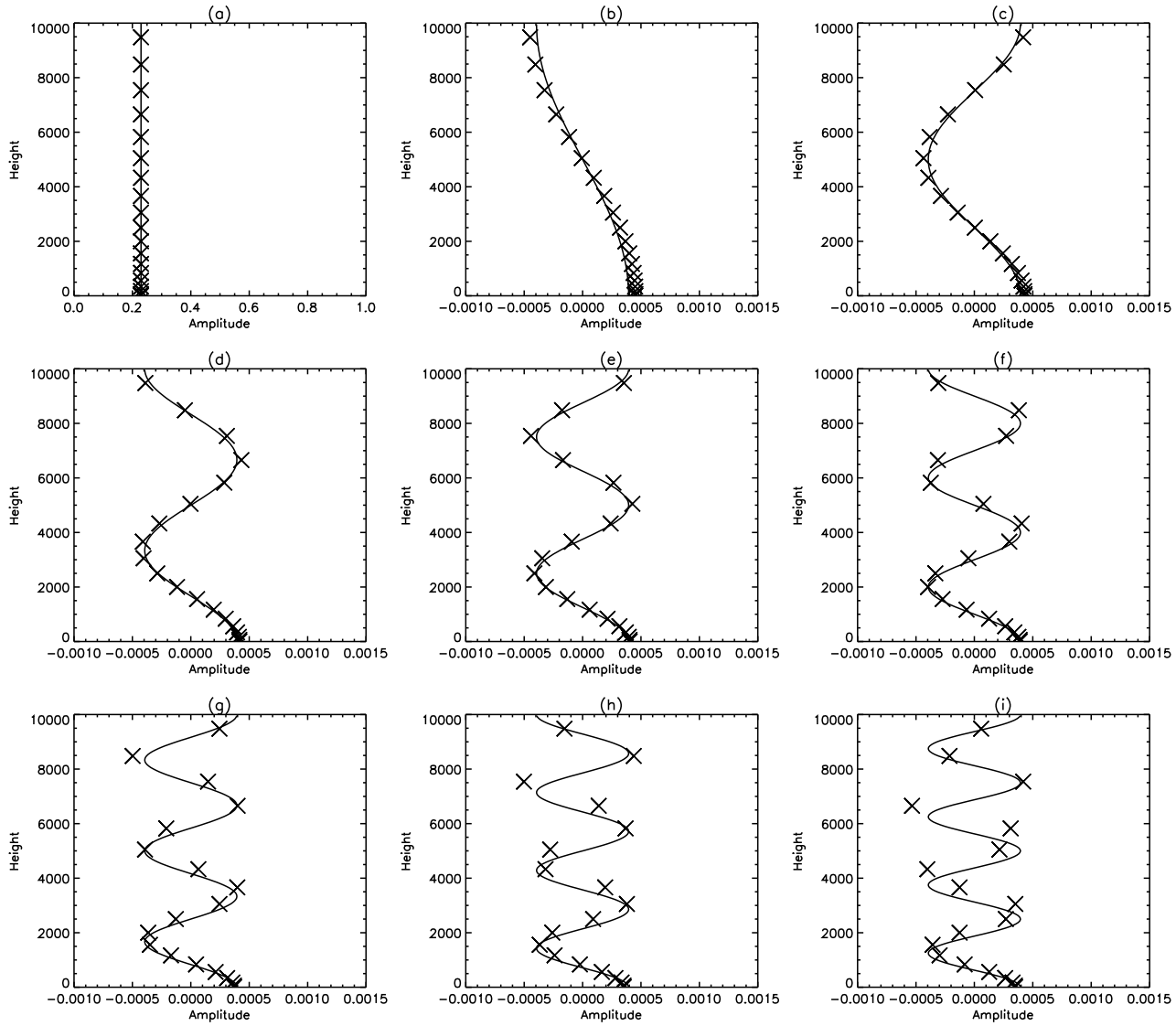

Figure 12: $\underline{\Pi}-$modes of index $m = 1, ..., 9$ for a quadratic grid with $N = 19$. The continuous line denotes the analytic continuous normal modes, the crosses the numerical ones.

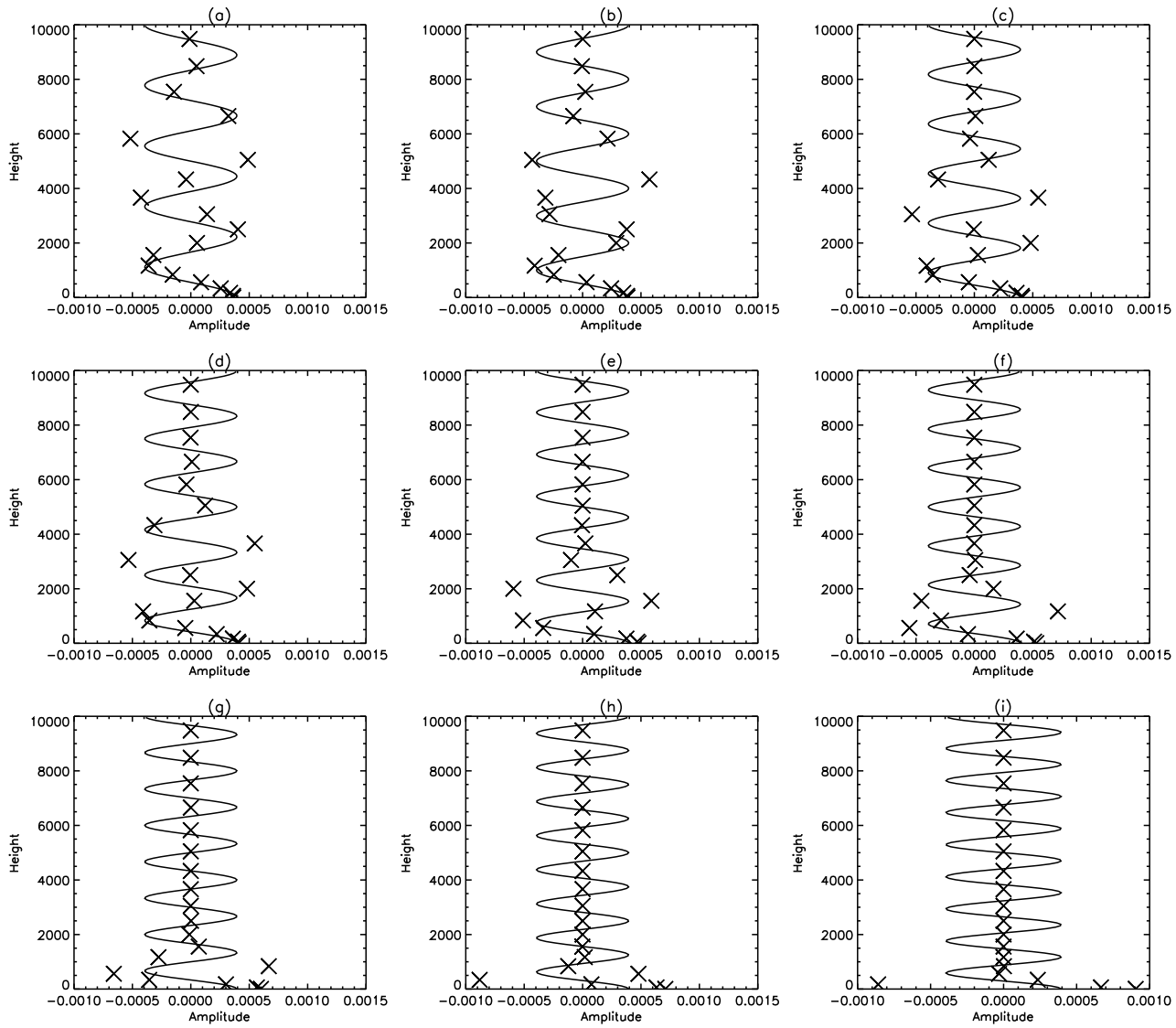

Figure 13: $\underline{\Pi}-$modes of index $m = 10, ..., 18$ for a quadratic grid with $N = 19$.

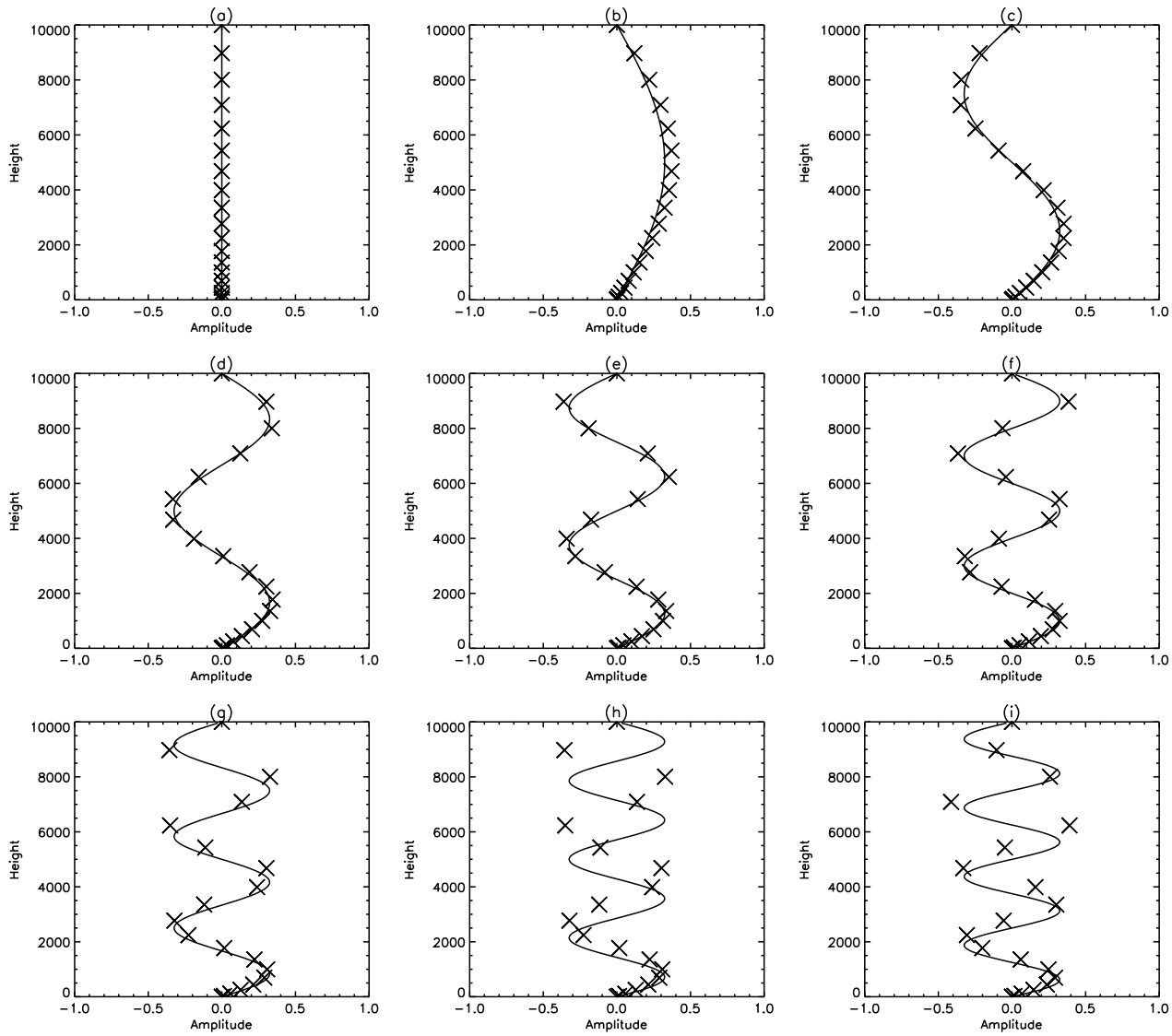

Figure 14: $\underline{w}-$modes of index $m = 1, ..., 9$ for a quadratic grid with $N = 19$.

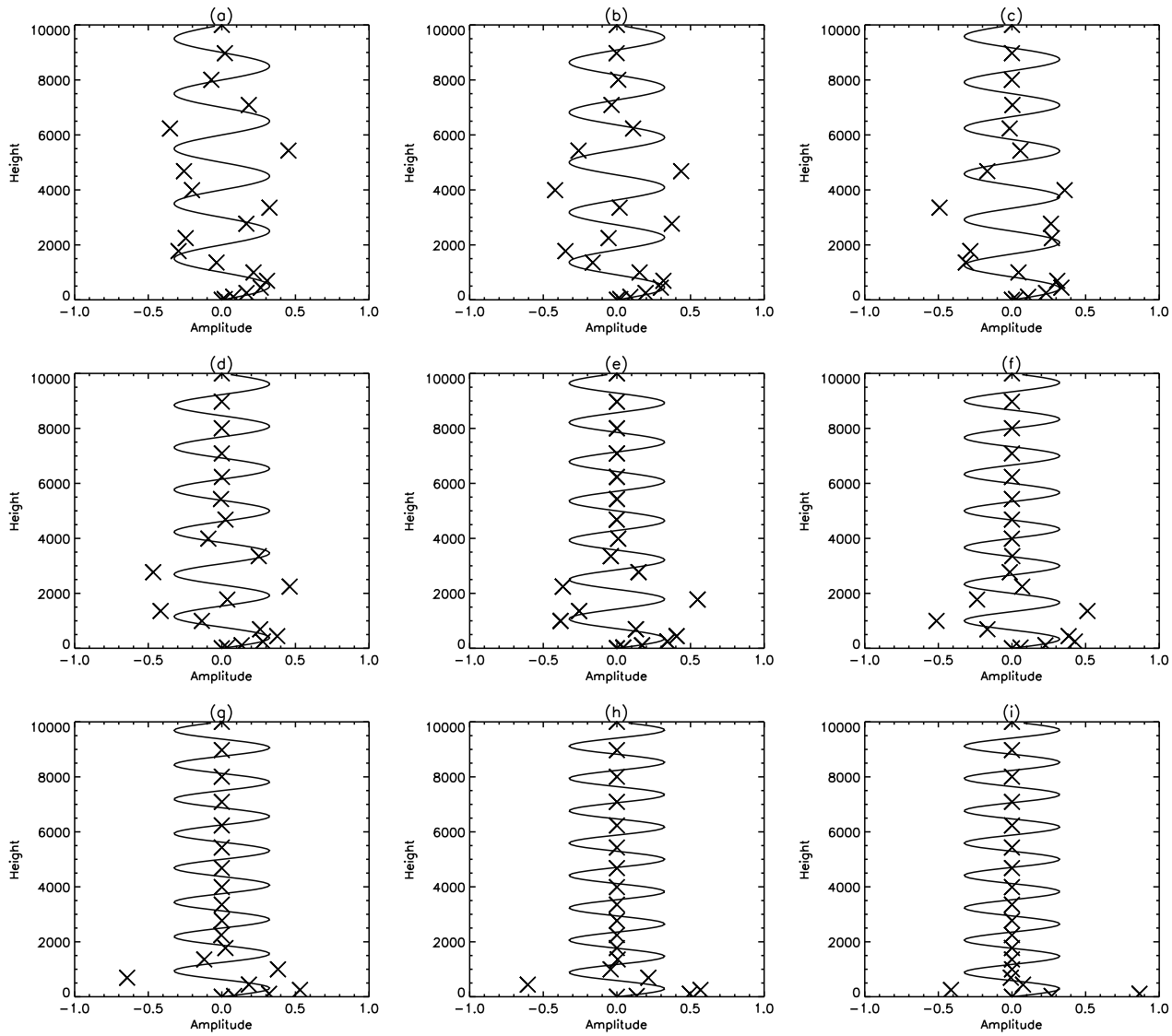

Figure 15: $\underline{w}-$modes of index $m = 10, ..., 18$ for a quadratic grid with $N = 19$.

are easily ordered with respect to increasing mode index m. For the numerical ones, there is no such reference, but they have been ranked with respect to decreasing modulus of their associated eigenvalue, i.e. $|\lambda| = \sqrt{\Re^2(\lambda) + \Im^2(\lambda)}$, and this ordering is found to be consistent with that of the analytic normal modes. This indicates that the modulus of the eigenvalue may be a measure of the importance of the associated normal mode. This property is thought to mimic the ordering of the normal modes of the discrete problems computed analytically (cf. Section 3.4.6), which have the associated eigenvalues decreasing in magnitude as the index m increases. This can be seen from the results:

$$|\lambda_m|^2 = \frac{1 + (1-\alpha)^2 \beta_m^2 c_s^2}{1 + \alpha^2 \beta_m^2 c_s^2} = 1 + \frac{(1-2\alpha)\beta_m^2 c_s^2}{1 + \alpha^2 \beta_m^2 c_s^2}, \tag{4.15}$$

where β_m is defined as in (3.69), and $\alpha \geq 1/2$ for stability considerations. By differentiating (4.15) with respect to β_m , it is found that $|\lambda_m|^2$ is a decreasing function of β_m and β_m is an increasing function of m, for $m = 0, ..., N$, so that $|\lambda_m|^2$ is a decreasing function of m. Thus the numerical normal modes have been ordered according to the magnitude of their eigenvalues.

5 The eigenvalue problem for the 1D isothermal basic state case

The general framework developed in Section 2 with matrices defined as in (2.80) - (2.106), allows us to analyse the 2D New Dynamics discretisation under the assumptions stated at the beginning of Section 2.1. Further, by modifying appropriately the definitions of the sub-matrices defining the matrices A and B, its relevant subsets and special cases can also be analysed.

In particular in the present section the special case of the 1D column model is presented: the equations and their analytic solution are summarised, the definition of the matrices is given and various boundary conditions imposed on the potential temperature are discussed.

Next the normal modes are computed numerically and used as perturbations to the initial state of the 1D version of the New Dynamics model (cf. "New Dynamics formulation: 1-D dry column model", M. Zerroukat, A. Staniforth and T. Davies) with an isothermal basic state. The non-linear evolution of the modes computed by the 1D model is compared with the linear evolution predicted by the linear normal mode analysis and the impact on the behaviour of the modes of the boundary conditions imposed on the potential temperature is discussed in Section 6.

5.1 The linearised continuous governing equations

In the 1D case and for an isothermal basic state at rest ($u_s = 0$) the set of linearised continuous equations (3.16) - (3.19) subject to $w = 0$ at the top and bottom of the domain, can be solved analytically.

The solution for the internal modes to (3.16) - (3.19) is:

$$w(z,t) = w_0 \exp(i\omega t) \sin\left(\frac{m\pi}{z_T} z\right) \exp\left(\frac{z}{2H}\right), \tag{5.1}$$

$$\Pi(z,t) = \Pi_0 \exp(i\omega t) \left[\frac{m\pi}{z_T} \cos\left(\frac{m\pi}{z_T} z\right) - \frac{1-2\kappa_d}{2H} \sin\left(\frac{m\pi}{z_T} z\right)\right] \exp\left(\frac{1-2\kappa_d}{2H} z\right), \tag{5.2}$$

$$\theta(z,t) = \theta_0 \exp(i\omega t) \sin\left(\frac{m\pi}{z_T} z\right) \exp\left(\frac{1+2\kappa_d}{2H} z\right), \tag{5.3}$$

$$\rho(z,t) = \rho_0 \exp(i\omega t) \left[\frac{m\pi}{z_T} \cos\left(\frac{m\pi}{z_T} z\right) - \frac{1}{2H} \sin\left(\frac{m\pi}{z_T} z\right)\right] \exp\left(-\frac{z}{2H}\right), \tag{5.4}$$

where w_0 is an arbitrary constant,

$$\Pi_0 = \frac{\kappa_d}{1-\kappa_d}\left(i\frac{w_0}{\omega}\right), \tag{5.5}$$

$$\theta_0 = T_s\frac{\kappa_d}{H}\left(i\frac{w_0}{\omega}\right), \tag{5.6}$$

$$\rho_0 = \frac{p_0}{\kappa_d c_{pd} T_s}\left(i\frac{w_0}{\omega}\right), \tag{5.7}$$

$$\omega = \pm c_s\sqrt{\left(\frac{m\pi}{z_T}\right)^2 + \frac{1}{4H^2}}, \tag{5.8}$$

$$c_s^2 = \frac{R_d T_s}{1-\kappa_d}, \quad H = \frac{R_d T_s}{g}, \quad \kappa_d = R_d/c_{pd}\,, \tag{5.9}$$

z_T is the height of the top of the domain and $m = 1, ..., N-1$ is the internal mode index.

The external mode has $w = 0$, which implies θ, ρ, and Π are functions of height only, so that its frequency is $\omega = 0$. Π is an arbitrary function of height, whilst θ and ρ are calculated from Π via the vertical momentum equation and the linearised gas law respectively. Thus:

$$w = 0, \tag{5.10}$$

$$\Pi = \Pi(z), \tag{5.11}$$

$$\theta = -\theta_s(z)\left(\frac{d\Pi(z)}{dz}\Big/\frac{d\Pi_s(z)}{dz}\right), \tag{5.12}$$

$$\rho = \rho_s(z)\left[\frac{1-\kappa_d}{\kappa_d}\left(\frac{\Pi(z)}{\Pi_s(z)}\right) - \frac{\theta(z)}{\theta_s(z)}\right]. \tag{5.13}$$

The set of linearised equations (3.16) - (3.19) and the expression for the internal normal modes (5.1) - (5.4) are consistent with the corresponding equations reported in Thuburn, Wood & Staniforth (2002), which are written for variables u, v, w, p, and θ. In the latter paper the coefficient of the internal modes associated with pressure, p_0, has been set to unity. This choice corresponds to setting $w_0 = -i\omega(1-\kappa_d)/p_0$ in (5.1). The analysis reported in Thuburn et al. (2002) allows both for variations in the x and y directions and the effect of rotation and therefore the external mode computed therein differs from the less constrained solution of (5.10) - (5.13). In particular Π is no longer arbitrary and θ is zero, with consequent impact on ρ.

5.2 Linearised discrete equations and resulting matrices for the associated eigenvalue problem

The linearised discrete equations for the 1D isothermal basic state are obtained by setting $F = 0$, $u_s = 0$ (and therefore $()_d^n = ()^n$), and $\partial/\partial x \equiv 0$ in the linearised time-discretised equations of the full model (i.e. (2.50) - (2.61)):

5.2.1 Horizontal momentum at levels $k = 1/2, ..., N - 1/2$

$$\frac{u^{n+1} - u^n}{\Delta t} = 0, \tag{5.14}$$

$$\frac{v^{n+1} - v^n}{\Delta t} = 0. \tag{5.15}$$

5.2.2 Vertical momentum at levels $k = 0, ..., N$

$$w^{n+1}\Big|_{z_{0\equiv 0}} = 0, \tag{5.16}$$

$$\begin{aligned} I_h \frac{w^{n+1} - w^n}{\Delta t} &= -c_{pd}\theta_s \left[\alpha_4 \delta_z \Pi^{n+1} + (1-\alpha_4)\,\delta_z \Pi^n\right] \\ &\quad -c_{pd}\delta_z \Pi_s \left[\alpha_4 \theta^{n+1} + (1-\alpha_4)\,\theta^n\right], \end{aligned} \tag{5.17}$$

at levels $k = 1, ..., N - 1$ and

$$w^{n+1}\Big|_{z_N} = 0. \tag{5.18}$$

5.2.3 Thermodynamics at levels $k = 0, ..., N$

$$\theta^{n+1}\Big|_{z_{0\equiv 0}} = \theta^n|_{z_{0\equiv 0}}\,, \tag{5.19}$$

$$\frac{\theta^{n+1} - \theta^n}{\Delta t} = -\delta_{2z}\theta_s \left[\alpha_2 w^{n+1} + (1-\alpha_2)\,w^n\right], \tag{5.20}$$

at levels $k = 1, ..., N - 1$ and

$$\theta^{n+1}\Big|_{z_N} = \theta^n|_{z_N}\,. \tag{5.21}$$

5.2.4 Continuity at levels $k = 1/2, ..., N - 1/2$

$$\left(\frac{\rho^{n+1} - \rho^n}{\Delta t}\right)\Big|_{z_{1/2}} = -\left(\frac{1}{\Delta z}\right)\Big|_{z_{1/2}} \left[\alpha_2 \overline{\rho}_s^z w^{n+1} + (1-\alpha_2)\,\overline{\rho}_s^z w^n\right]\Big|_{z_1}, \tag{5.22}$$

$$\frac{\rho^{n+1} - \rho^n}{\Delta t} = -\left[\alpha_2 \delta_z \left(\overline{\rho}_s^z w^{n+1}\right) + (1-\alpha_2)\,\delta_z \left(\overline{\rho}_s^z w^n\right)\right], \tag{5.23}$$

at levels $k = 1/2, ..., N - 3/2$ and

$$\left(\frac{\rho^{n+1} - \rho^n}{\Delta t}\right)\Big|_{z_{1/2}} = \left(\frac{1}{\Delta z}\right)\Big|_{z_{N-1/2}} \left[\alpha_2 \overline{\rho}_s^z w^{n+1} + (1-\alpha_2)\,\overline{\rho}_s^z w^n\right]\Big|_{z_{N-1}}. \tag{5.24}$$

5.2.5 Linearised gas law at levels $k = 1/2, ..., N - 1/2$

$$\left(\frac{1-\kappa_d}{\kappa_d}\right)\frac{\Pi^{n+1}}{\Pi_s} = \frac{\rho^{n+1}}{\rho_s} + \frac{\overline{\theta^{n+1}}^z}{\overline{\theta_s}^z}. \tag{5.25}$$

The set of discrete equations (5.14) - (5.25) corresponds to that derived in Section 3.2 (cf. (3.30) - (3.39)) with the addition of the horizontal momentum equations (5.14) and (5.15). The horizontal momentum equations are not genuine equations of the 1D $z-$column model (in fact u and v are not effective variables in this case) and they reduce to trivial equations. They appear in the equation set, and therefore in the matrices defining the eigenvalue problem, because of the general framework set up to solve it, and introduced in Section 2. They are expected to produce $2N$ trivial eigenmodes (owing to the $2N$ trivial equations appearing in the linear system (2.79)) in the 1D case.

Also the bottom boundary condition for the potential temperature, (5.19) i.e. θ active at the bottom, is different from (2.55) and (3.33), which assume an isentropic bottom layer. Different boundary conditions however can be analysed, by changing the definition of the matrices. The top and bottom boundary conditions used in the New Dynamics discretisation are discussed in Section 5.3.

Unlike the case of the 1D constant basic state case, it is not straightforward to derive the analytic discrete expression for the internal normal modes of the system. As to the external modes, their analytic discrete expressions is obtained by setting $w = 0$ in (5.17) - (5.25), which implies that Π, θ, and ρ are independent of time, Π is an arbitrary function of z_k and θ and ρ are determined by (5.17) and (5.25) respectively. Thus:

$$w(z_k) = 0, \quad k = 0, ..., N \tag{5.26}$$

$$\Pi(z_k) = \Pi(z_k), \quad k = 1/2, ..., N - 1/2 \tag{5.27}$$

$$\theta(z_k) = -\frac{\theta_s(z_k)}{\delta_z \Pi_s(z_k)} \delta_z \Pi(z_k), \quad k = 1, N-1 \tag{5.28}$$

$$\rho(z_k) = \frac{1-\kappa_d}{\kappa_d}\frac{\rho_s(z_k)}{\Pi_s(z_k)}\Pi(z_k) - \rho_s(z_k)\frac{\overline{\theta}^z(z_k)}{\overline{\theta_s}^z(z_k)}, \quad k = 1/2, ..., N - 1/2 \tag{5.29}$$

and θ at the top is arbitrary, whilst θ at the bottom is either arbitrary, if the active bottom boundary is used, or determined by its value at the first integer model level, if the isentropic

bottom boundary condition is used.

It is worth noting that in computing the analytic discrete external modes there are $N+2$ or $N+1$ degrees of freedom respectively for the θ active at the bottom or isentropic bottom boundary condition respectively: N are due to the arbitrariness of Π, the remaining one (or two) are due to the active boundary condition(s). Thus $N+2$ or $N+1$ independent external modes are expected to be found numerically.

5.2.6 Definition of the matrices defining the eigenvalue problem

The sub-matrices composing the matrices A and B of the eigenvalue problem (2.121) in the special case of the 1D isothermal basic state $z-$column model and corresponding to the equation set (5.14) - (5.25) are defined by (2.89) - (2.96), (2.98), (2.100), (2.105) - (2.106), and

$$B'_{w,u} = A_{\rho,u} = B'_{\rho,u} = A_{u,\Pi} = B'_{u,\Pi} = B'_{u,w} = 0. \tag{5.30}$$

Since in the linearised discrete equations derived in this section the bottom boundary condition (5.19) is used instead of the isentropic bottom boundary condition (3.33) employed in the matrix formulation developed in Section 2.6, the first rows in the sub-matrices $A_{\theta,w}$ and $B_{\theta,w}$ defined in (2.91) and (2.92) are replaced by zeros, for the sub-matrices to be consistent with the boundary condition (5.19). The issue of the boundary conditions imposed on the potential temperature is discussed in Section 5.3.

Further, since in the 1D case $u_s = 0$ and $\partial/\partial x \equiv 0$, l is set to zero in the definition (2.86) of the matrix B.

5.3 Top and bottom boundary conditions for the potential temperature

In the discrete equation set of Section 5.2, the values of θ at the top and bottom boundaries are determined by horizontal advection (i.e. by applying $w = 0$ in (5.20)), without the need for imposing any special boundary conditions on θ - for convenience this approach is referred to henceforth as "active boundary conditions".

However, application of boundary conditions on θ at the top and bottom, namely an isentropic layer at the bottom and / or an isothermal layer at the top have also been considered, since they are relevant to the New Dynamics: the isentropic bottom layer with θ

active at the top are the boundary conditions used currently, whilst the isothermal top layer was used in previous versions of the New Dynamics.

It is however possible to use the active boundary conditions in the present analysis, because all options (active boundary conditions; the isentropic bottom layer; and the isothermal top layer) are coded into the 1D column model, with a switch to choose between their combinations. The non-active boundary conditions can be analysed by changing the definition of the sub-matrices $A_{\theta,\theta}$, $A_{\theta,w}$, $B'_{\theta,\theta}$, and $B'_{\theta,w}$ as explained in the following sections. In the normal mode code a switch has been included to choose between the different boundary conditions. The numerical results obtained with the active or the non-active (isothermal top or isentropic bottom) boundary conditions are discussed in Sections 6.1 - 6.2.

5.3.1 Isothermal top layer

With the isothermal top layer, the value of potential temperature at the top of the model, θ_N, defined as

$$\theta^{n+1}\Big|_{z_N} = \theta^n|_{z_N}\,, \tag{5.31}$$

is not used in the dynamics. The usual vertical average of potential temperature at level $N-\frac{1}{2}$ (which involves θ_N),

$$\overline{\theta}^z\Big|_{z_{N-\frac{1}{2}}} = \frac{\left(z_{N-\frac{1}{2}} - z_{N-1}\right)\theta_N + \left(z_N - z_{N-\frac{1}{2}}\right)\theta_{N-1}}{z_N - z_{N-1}}, \tag{5.32}$$

is replaced by a special average over the layer, defined by assuming the temperature T to be constant over the layer $\left[z_{N-\frac{3}{2}},\, z_N\right]$. This vertical average is given by:

$$\overline{\theta}^z\Big|_{z_{N-\frac{1}{2}}} = \frac{\theta|_{z_{N-1}}\ \overline{\Pi}^z\Big|_{z_{N-1}}}{\Pi|_{z_{N-\frac{1}{2}}}}. \tag{5.33}$$

Further the term $\delta_{2z}\theta_s|_{z_{N-1}}$ in the thermodynamic equation (5.20) at level $N-1$ is discretised over the layer $\left[z_{N-\frac{3}{2}},\, z_{N-\frac{1}{2}}\right]$ as:

$$\delta_{2z}\theta_s|_{z_{N-1}} = \frac{\overline{\theta}^z_s\Big|_{z_{N-\frac{1}{2}}} - \overline{\theta}^z_s\Big|_{z_{N-\frac{3}{2}}}}{\Delta z|_{z_{N-1}}}, \tag{5.34}$$

(as opposed to the standard definition over the two layers $[z_{N-2},\, z_N]$).

The special form for $\delta_{2z}\theta_s|_{z_{N-1}}$ i.e. (5.34) is used in the thermodynamic equation (5.20) at level $N-1$. The special form for the averaged potential temperature (5.33) is used to define $\overline{\theta}^z_s\Big|_{z_{N-\frac{1}{2}}}$ in the equation of state (5.25) at level $N-\frac{1}{2}$ and its linearised form,

$$\overline{\theta}^z\Big|_{z_{N-\frac{1}{2}}} = \frac{1}{\Pi_s|_{z_{N-\frac{1}{2}}}}\left\{\frac{\theta_s|_{z_{N-1}}\ \overline{\Pi}^z_s\Big|_{z_{N-1}}\ \Pi|_{z_{N-\frac{1}{2}}}}{\Pi_s|_{z_{N-\frac{1}{2}}}} - \theta|_{z_{N-1}}\ \overline{\Pi}^z_s\Big|_{z_{N-1}} - \theta_s|_{z_{N-1}}\ \overline{\Pi}^z\Big|_{z_{N-1}}\right\}, \quad (5.35)$$

is used for $\overline{\theta}^z\Big|_{z_{N-\frac{1}{2}}}$ in the equation of state (5.25).

Following these changes in the thermodynamic equation and in the linearised gas law, the last rows in the sub-matrices $A_{\Pi,\Pi}$ and $A_{\Pi,\theta}$ are modified as follows:

$$[A_{\Pi,\Pi}]_N = \left[\ 0,\ \ 0,\ \ 0,\ \ -\frac{\kappa_d}{1-\kappa_d}\frac{\Pi_s|_{z_{N-\frac{1}{2}}}}{\overline{\Pi}^z_s\Big|_{z_{N-1}}}\ a|_{z_{N-1}}\ ,\ \ 1+\frac{\kappa_d}{1-\kappa_d}\left(1-\frac{\Pi_s|_{z_{N-\frac{1}{2}}}}{\overline{\Pi}^z_s\Big|_{z_{N-1}}}\ b|_{z_{N-1}}\right)\ \right], \quad (5.36)$$

where

$$a|_{z_k} = \left(\frac{z_{k+\frac{1}{2}}-z_k}{z_{k+\frac{1}{2}}-z_{k-\frac{1}{2}}}\right) = \frac{z_{k+\frac{1}{2}}-z_k}{\Delta z_k}, \quad b|_{z_k} = \left(\frac{z_k-z_{k-\frac{1}{2}}}{z_{k+\frac{1}{2}}-z_{k-\frac{1}{2}}}\right) = \frac{z_k-z_{k-\frac{1}{2}}}{\Delta z_k}, \quad (5.37)$$

for $k=1,...,N-1$, and

$$[A_{\Pi,\theta}]_N = \left[\ 0,\ \ 0,\ \ 0,\ \ 0,\ \ -\frac{\kappa_d}{1-\kappa_d}\frac{\Pi_s|_{z_{N-\frac{1}{2}}}}{\theta_s|_{z_{N-1}}},\ \ 0\ \right]. \quad (5.38)$$

Further, although the sub-matrices $A_{\theta,w}$ and $B'_{\theta,w}$ remain formally the same as in (2.91) and (2.92) (but with the first row in both matrices replaced by zeros), when the isothermal top layer is assumed the definition of $\delta_{2z}\theta_s|_{z_{N-1}}$ which appears in them is (5.34).

5.3.2 Isentropic bottom layer

The isentropic bottom layer assumption prescribes the potential temperature to be constant in the bottom layer. Thus:

$$\theta^{n+1}\Big|_{z_{0\equiv 0}} = \theta^{n+1}\Big|_{z_1}. \quad (5.39)$$

When the boundary condition (5.39) is applied in place of (5.19), the first rows of the sub-matrices $A_{\theta,\theta}$ and $B'_{\theta,\theta}$, are modified as follows (the others remain unchanged):

$$[A_{\theta,\theta}]_1 = \left[\ 1,\ \ -1,\ \ 0,\ \ 0,\ \ 0,\ \ 0\ \right], \quad (5.40)$$

$$\left[B'_{\theta,\theta}\right]_1 = \left[\ 0,\ \ 0,\ \ 0,\ \ 0,\ \ 0,\ \ 0\ \right]. \quad (5.41)$$

A different form of isentropic bottom boundary condition is obtained by combining (5.39) and the thermodynamic equation (5.20) evaluated at level $k = 1$, as is explained in Section 2 (below (2.108) - (2.109)):

$$\theta^{n+1}\Big|_{z_0 \equiv 0} = \theta^n\big|_{z_0 \equiv 0} - \delta_{2z}\theta_s \Delta t \left[\alpha_2 \, w^{n+1}\Big|_{z_1} + (1-\alpha_2)\, w^n\big|_{z_1}\right]. \tag{5.42}$$

When the boundary condition (5.42) is used, the first row of the sub-matrices $A_{\theta,w}$ and $B'_{\theta,w}$ is modified as follows:

$$[A_{\theta,w}]_1 = \left[\; 0, \quad \delta_{2z}\theta_s\big|_{z_1}, \quad 0, \quad 0, \quad 0, \quad 0 \;\right], \tag{5.43}$$

$$\left[B'_{\theta,w}\right]_1 = \left[\; 0, \quad \delta_{2z}\theta_s\big|_{z_1}, \quad 0, \quad 0, \quad 0, \quad 0 \;\right]. \tag{5.44}$$

To understand the link between the isentropic boundary conditions (5.39) and (5.42), note that (5.39) is a discretised form of the isentropic condition:

$$\left(\frac{\partial \theta}{\partial z}\right)^{n+1} = 0, \tag{5.45}$$

whereas (5.42) is a discretised form of D^L/Dt of (5.45):

$$\frac{D^L}{Dt}\left(\left.\frac{\partial \theta}{\partial z}\right|_{z_{1/2}}\right) = 0 \iff \left.\frac{D^L\theta}{Dt}\right|_{z_1} = \left.\frac{D^L\theta}{Dt}\right|_{z_0 \equiv 0}. \tag{5.46}$$

Under the assumption $\left.\dfrac{d\theta^0}{dz}\right|_{z_{1/2}} = 0$ (i.e. assuming the lowest level to be isentropic at the initial time) (5.45) and (5.46) are equivalent boundary conditions for the underlying continuous problem. However the normal mode analysis has no information regarding initial conditions, hence the discrete counterparts of (5.45) and (5.46) are not equivalent for the eigenvalue problem. This is due to the fact that applying (2.123) to the $\underline{\theta}$ components of $\underline{x}$, (5.46) yields:

$$(\lambda - 1)\left(\theta^n\big|_{z_1} - \theta^n\big|_{z_0 \equiv 0}\right) = 0. \tag{5.47}$$

Eq. (5.47) is equivalent to the isentropic assumption (5.39) only for the normal modes with eigenvalues $\lambda \neq 1$. This is consistent with the numerical results: the normal modes associated with the eigenvalue $\lambda = 1$ computed using (5.42), and therefore with the sub-matrices $A_{\theta,w}$ and $B'_{\theta,w}$ modified as in (5.43) - (5.44), do not satisfy the original isentropic boundary condition (5.39). This is because for the normal modes with $\lambda = 1$, $\theta\big|_{z_0}$ can be chosen independently of $\theta\big|_{z_1}$ and still satisfy (5.42) (since when $\lambda = 1$ the square bracketed term in (5.42) must vanish).

6 Numerical normal modes of the 1D isothermal basic state column model

The eigenvalue problem (2.121), where the sub-matrices composing the matrices A and B are defined in Section 5.2.6, is solved numerically using the $Fortran90$ code *full_isoth_new.f90* calling the $Fortran77$ NAG (Numerical Algorithm Group) library routine $F02BJF$.

The first issue to be dealt with when computing the eigenvalues and eigenmodes is the counting of the modes, since using the general (2D) framework for the special 1D case, for which the horizontal momentum equations reduce to trivial relations for the variables u and v written at the N half-integer model levels, yields $2N$ trivial modes. The trivial modes are associated with the eigenvalue $\lambda = \exp(i\omega\Delta t) = 1$, which corresponds to the frequency $\omega = 0$, which is the frequency of the gravity and Rossby modes in the special case of the 1D $z-$column model.

The number of expected eigenvalues and eigenmodes is given asymptotically by the number of prognostic equations times the number of interior model levels or, more precisely, by the degrees of freedom (i.e. the number of prognostic variables times the number of levels at which they are stored minus the number of Dirichlet boundary conditions imposed on them). The problem under examination is characterised by three prognostic equations, for the variables θ, w, and ρ; $N-1$ interior model levels, and $3N$ degrees of freedom (or $3N-1$ when the isentropic bottom boundary condition is used), which are counted as follows. There are: $N+1$ (or N, if the isentropic bottom boundary condition is imposed) degrees of freedom for θ, $N-1=(N+1)-2$ for w, and N for ρ, yielding $3N$ (or $3N-1$ if the isentropic bottom boundary condition is used) expected eigenmodes.

The number of eigenmodes computed numerically corresponds to the dimension of the square matrices defining the eigenvalue problem, i.e. $6N+2$ for the Charney-Phillips grid staggering. Alongside the $2N$ trivial modes mentioned above, $N+2$ (or $N+3$ when the isentropic boundary condition is used in the original form (5.39)) spurious modes, associated with the eigenvalue $\lambda = 0$, are found.

The $N+2$ spurious modes are due to: the linearised gas law (5.25), which is a diagnostic relation, being discretised for convenience as N prognostic equations (at time level $n+1$); and the top and bottom boundary conditions on w, (5.18) and (5.16), being imposed at time

level $n+1$, and retained again for convenience as prognostic equations in the system, so that $B'_{\Pi,\cdot} = 0$ and the first and last row in the matrices $B'_{w,\cdot}$ are also zero. This yields $N+2$ null rows in the matrix B. If the isentropic bottom boundary condition (5.39) is used, there is a further null row in the matrix B (the first row in the matrices $B_{\theta,\cdot}$), leading to $N+3$ spurious modes in total. These modes are spurious in the sense that they do not satisfy all of the equations and are therefore not solutions to the problem and are not considered in the analysis; they are introduced by the choice of evaluating the linearised gas law and the boundary conditions at time $n+1$, as explained above.

Of the remaining (and expected) $3N$ (or $3N-1$ when the isentropic bottom boundary condition (5.39) is used) eigenmodes, it is found that $2(N-1)$ form $N-1$ complex conjugate pairs, one for each of the interior model levels: these are the internal modes, whose analytic continuous counterparts are defined by (5.1) - (5.4).

The remaining $N+2$ (or $N+1$, when the isentropic bottom boundary condition (5.39) is used) normal modes are real and correspond to the external modes. The number of external modes computed numerically agrees with the number of discrete external modes computed analytically in Section 5.2. It is also verified that the external modes computed numerically agree well with their analytic discrete expressions defined by (5.26) - (5.29). This is done by: setting the arbitrary components (i.e. $\underline{\Pi}$ and the components of $\underline{\theta}$ at the active boundaries) of the analytic discrete external modes (5.26) - (5.29) to be equal to the corresponding components of each of the numerical external normal modes in turn; defining the analytic discrete $\underline{\theta}$ and $\underline{\rho}$ components from $\underline{\Pi}$ via (5.28) and (5.29); and computing the differences between the analytic discrete and the numerical values. These differences are found to be at most of order 10^{-11}.

The second aspect is related to the interpretation of the results, in particular how to obtain real, physically meaningful values for the variables Π, θ, w, and ρ (the $\underline{u}$ and $\underline{v}$ components of the modes are discarded, since u and v are not active variables of the 1D column model) from the complex eigenmodes.

By analogy with the 1D constant basic state model, in which the solution of the continuous problem was found as the real part of a more general complex solution (cf. Section 4, (3.28) - (3.29) and (4.2) - (4.3)), the complex numerical eigenmodes computed in the isothermal basic state case can be interpreted as the discrete analogues of the more general complex

solution, the real part of which constitutes the physically meaningful discrete solution. The imaginary part of the modes is not however discarded, but it is used to predict the time evolution of the modes, when they are input into the 1D column model version of the New Dynamics.

In fact, by applying (2.123) recursively and taking the real part, it follows that the expected value of the variables at any given time-step n is given by:

$$\begin{aligned} \Re\left(\underline{x}^n\right) &= \Re\left(\lambda^n \underline{x}^0\right) \\ &= \Re\left(\lambda^n\right)\Re\left(\underline{x}^0\right) - \Im\left(\lambda^n\right)\Im\left(\underline{x}^0\right). \end{aligned} \tag{6.1}$$

The value $\Re\left(\lambda^n \underline{x}^0\right)$ defined by (6.1) and predicted by the normal mode analysis will be referred to henceforth as "linear analysis".

As a validation of the 2D code, the eigenvalues and eigenmodes of the 1D constant basic state column model have been computed and compared with those obtained by solving the 1D simplified problem described in Section 3. The same results have been found, apart from the null space modes (i.e. those associated with the $\lambda = 0$ eigenvalue, as discussed above), which differ, and the trivial ones, which are absent from the 1D code.

Next the eigenvalues and eigenmodes of the 1D isothermal basic state column model are computed and used to initialise the 1D column model with an isothermal basic state.

More precisely the modes $\underline{x}_m = \left[\begin{array}{cccc} \underline{\Pi}, & \underline{\theta}, & \underline{w}, & \underline{\rho} \end{array} \right]^T$, taken one at a time, represent perturbations about the initial isothermal basic state of the 1D column model, $\left[\begin{array}{cccc} \underline{\Pi}_s, & \underline{\theta}_s, & \underline{w}_s = 0, & \underline{\rho}_s \end{array} \right]^T$. The isothermal basic state is defined either analytically (cf. (2.28), (2.27), and (2.31)) or by solving the hydrostatic relationship and the equation of state in discrete form on the grid and exploiting the definition of potential temperature. The initial state of the 1D model is then given by the sum of the isothermal basic state and a perturbation defined by one of the normal modes.

The parameters used in the runs are the same as those in Mohamed Zerroukat's "On the boundary conditions in the column model" (BC1D): the top of the domain is set at $z_T = 12000\,\mathrm{m}$, the domain is discretised using a uniform vertical grid comprising 40 levels, yielding $\Delta z = 300\,\mathrm{m}$ and the basic state constant temperature is $T_s = 290\,\mathrm{K}$; in the standard run the semi-implicit weights are $\alpha_2 = \alpha_4 = 0.51$, and the time step is $\Delta t = 60\,\mathrm{s}$, but the runs have been repeated reducing the time-step down to $\Delta t = 1\,\mathrm{s}$ and increasing the weights

up to $\alpha_2 = \alpha_4 = 1$. The model was initially run with θ active at the top and bottom, then the runs were repeated with the isentropic bottom boundary condition and the isothermal top layer, in order to verify the impact of the boundary conditions on the numerical normal modes.

For the internal modes, the model is run for a number of time-steps greater than those required to complete an oscillation cycle of the mode, which is defined as 2π times the reciprocal of the numerical frequency and is computed as:

$$N_{cycle} = \frac{2\pi}{|\omega_R \Delta t|}, \tag{6.2}$$

where the numerical frequency is

$$\omega_R \Delta t = \tan^{-1}\left(\Im\left(\lambda\right)/\Re\left(\lambda\right)\right), \tag{6.3}$$

and it is related to the eigenvalues via:

$$\lambda = \exp\left(i\omega\Delta t\right) = \exp\left(-\omega_I \Delta t\right)\exp\left(i\omega_R \Delta t\right). \tag{6.4}$$

The inverse of the tangent in (6.3) is computed using the *Fortran*90 intrinsic function *atan*2, which returns values in the range $[-\pi, \pi]$, i.e. the principal argument of the function. For the external modes, it is not meaningful to define an oscillation cycle, since they are not wave-like (i.e. $\omega_R = 0$) but grow (if $\omega_I < 0$), decay (if $\omega_I > 0$), or remain neutral (if $\omega_I = 0$), depending on the associated eigenvalue.

The perturbations (i.e. the values of the variables computed by the 1D model at the appropriate integer or half-integer model levels minus their basic state values) produced by the 1D model are compared with the linear analysis (6.1).

As a measure of the accuracy of the numerical results with respect to the predicted values, the absolute and relative errors at a given time-step n are defined respectively as:

$$e_{abs} = \underline{x}^n_{model} - \Re\left(\lambda^n \underline{x}_0\right), \tag{6.5}$$

and

$$e_{rel} = \frac{e_{abs}}{\Re\left(\lambda^n \underline{x}_0\right)}, \tag{6.6}$$

where $\underline{x}^n_{model} = \left[\begin{array}{cccc} \underline{\Pi}^n_{model}, & \underline{\theta}^n_{model}, & \underline{w}^n_{model}, & \underline{\rho}^n_{model} \end{array}\right]^T$ denotes the numerical solution computed at time-step n by the 1D model initialised with the normal mode $\underline{x}_0$ as a perturbation of the basic state, and $\Re\left(\lambda^n \underline{x}_0\right)$ is the value predicted by the normal mode analysis.

For small values of the time-step ($\Delta t < 1\,s$) the numerical frequencies relative to the complex eigenvalues (i.e. those associated with the internal modes) computed numerically are also compared with the analytical ones defined in (5.8) and it is found that they agree well for frequencies up to $\omega_R \Delta t \approx 2.2$. This can be explained by recalling that the numerical frequencies are expected to converge to the analytical ones for Δt, $\Delta z \to 0$. In our runs $\Delta z = 300\,\mathrm{m}$, which for high frequency waves (smaller scales) is too large, compared with their wavelengths, to ensure convergence to the physical frequency, even for small values of the time-step Δt (since Δz does not tend to zero).

The numerical frequency computed as in (6.3) also provides the correct ordering of the internal modes: (5.8) shows that the physical frequency increases as the mode index m increases. Since there is a one to one correspondence between the numerical eigenmodes associated with the interior model levels and the analytic ones, the numerical eigenmodes can be ordered according to increasing values of the numerical frequency $\omega_R \Delta t$: this ordering provides the mode index m for the internal modes computed numerically, by analogy to the indexing of the corresponding physical internal modes. This feature enables us to identify the correspondence between the internal modes obtained in different runs of the model.

The normal modes computed numerically for the various top and bottom boundary conditions are presented in the following sections, starting with the case of θ active at the top and bottom.

6.1 Numerical normal modes with θ active at the top and bottom

The 1D model with an isothermal basic state and initial perturbations defined by one of the normal modes is first run with active top and bottom boundaries.

As an example of the internal modes, in Fig. 16 the $\underline{\Pi}$, $\underline{\theta}$, $\underline{\rho}$, and $\underline{w}$ numerical perturbations (i.e. numerical solution minus basic state values) computed by the 1D model for the normal mode of index $m = 3$ and for $\Delta t = 60\,\mathrm{s}$ are plotted at time-step $n = 13$. The numerical results, denoted by asterisks, are compared with the linear analysis (6.1) (solid line); the analytic continuous expression for the internal modes is given by (5.1) - (5.4).

There is good agreement between the computed and the predicted values for the $\underline{\Pi}$ and $\underline{w}$ components of the normal mode, whilst a weak discrepancy starts to appear in the $\underline{\rho}$ component, which is slightly affected by the introduction of the mode of index $2m$. The $\underline{\theta}$ component is again affected by the introduction of the mode of index $2m$, and dominated by it. The introduction of the mode of index $2m$ is consistent with what would be expected from a non-linear interaction of a mode with itself. In the case of the time-step $\Delta t = 60\,\mathrm{s}$ this effect starts to appear in the $\underline{\theta}$ component of the numerical mode at time-step $n = 11$ and remains as a persistent feature in all of the following steps.

The discrepancies observed in Fig. 16 may be ascribed to the non-linearity of the 1D column model: if the latter were linear, the evolution of the internal modes $\underline{x}^0 = \left[\begin{array}{cccc} \underline{\Pi}^0, & \underline{\theta}^0, & \underline{w}^0, & \underline{\rho}^0 \end{array} \right]^T$ when they are input as perturbations about its initial state would follow (6.1) and no discrepancies should be observed in the plots; but since the column model computes the non-linear evolution of the modes, differences between the perturbations computed by the 1D model and the linear analysis (6.1) are expected.

An error analysis is performed to verify whether the observed discrepancies are indeed due to the non-linearity of the 1D model. If the error of the model is non-linear, then we expect:

$$\underline{x}^n_{model} = \Re\left(\lambda^n \underline{x}^0\right) + O\left(\left(\underline{x}_{model}\right)^2\right), \tag{6.7}$$

where $\underline{x}_{model} \equiv \Re\left(\underline{x}^0\right)$, i.e. the real part of the mode $\underline{x}^0$, introduced as a perturbation to the initial state of the 1D column model. If the initial perturbations are then rescaled by the factor ϵ, the corresponding numerical solution computed by the 1D model becomes: $\underline{x}^n_{model,\epsilon} = \Re\left(\epsilon \underline{x}^0\right) = \epsilon \Re\left(\underline{x}^0\right)$, which, again if the model is nonlinear, can be expected to be:

$$\underline{x}^n_{model,\epsilon} = \epsilon \Re\left(\lambda^n \underline{x}^0\right) + O\left(\left(\epsilon \underline{x}_{model}\right)^2\right). \tag{6.8}$$

Using (6.5) - (6.6) and (6.7) - (6.8) the ratio between the relative errors obtained with and without rescaling the perturbations is expected to be given by:

$$\frac{e_{rel,\epsilon}}{e_{rel}} = \frac{O\left(\left(\epsilon \underline{x}_{model}\right)^2\right)}{\epsilon O\left(\left(\underline{x}_{model}\right)^2\right)} = O\left(\epsilon\right). \tag{6.9}$$

In order to verify whether the differences between the numerical results and their predicted value (6.1) are due to the non-linearity of the 1D column model only, the 1D model was first rerun with the same parameters, but using as initial perturbations the eigenmodes rescaled by a factor $\epsilon = 0.1$ (this is permissible, since the eigenmodes of a problem are defined only to within a multiplicative constant).

It is found (the results are not plotted) that when the perturbations are rescaled by the factor ϵ, the relative error is also rescaled by the same factor, as predicted by (6.9): this suggests that the errors observed are consistent with them being due to the non-linearity of the full 1D model.

Further tests were performed, varying the time-step, which was reduced down to $\Delta t = 1\,\mathrm{s}$, and increasing the semi-implicit weights up to $\alpha_2 = \alpha_4 = 1$: the non-linear evolution of the internal mode of index $m = 3$ computed by the 1D model run with different values of the time-step Δt and the same semi-implicit weights is plotted in Figs. 17 - 19.

In Fig. 17 the results obtained with a time-step $\Delta t = 30\,\mathrm{s}$ are plotted at time-step $n = 26$, which corresponds to the same physical time ($t_n = 780\,\mathrm{s}$) as in Fig. 16. Similarly to Fig. 16 there is good agreement between the non-linear evolution of the $\underline{\Pi}$ and $\underline{w}$ components of the internal mode computed by the 1D model and their linear evolution predicted by (6.1). The non-linear behaviour is still evident in the $\underline{\theta}$ component of the results, but no discrepancies between the numerical mode and the linear analysis are observed in the $\underline{\rho}$ one. The non-linear behaviour starts to appear at time-step $n = 13$ (even though it is plotted at time-step $n = 26$, in order to compare the results with those obtained with a time-step of $\Delta t = 60\,\mathrm{s}$). It is not as persistent at following time-steps as the $\Delta t = 60\,\mathrm{s}$ case, but it is visible in a number of the following steps.

In Fig. 18 the results obtained with a time-step $\Delta t = 10\,\mathrm{s}$ are plotted at time-step $n = 49$, which corresponds to the physical time ($t_n = 490\,\mathrm{s}$). Similarly to the results obtained with $\Delta t = 60\,\mathrm{s}$ and $\Delta t = 30\,\mathrm{s}$ plotted in Figs. 16 and 17 respectively there is good agreement between the numerical mode and the linear analysis (6.1). The non-linear behaviour is still

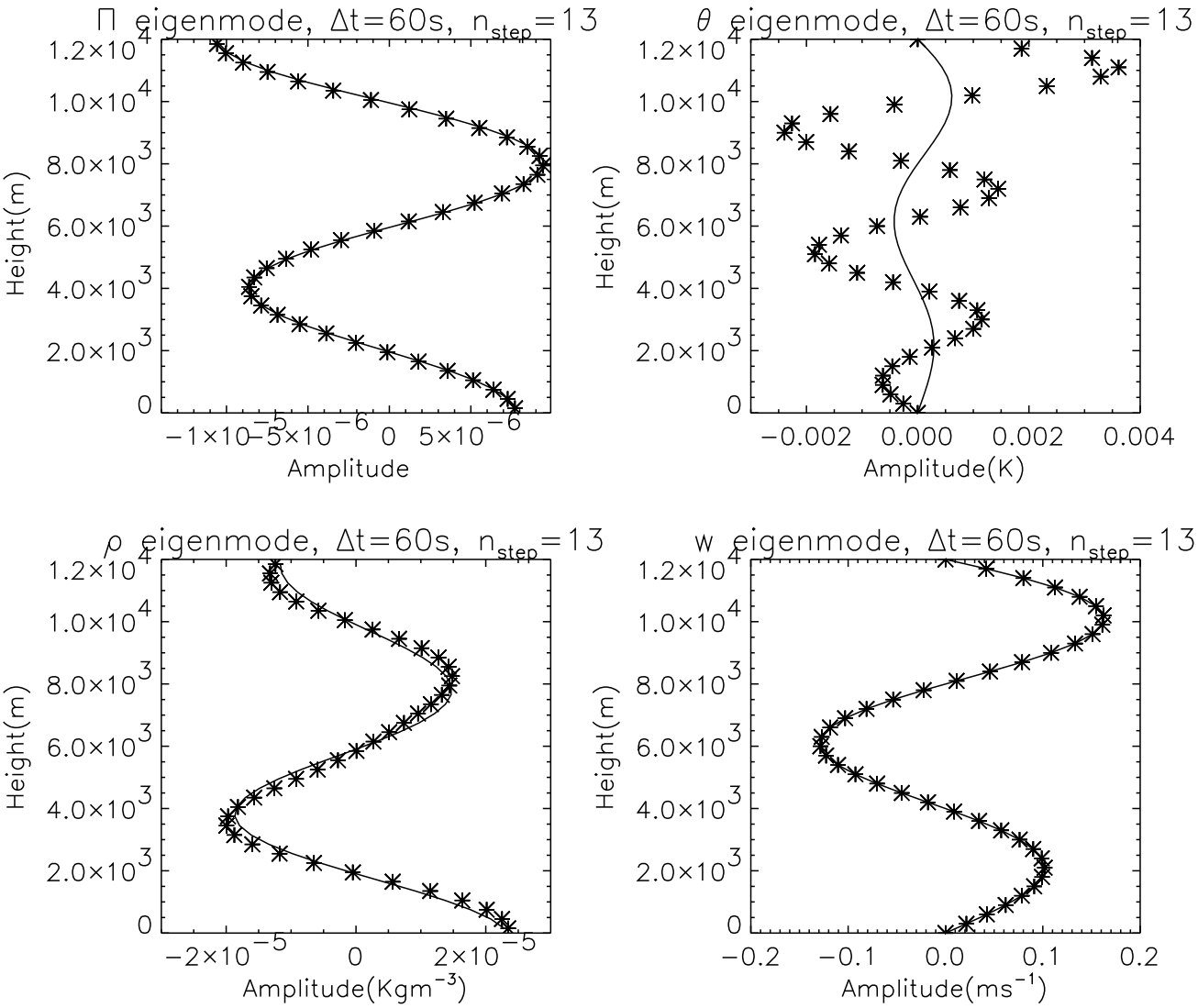

Figure 16: $\underline{\Pi}$, $\underline{\theta}$, $\underline{\rho}$, and $\underline{w}$ perturbations computed by the 1D model, with initial perturbation defined by the internal mode of index $m = 3$, and for a time-step $\Delta t = 60\,\mathrm{s}$, at time-step $n = 13$, corresponding to $t_n = 780\,\mathrm{s}$. The asterisks denote the numerical results, the continuous line represents the value predicted by the eigenvalue analysis, (6.1). The results are plotted against height ($z \in [0, 12000]$ m).

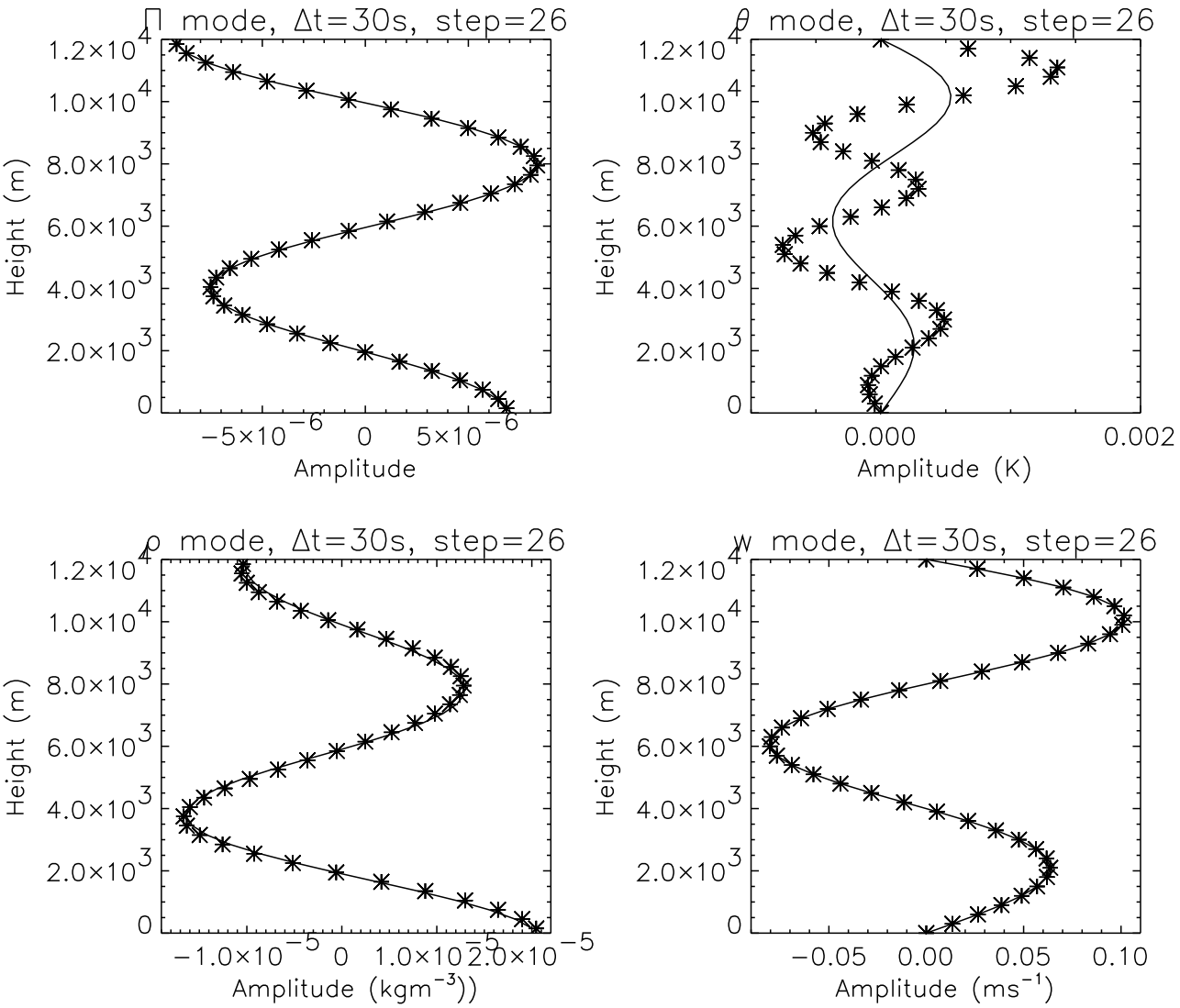

Figure 17: Same as in Fig. 16, but for $\Delta t = 30\,\mathrm{s}$ and time-step $n = 26$, corresponding to the same physical time $t_n = 780\,\mathrm{s}$

evident in the $\underline{\theta}$ component of the results, but as for $\Delta t = 30\,\mathrm{s}$ no discrepancies between the numerical mode and the linear analysis are observed in the $\underline{\rho}$ one. For $\Delta t = 10\,\mathrm{s}$ the non-linear effect starts to appear at time-step $n = 26$, corresponding to a physical time $t_n = 260\,\mathrm{s}$, again it is not persistent, it appears in a few of the following time-steps, but it is not observed at time-step $n = 13$, nor at the physical time $t_n = 780\,\mathrm{s}$, (when it is present for both the runs with $\Delta t = 60\,\mathrm{s}$ and $\Delta t = 30\,\mathrm{s}$).

Finally for $\Delta t = 1\,\mathrm{s}$ the nonlinear behaviour is only visible in a rare number of time-steps. As an example the results obtained at time-step $n = 907$, corresponding to a physical time $t_n = 907\,\mathrm{s}$ are plotted in Fig 19. Similarly to the previous examples (see Figs. 16 - 18) the numerical results generally agree well with the linear analysis except for the non-linear behaviour evident in the $\underline{\theta}$ component of the mode. Unlike the previous cases, a weak discrepancy between the numerical mode and the linear analysis appears also in the $\underline{\Pi}$ component, as well as the $\underline{\rho}$ one.

In summary, the numerical results computed varying the time-step exhibit good agreement between the non-linear evolution computed by the 1D column model and the corresponding linear analysis (6.1), with the non-linear behaviour appearing consistently in all the runs and primarily in the $\underline{\theta}$ components of the modes. In order to understand which of the terms could be responsible for the observed non-linear behaviour, and why its effect appears to be much more evident in the $\underline{\theta}$ components of the normal modes, the non-linear equations (in particular the thermodynamic one) have been compared with their linear approximations, but the answer is not obvious. The speculation is that the non-linear terms may be compounding each other in the thermodynamic equation, whilst (partly) cancelling each other in the others.

The runs differ in the physical time and the number of time-steps required for the non-linear behaviour to manifest itself - in general it takes a larger number of time-steps for the non-linearity to appear as the time-step is reduced. This is thought to be due to the fact that the same normal mode of the problem (the one of index $m = 3$ in the figures) has a smaller non-dimensional numerical frequency $\omega_R \Delta t$ (as computed in (6.3)) as the time-step Δt is reduced, so that it is less prone to the non-linear effect. For example, the non-dimensional numerical frequencies corresponding to the results plotted in Figs. 16 - 19 are as follows.

For $\Delta t = 60\,\mathrm{s}$ the numerical non-dimensional frequency of the internal mode of index

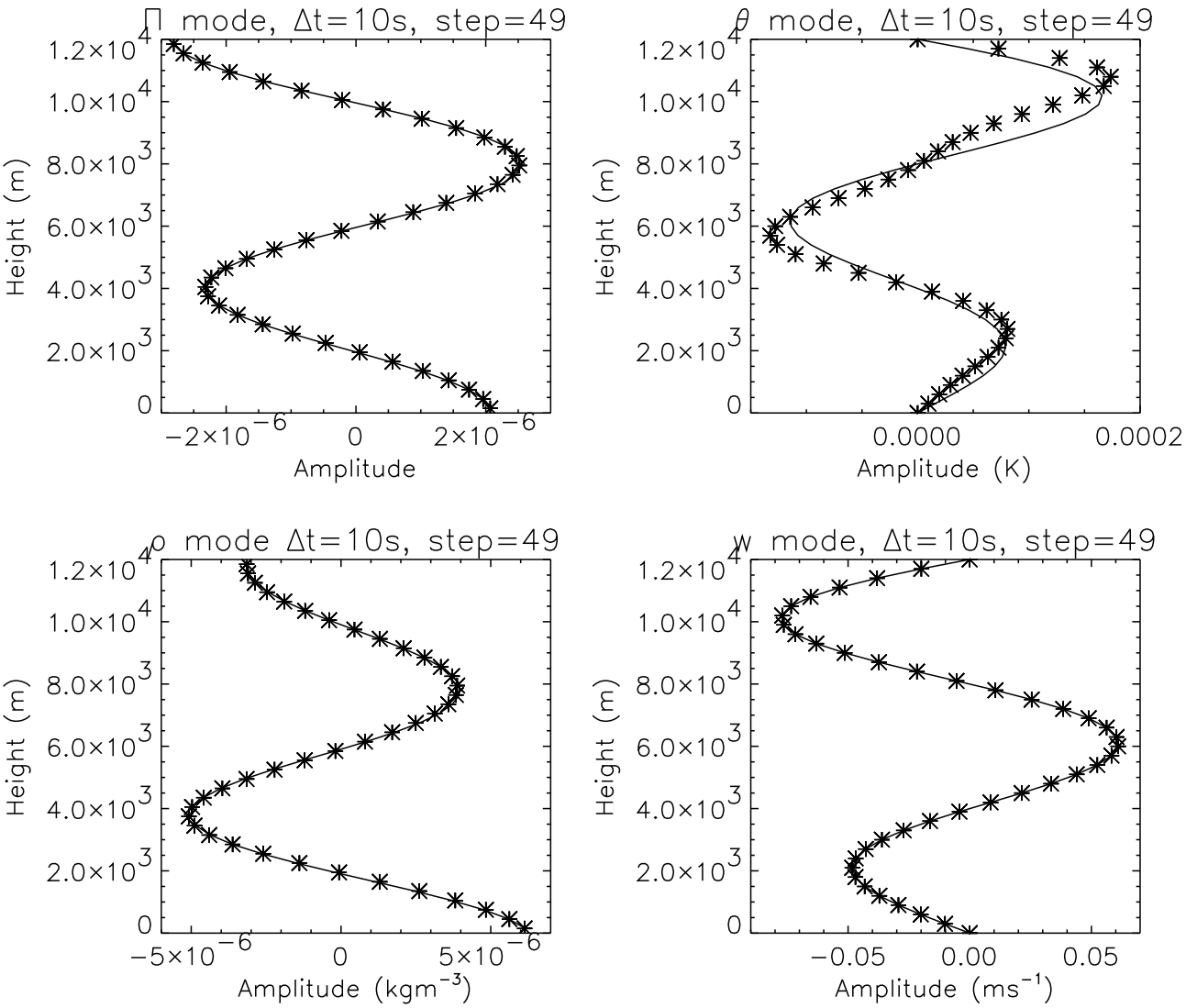

Figure 18: Same as in Figs. 16 and 17, but for $\Delta t = 10\,\mathrm{s}$ and time-step $n = 49$, corresponding to a physical time $t_n = 490\,\mathrm{s}$.

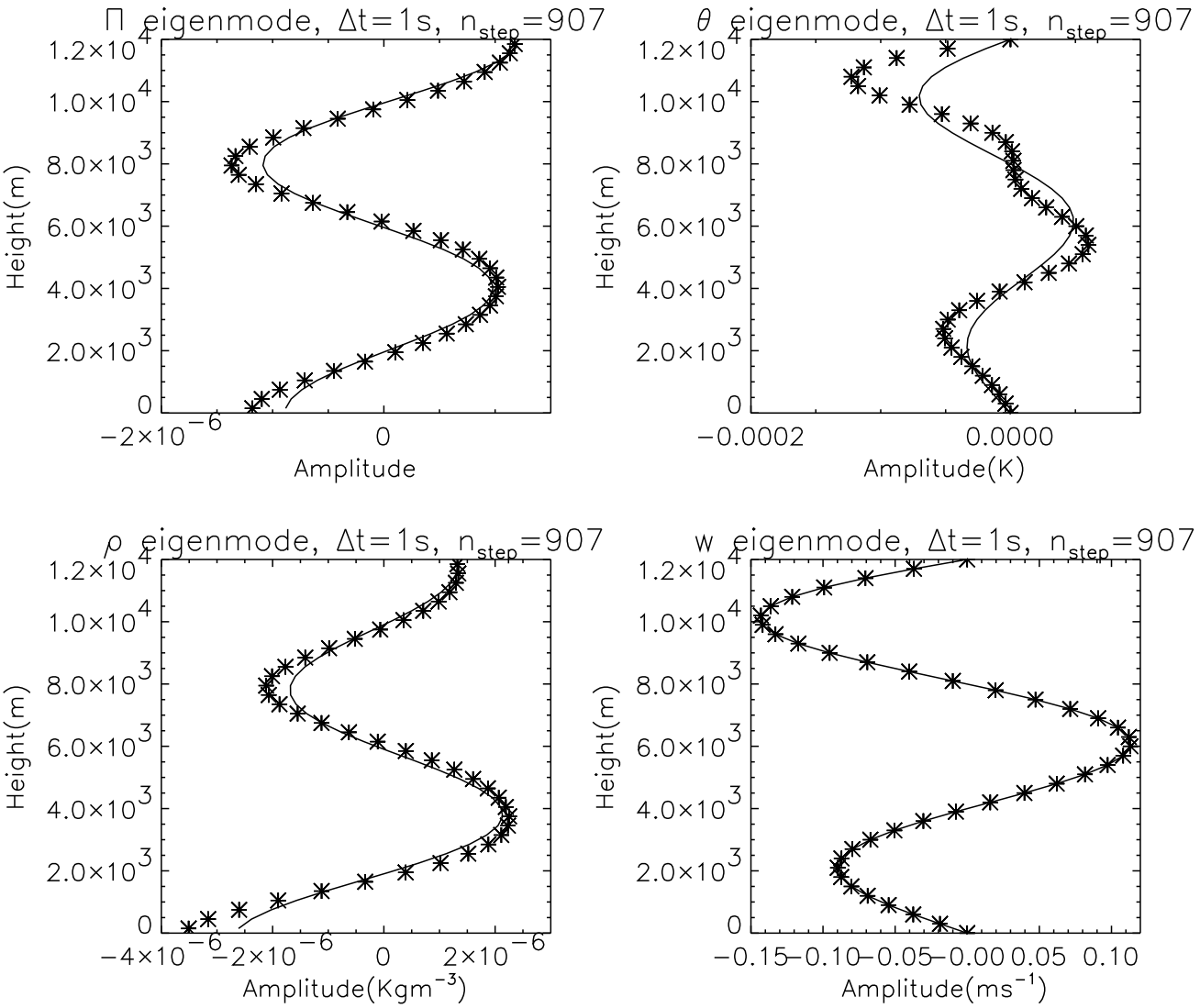

Figure 19: Same as in Figs. 16 - 18, but for $\Delta t = 1\,\mathrm{s}$ and time-step $n = 907$, corresponding to a physical time $t_n = 907\,\mathrm{s}$.

$m = 3$ computed using (6.3), is $\omega_R \Delta t \approx 2.9$, corresponding to a frequency of $\omega_R = 0.048\,\mathrm{s}^{-1}$, the number of time-steps required to complete an oscillation cycle of the mode (computed using (6.2)) is $N_{cycle} \approx 2.17$, and the non-linear effects start to appear at time-step $n = 11$.

For $\Delta t = 30\,\mathrm{s}$ the numerical non-dimensional frequency of the internal mode of index $m = 3$ is $\omega_R \Delta t \approx 2.43$, corresponding to a frequency of $\omega_R = 0.08\,\mathrm{s}^{-1}$, the number of time-steps required to complete a mode cycle is $N_{cycle} \approx 2.37$, and the non-linear effects start to appear at time-step $n = 13$.

For $\Delta t = 10\,\mathrm{s}$ the numerical non-dimensional frequency of the internal mode of index $m = 3$ is $\omega_R \Delta t \approx 1.86$, corresponding to a frequency of $\omega_R = 0.186\,\mathrm{s}^{-1}$, the number of time-steps required to complete a mode cycle is $N_{cycle} \approx 3.38$, and the non-linear effects start to appear at time-step $n = 26$.

For $\Delta t = 1\,\mathrm{s}$ the numerical non-dimensional frequency of the normal mode of index $m = 3$ is $\omega_R \Delta t \approx 0.27$, corresponding to a frequency of $\omega_R = 0.27\,\mathrm{s}^{-1}$, the number of time-steps required to complete a mode cycle is $N_{cycle} \approx 23.56$ and the non-linearity is so weak that it is only visible in an occasional number of time-steps.

It is also worth noting that the non-linear behaviour starts to appear at a later time-step than the number of steps required to complete a cycle of the mode. The non-linearity of the full 1D column model therefore introduces a behaviour non-periodic in time in the otherwise periodic linear normal modes.

Although the results plotted in Figs. 16 - 19 are relative to the normal mode of index $m = 3$, the evolution of a number of other modes has been examined for all the runs with different time-steps Δt and their behaviour is found to be similar, with the non-linear effects being more pronounced and more persistent for higher frequencies $\omega_R \Delta t$. However, for the purposes of comparing the results when varying the parameters of the runs and the top and bottom boundary conditions, the mode of index $m = 3$ has been chosen as representative and the attention has been focussed on it.

The external modes are real and are associated with eigenvalues $\lambda \approx 1$ (i.e. $\omega_R = 0$). In all of the runs performed for which the time-step Δt is varied, some of the eigenvalues are found to exceed unity, but only in the 12^{th} or 13^{th} decimal places, the latter being found for the runs with $\Delta t = 10\,\mathrm{s}$ or with the isentropic bottom boundary condition. It is therefore impossible to decide whether these eigenvalues genuinely have magnitude greater than unity, which

would indicate an instability of the model for the present choice of parameters, or whether their amplitude is due to round-off error.

The behaviour of the external modes is similar in all the runs for different time-steps Δt. As an example, the numerical perturbations computed by the 1D model when one of the external modes is introduced as initial perturbation on the isothermal basic state is shown in Fig. 20 at step $n = 1$ for the run with a time-step $\Delta t = 60\,\mathrm{s}$.

Consistent with the analytic discrete expression for the external modes (5.26) - (5.29), at the initial time the external modes are found to have: $w_k = O\left(10^{-11}\right)$, for $k = 1, ..., N-1$; Π_k arbitrary, for $k = 1/2, ..., N-1/2$; and the $\underline{\theta}$ and $\underline{\rho}$ components in agreement with (5.28) and (5.29), with maximum differences from the analytic values of the order $O\left(10^{-11}\right)$.

If the 1D model were linear, then since the eigenvalues associated with the external modes are $\lambda \approx 1$, the initial perturbations (i.e. the external modes) should remain approximately constant throughout the run of the 1D model. In the tests it is however observed that the $\underline{\Pi}$, $\underline{\theta}$, and $\underline{\rho}$ components of the external modes remain constant, whereas the $\underline{w}$ components attain a value of the order $O\left(10^{-5}\right)$ at the first step, after which they appear to oscillate with an amplitude decreasing at each time-step. (For example, the value of the $\underline{w}$ component of the external mode computed with $\Delta t = 60\,\mathrm{s}$ and shown in Fig. 20 after 1 time-step, is reduced by an order of magnitude after 100 time-steps.)

This perturbation observed in the $\underline{w}$ components of the external modes is believed to be introduced by the non-linearity of the 1D model, as is verified by means of an error analysis similar to that performed for the internal modes at the beginning of the present section. Namely the runs are repeated after rescaling the initial perturbations by a factor $\epsilon = 0.1$ and it is found that the relative errors in the $\underline{w}$ components of the external modes computed in the rescaled run are reduced by a factor ϵ with respect to those of the original run. Using (6.7) - (6.9), where the real part $\Re$ can be omitted, since the external modes are real, this implies that the perturbation observed in the $\underline{w}$ components of the external modes is consistent to it being due to the non-linearity of the 1D model.

The damping effect observed in the non-linear response of the 1D model (combined with the oscillatory behaviour) is possibly due to the small off-centring of the semi-implicit discretisation ($\alpha_2 = \alpha_4 = 0.51$).

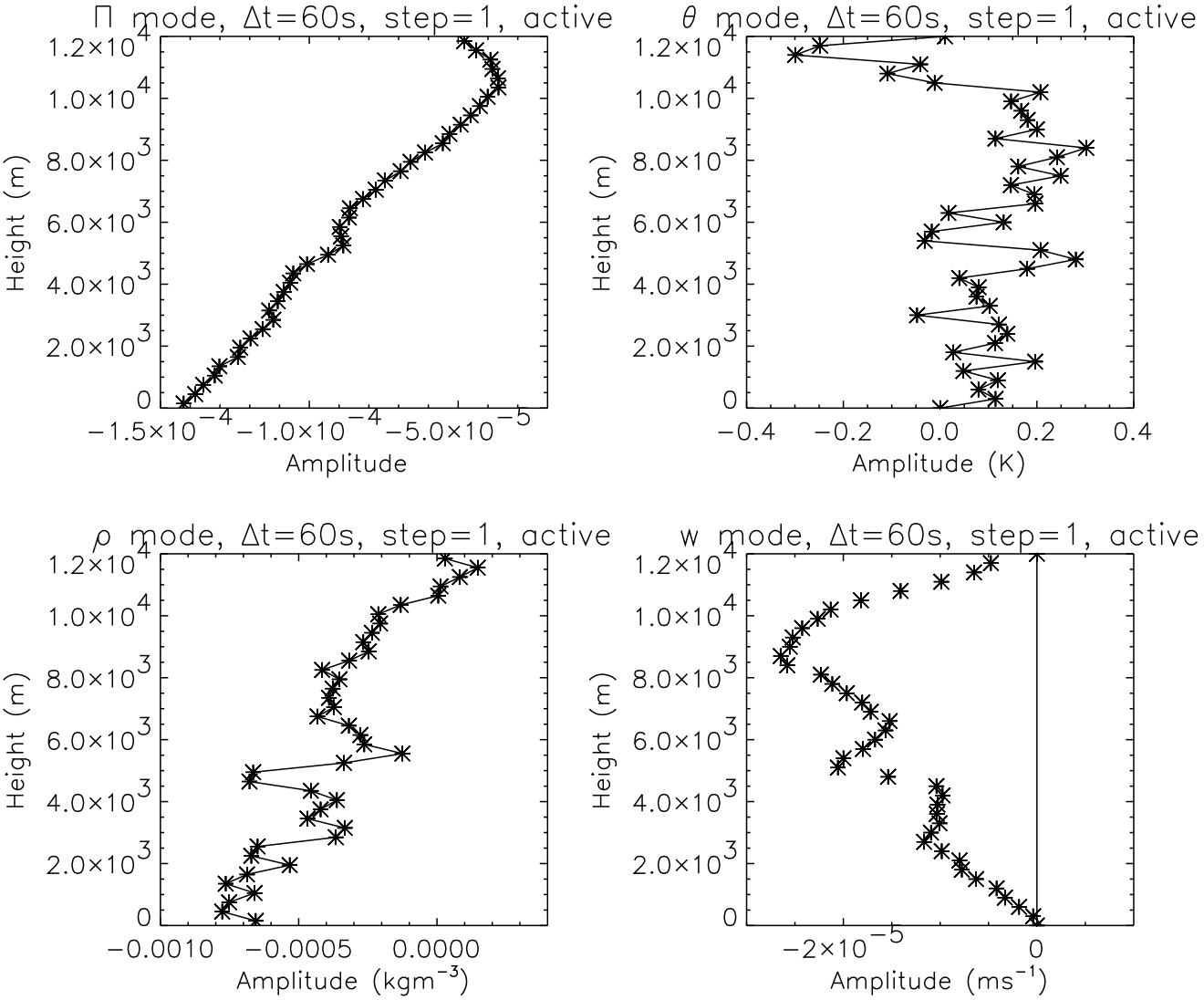

Figure 20: $\underline{\Pi}$, $\underline{\theta}$, $\underline{\rho}$, and $\underline{w}$ and perturbations computed at the first step by the 1D model having one of the external modes as initial perturbation and run with a time-step $\Delta t = 60\,\mathrm{s}$.

6.2 Numerical normal modes with non-active boundary conditions

The runs performed using active boundary conditions, the results of which are summarised in Section 6.1, have been repeated using the non-active boundary conditions, and the results computed for internal and external modes using the three types (active, isentropic bottom, isothermal top) of boundary conditions have been compared. The modes are used to initialise the 1D column model, which is run with a value of the off-centring parameter of $\alpha = 0.51$, for a time-step of $\Delta t = 10\,\mathrm{s}$, $\Delta t = 30\,\mathrm{s}$, or $\Delta t = 60\,\mathrm{s}$.

The external modes, for which the results are not plotted, exhibit a behaviour similar to that of the active boundaries case, an example of which is shown in Fig. 20: with the small value of the off-centring parameter $\alpha = 0.51$ used in the runs, the external modes are associated with the real eigenvalue $\lambda \approx 1$ (i.e. $\omega_R = 0$), and they are approximately stationary, apart from a non-linear oscillation in their $\underline{w}$ components.

The main difference between the external modes computed with the various boundary conditions is their number: there is one less when the isentropic bottom boundary condition is used.

As mentioned at the beginning of Section 6, when the isentropic bottom boundary condition is used in the form

$$\theta^{n+1}\Big|_{z_0 \equiv 0} = \theta^{n+1}\Big|_{z_1}\,, \tag{6.10}$$

an extra spurious mode is found with respect to the case of θ active at the bottom, due to the isentropic bottom boundary condition being imposed at time level $n+1$, so that the matrix B has one extra null row and therefore an extra $\lambda = 0$ eigenvalue. As in the case of the active boundaries, there are $N-1$ complex conjugate pairs of modes, corresponding to $N-1$ internal modes, one for each of the interior integer model levels, but there are now only $N+1$ (real) external modes, as opposed to the $N+2$ of the θ active case: one of the real modes is lost in favour of the spurious one introduced by the boundary condition.

This is consistent with the fact that when the active or the isothermal top boundary conditions are used, the number of degrees of freedom associated with the external mode is given by $N+2$: N of these are introduced by the $\underline{\Pi}$ component of the modes, which is arbitrary for the external modes, and two by the values of potential temperature at the top and bottom boundaries of the domain, where θ is let free to be advected with the horizontal flow.

By contrast, when the active boundary condition is used, the value of θ at the bottom of the domain is no longer arbitrary, but it is prescribed by (6.10), so that the number of degrees of freedom associated with the external modes is reduced to $N+1$.

The behaviour of the internal modes computed using the active or non-active boundary conditions is investigated by comparing first their linear evolution:

$$L^n = \Re\left(\lambda^n \underline{x}^0\right). \tag{6.11}$$

This comparison is meaningful since in Section 6.1 it was found that the linear evolution of the modes with active boundary conditions agrees with the non-linear one computed by the 1D column model apart from the non-linear effects, so that the linear evolution (6.11) provides a reliable guideline for the analysis of the results.

Since differences between the linear and non-linear evolutions were however observed in the modes computed using the active boundary conditions, it is also worth investigating the impact of the various boundary conditions on the non-linear response of the 1D model. This is done by comparing:

$$(NL)^n = \underline{x}^n_{model} - L^n, \tag{6.12}$$

i.e. the difference between the non-linear and linear evolution, for the internal modes computed with: active boundary conditions; isentropic bottom boundary condition; and isothermal top layer.

Further the phase of the modes has been computed by determining the indices of the time-steps at which the amplitude of the linear evolution of each of the components of the modes attains a maximum in magnitude, which is defined as

$$\left|\underline{y}\right| = \left(\sum_{l=1}^{N_y} |y_l|^2\right)^{1/2} \tag{6.13}$$

for each of the components, $\underline{y} = \left\{\underline{\Pi}, \underline{\theta}, \underline{\rho}, \underline{w}\right\}$ considered separately. N_y in (6.13) corresponds to $N+1$ or N, for variables held at integer or half-integer model levels respectively. The linear rather than the non-linear evolution of the modes is used to determine the phase, in order for the results not to be affected by the non-linear behaviour of the modes, which has been already been observed and discussed in Section 6.1 in the case of the active boundary conditions.

In all the runs the $\underline{w}$ component is found to have a phase different to that of the $\underline{\Pi}$, $\underline{\theta}$, and $\underline{\rho}$, which are in phase. The modes computed using the same time-step Δt have the same phase for all the boundary conditions: varying the boundary conditions affects the amplitude but not the phase of the modes.

In all the runs and at most of the time-steps it is found that the linear evolutions of the internal modes computed with the various boundary conditions are practically identical in the interior of the domain, with some differences at the boundaries. These are minor and limited to the lowest layer only when the isentropic bottom boundary condition is used, but are larger and limited to the upper layers of the domain (but not necessarily the uppermost only) when the isothermal top boundary condition is used. At a few time-steps however differences in the amplitude of the internal modes, which are larger as the time-step Δt is reduced, are also visible both at the boundaries and in the interior of the domain.

As an example of the results, the linear evolution of the internal mode of index $m = 3$ computed at time-step $n = 116$ using the active and non-active boundary conditions and $\Delta t = 30\,\mathrm{s}$ is plotted in Fig. 21. The active case is denoted by the solid line, the isentropic bottom boundary condition is represented by the plus symbols, and the isothermal top layer by the dashed line. This time-step is chosen to illustrate the results instead of $n = 26$, at which the comparison between the linear and non-linear evolution of the mode computed with the active boundary conditions was illustrated in Fig. 17. This choice is due to the fact that $n = 116$ is one of the time-steps at which the differences between the linear evolutions of the mode computed with the three types of boundary conditions are most evident.

The evolutions of the $\underline{w}$ component of the mode appear to be very similar for all the boundary conditions used. In the other components differences are observed: in the $\underline{\Pi}$ and $\underline{\rho}$ components the differences in the linear evolutions are similar both at the boundaries and in the interior of the domain, whereas in the $\underline{\theta}$ component the largest difference is introduced by the isothermal top layer at the top of the domain: a peak value of $\theta = -1.3 \times 10^{-5}\,\mathrm{K}$ is attained at level $N - 1$. This is not plotted in the figure, where the scale has been limited in order to show the differences between the various modes, which would not be clearly visible on a larger scale.

Next the non-linear response of the model is examined, which is the difference between the non-linear evolution of the internal modes computed by the 1D column model and the

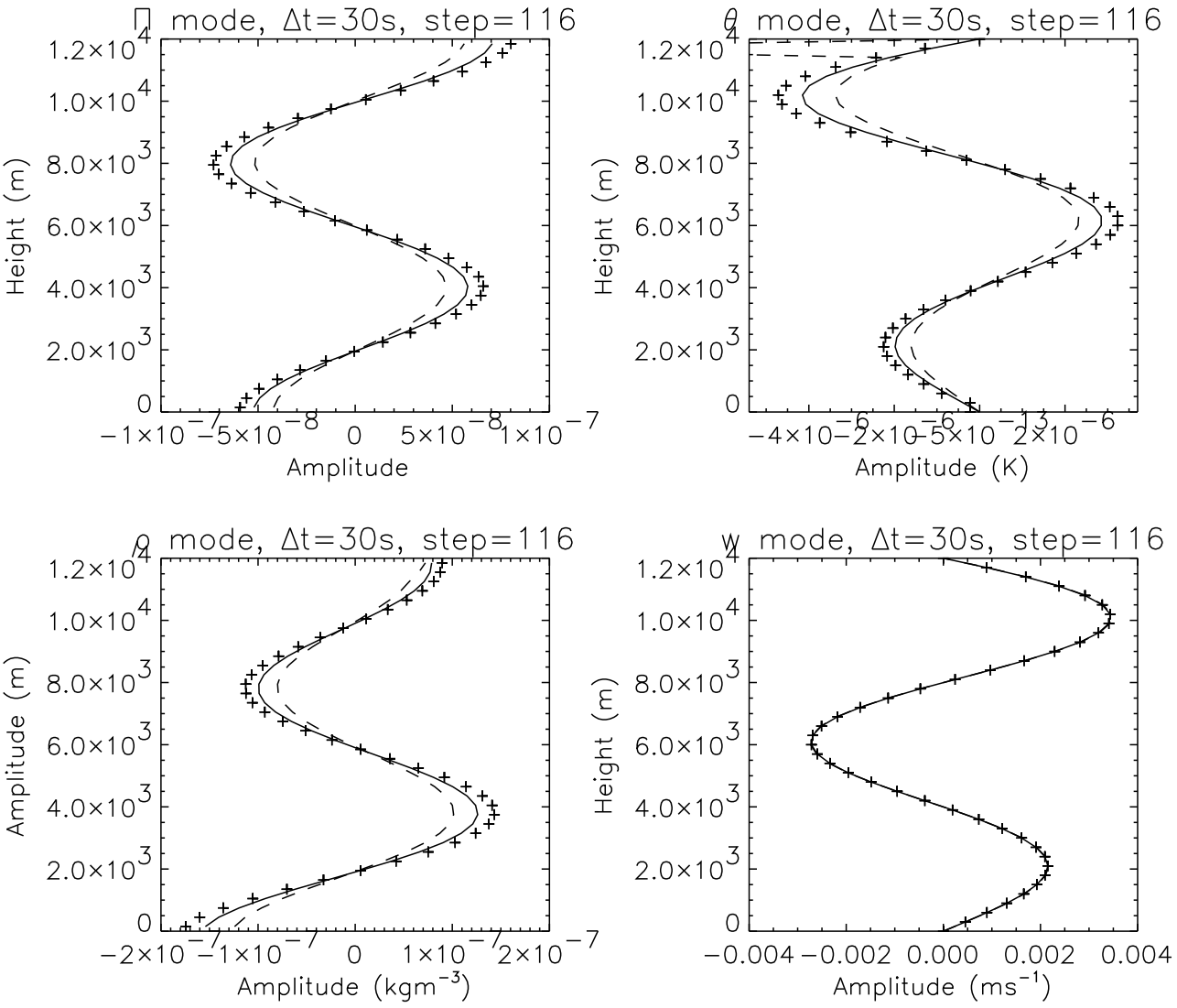

Figure 21: Linear evolution L^n (cf. (6.11)) of the internal mode of index $m = 3$ computed at time-step $n = 116$ with $\Delta t = 30\,\mathrm{s}$, and using: the active boundary conditions (solid line), the isentropic bottom boundary condition (plus symbols), and the isothermal top layer (dashed line).

linear evolution predicted by the normal mode analysis, $(NL)^n$ defined in (6.12).

In general the boundary conditions appear to have a bigger impact on the non-linear response of the 1D model, rather than on the linear evolution displayed in the previous figures and in both the linear and the non-linear evolutions larger differences are introduced by the isothermal top layer, which propagate from the top boundary throughout the domain.

The amplitude of the non-linear response of the modes computed with the non-active boundary conditions is generally larger than that of the active boundaries modes, with the isothermal being the largest. Since the non-linear response (6.12) is given by the difference between the non-linear evolution computed by the 1D model and the linear evolution predicted by the normal mode analysis, this means that the non-active boundary conditions enhance the non-linear effects already observed in the non-linear evolutions of the modes computed by the 1D model using the active boundary conditions and illustrated in Section 6.1.

As an example of the results, the non-linear response computed for the mode of index $m = 3$ and with $\Delta t = 30\,\mathrm{s}$ is plotted in Fig. 22 at time-step $n = 116$, for which the corresponding linear evolution is displayed in Fig. 21. In Fig. 22 the non-linear response computed with the active boundaries are denoted by the solid line, that computed with the isentropic bottom boundary condition is identified by plus symbols, and that computed with the isothermal top boundary condition is denoted by the dashed line.

In all the components of the mode, the largest differences between the non-linear evolutions of the mode are introduced by the isothermal top layer, and are distributed throughout the domain, with larger peaks at the top. These are no longer limited to the $\underline{\theta}$ component, as for the linear evolution, but are present in all of them. The $\underline{\Pi}$ component attains a value of $\Pi = -0.0015$ at level N, i.e. the top boundary of the domain; for the $\underline{\theta}$ component the peak value is $\theta = -1.37\,\mathrm{K}$ at level $N - 1$; the $\underline{\rho}$ component reaches $\rho = -0.00024\,\mathrm{kg\,m^{-3}}$ at level $N - 3/2$ and $\rho = 0.0018\,\mathrm{kg\,m^{-3}}$ at level $N - 1/2$; and the $\underline{w}$ component attains the values $w = -0.02\,\mathrm{m\,s^{-1}}$ at level $N - 3$ and $w = 2.37\,\mathrm{m\,s^{-1}}$ at level $N - 1$. The non-linear evolution computed using the isentropic bottom boundary condition also differs from that of the active case in the $\underline{\Pi}$, $\underline{\rho}$, and $\underline{w}$ components, although this is not clearly visible in the plots.

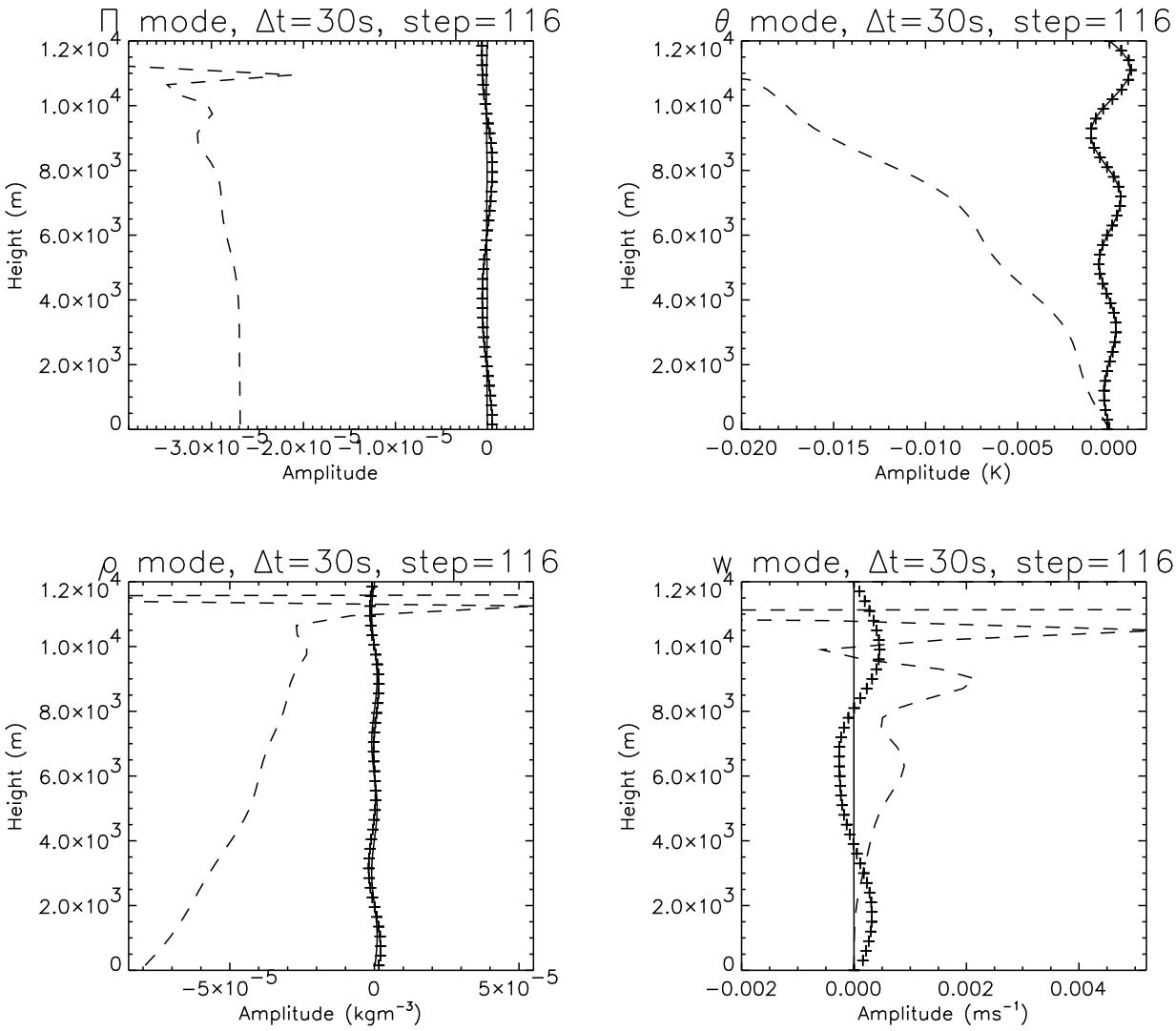

Figure 22: Non-linear response $(NL)^n$ (cf. (6.12)) of the mode of index $m = 3$, computed at time-step $n = 116$, with $\Delta t = 30\,\mathrm{s}$. The corresponding linear evolution is plotted in Fig. 21.

6.3 Numerical normal modes with the isentropic boundary condition imposed within a thin bottom layer

In Section 6.2 the impact of the non-active boundary conditions on the behaviour of the normal modes of the 1D isothermal basic state New Dynamics was discussed. It was found that the accuracy of the numerical results is seriously affected by the isothermal top boundary condition, particularly in the non-linear response of the 1D model (see Fig. 22). The isentropic bottom boundary condition was found to introduce smaller inaccuracies. In the linear response of the 1D model, at most time-steps these are limited to the lowest layer of the model, although there are examples (see Fig. 21) in which they are distributed throughout the domain. In the non-linear response (see Fig. 22) the inaccuracies are present in the whole domain, but they remain small.

The object of the present section is to test whether the inaccuracies introduced by the isentropic bottom boundary condition can be reduced by imposing it within a very thin layer added at the bottom of the domain.

For this purpose the uniform vertical grid of Section 6 has been extended by an extra layer of depth one tenth of the other layers. The original domain, with top and bottom boundaries respectively set at $z_0 = 0$ and $z_T = 12000\,\mathrm{m}$ is now discretised using 41 vertical levels. The first interior integer level is set at $z_1 = 30\,\mathrm{m}$, the remaining 39 integer levels are uniformly distributed as before, from $z_2 = 300\,\mathrm{m}$ to the top of the domain, with an increment of $\Delta z = 300\,\mathrm{m}$. The first half-integer model level is set at $z_{1/2} = 15\,\mathrm{m}$, the second one at $z_{3/2} = 150\,\mathrm{m}$ and the remaining 38 are placed half-way between two adjacent integer model levels.

Note that with the definition of the grid described above, the half-integer level of index $k = 3/2$ is not placed half-way between the integer levels of indices $k = 1$ and $k = 2$. This definition was chosen in order to preserve the same distribution of the integer and half-integer model levels as in the original uniform grid, apart from the addition of the extra levels set at $z_{1/2} = 15\,\mathrm{m}$ and $z_1 = 30\,\mathrm{m}$. This was done to compare the results obtained using the isentropic boundary condition imposed within the extra thin bottom layer with those computed previously with the active or the standard isentropic boundary conditions. As in the previous tests, the time-step has been varied from $\Delta t = 60\,\mathrm{s}$ down to $\Delta t = 10\,\mathrm{s}$.

The linear evolution of the modes (defined in (6.1)) has been used for the comparison: this

is meaningful, since it has been verified in Section 6.2 that the linear evolution of the modes provides a good estimate of the linear response of the 1D model. The non-linear response of the model has not been examined, since the flexibility of adding an extra arbitrary thin layer to the grid of the 1D column model is not available as a switch.

In the previous sections it was found that the linear evolutions of the modes computed using the three types (active; isentropic bottom; and isothermal top) of boundary conditions were almost coincident at most time-steps, apart from minor inaccuracies introduced by the isentropic boundary condition at the bottom of the domain, and larger ones introduced by the isothermal boundary condition at the top. Some time-steps were however found (see Fig. 21) at which the linear evolutions of the modes computed using the various boundary conditions exhibit small differences among themselves, distributed throughout the domain.

When the isentropic boundary condition is imposed within the extra thin bottom layer, at most time-steps (those at which the linear evolution computed with the standard boundary conditions were coincident) the linear evolution of the modes appears to be similar to those computed with the active or with the standard isentropic boundary conditions, although some small differences can be observed. An example of these results is shown in Fig. 23, where the linear evolution of the internal mode of index $m = 3$ computed with $\Delta t = 30\,\mathrm{s}$ is plotted at time-step $n = 26$. This is the same time-step for which the linear and non-linear evolutions computed using active boundary conditions were shown in Fig. 17.

In Fig. 23 the solid line denotes the results computed using active boundary conditions, the pluses denote the results computed with the standard isentropic bottom boundary condition, and the crosses those computed with the isentropic boundary condition imposed within the extra thin bottom layer. The linear evolution of the mode computed using the standard isentropic boundary condition is almost coincident with that computed using the active boundary condition, whilst that computed imposing the isentropic boundary condition within the extra thin bottom layer appears to be slightly less accurate, although the differences are very small. This is likely to be due to the fact that, with the introduction of the thin layer at the bottom of the domain, the vertical grid is no longer uniform in the two lowest layers. The difference operators appearing in the discretisation associated with the isentropic boundary condition imposed within the extra layer are therefore less accurate than those appearing in the discretisation associated with the active or standard isentropic

boundary conditions, which is based on a uniform grid.

In Fig. 24 an example is plotted of the results computed at a time-step at which the linear evolutions of the modes computed using the standard boundary conditions were found to differ slightly among themselves (see Fig. 21). In Fig. 24 the results computed for the same parameters of Fig. 21, $\Delta t = 30\,\mathrm{s}$ at time-step $n = 116$, but imposing the isentropic boundary condition within the extra thin bottom layer (denoted by the crosses) are compared with those obtained using the active (solid line) and the standard isentropic (pluses) boundary conditions. In this case the linear evolution of the mode computed imposing the isentropic boundary condition within the extra thin bottom layer is slightly different from that computed using the active boundary condition, but the differences appear to be generally smaller than those introduced by the standard isentropic boundary condition, apart from those observed in the $\underline{w}$ component of the mode.

In conclusion, imposing the isentropic boundary condition within an extra thin layer introduced at the bottom of the domain, as opposed to maintaining the vertical grid uniform and imposing isentropy within the bottom layer of the grid does not generally have a significant positive impact on the results. At most time-steps the thin bottom layer appears to degrade slightly the accuracy of the results, due to the grid being no longer uniform, so that the accuracy of the discrete operators appearing in the discretisation is reduced from second to first order. However at the few time-steps at which the linear evolution of the modes computed using the standard isentropic bottom boundary condition was found to differ from that computed using the active boundary condition, imposing isentropy within the thin layer added at the bottom of the domain seems to slightly improve the results. In this case the $\underline{\Pi}$, $\underline{\theta}$, and $\underline{\rho}$ components of the linear evolution of the mode appear to be slightly closer to those computed using the active boundary condition than those computed using the standard isentropic boundary condition. It should be noted though that the results discussed in this section have been obtained comparing the linear evolution of the modes only. Therefore no conclusions can be drawn on the effect of imposing the isentropic boundary condition in the extra thin bottom layer on the *non-linear* response of the 1D column model.

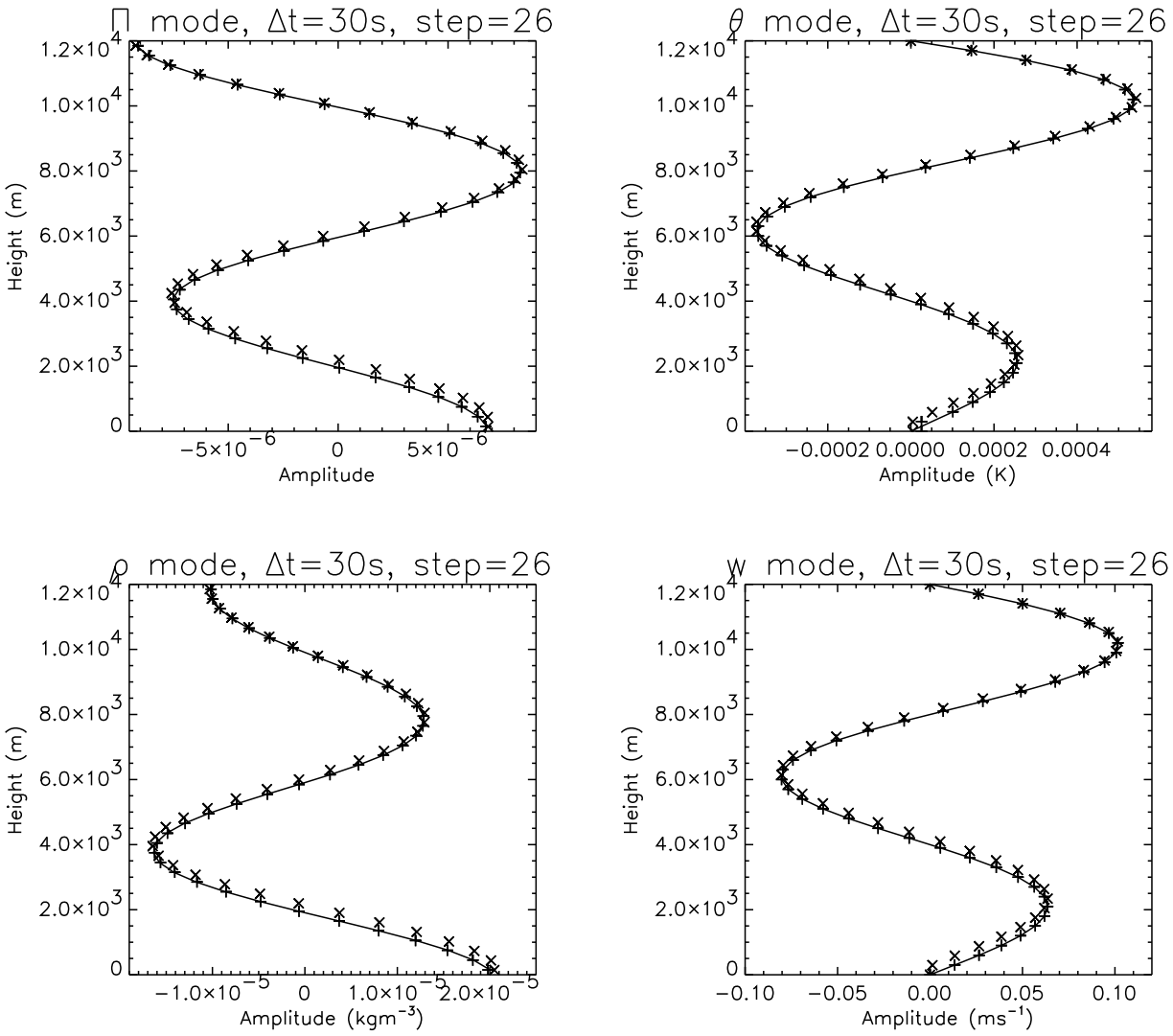

Figure 23: Linear evolution of the internal mode of index $m = 3$ computed with $\Delta t = 30\,\mathrm{s}$ at time-step $n = 26$. The results are computed using: the active boundary condition (solid line); the standard isentropic boundary condition (pluses); and the isentropic boundary condition imposed within the extra thin bottom layer (crosses).

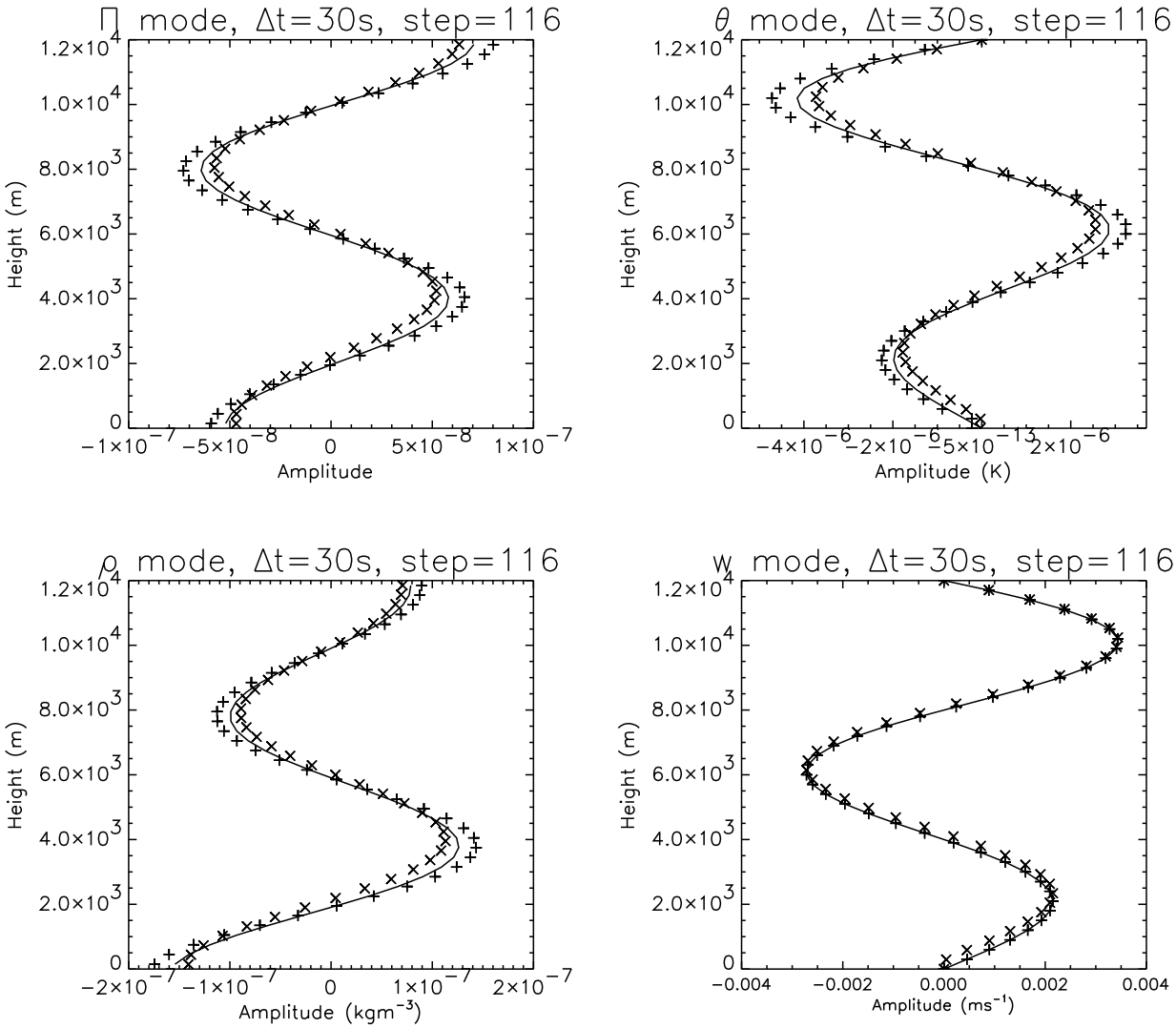

Figure 24: Same as in Fig. 24, but plotted at time-step $n = 116$.

7 Summary

In summary, a general 2D framework has been established to perform the normal mode analysis of the New Dynamics. This has lead to the development of a suite of $Fortran90$ programs to compute the numerical eigenvalues and normal modes of the discretisations, using NAG library routines.

The normal mode model has been applied to the analysis of the numerical properties of the 1D version of the New Dynamics in the cases of an isentropic and an isothermal basic state.

It is found that the eigenvalues and normal modes of the 1D New Dynamics with an isentropic basic state agree with the analytic ones, which are known in this particular case.

In the isothermal basic state case, the normal modes have been used to initialise the 1D column model, which is run using three types (active, isentropic bottom, and isothermal top) of boundary conditions.

In the case of active boundary conditions, the non-linear evolution computed by the 1D model is compared with the linear evolution predicted by the normal mode analysis, and it is found to agree in general, apart from the discrepancies due to the non-linearity of the 1D model. The linear evolution of the modes predicted by the normal mode analysis can therefore be considered a good estimate of the linear response of the 1D model.

Next the impact of the different boundary conditions (active, isentropic bottom, and isothermal top) on the behaviour of the modes is assessed by first comparing among themselves the linear evolutions of the modes computed using the three types of boundary conditions, for internal and external modes. Further, for internal modes, the non-linear evolutions computed using the various boundary conditions are also compared among themselves.

It is found that the behaviour of the external modes is similar for all the boundary conditions tested: the external modes are approximately stationary, as predicted by the linear normal mode analysis, apart from an oscillation in the $\underline{w}$ component, believed to be due to the non-linearity of the 1D model. The main difference is in the number of external modes: when the isentropic bottom boundary condition is used there is one less, since then one of the external modes is lost in favour of a spurious one, but apart from this, the boundary conditions do not affect the external modes present in each case.

For the internal modes, in general, it is found that the linear evolutions computed using

both the active and non-active boundary conditions are very similar at most time-steps, with small differences introduced at the bottom by the isentropic boundary condition, and more pronounced differences in the top layer, when this is assumed to be isothermal.

Unlike the linear evolutions, the non-linear responses $(NL)^n = \underline{x}^n_{model} - L^n$ of the internal modes differ in general among themselves when the boundary conditions are varied. This means that the boundary conditions have a larger impact on the non-linear response of the 1D model than on the linear one. This result suggest that the differences between the results obtained in the runs of the 1D model when the various boundary conditions were varied and discussed in BC1D were mainly due to the non-linear interaction between the boundary conditions and the 1D column model.

Further, in general it is found that the amplitude of the non-linear evolution of the internal modes computed using the non-active boundary conditions is larger than that computed using the active boundary conditions, that of the isothermal top layer case being generally the largest. This means that the non-active boundary conditions (and more so the isothermal top boundary condition) enhance the non-linear effects of the 1D model already observed in the active boundary condition case and discussed in detail in Section 6.1.

The conclusions drawn from the normal mode analysis and summarised above are consistent with and confirm the findings of BC1D, where the 1D column model with an isothermal basic state was run applying the different boundary conditions: θ active at the top and bottom; isentropic bottom boundary condition; and / or the isothermal top layer. It was found that both the isentropic and the isothermal boundary conditions worsened the numerical results, the latter having a bigger impact and leading to numerical instability. Unlike the BC1D analysis however this study does not show any particular instability due to the isothermal top boundary condition. It is found that the external modes have eigenvalues $\lambda \approx 1$, some of them exceeding unity by an amount of the order $O\left(10^{-12}\right)$ or smaller, but similar results were also obtained with the active top boundary condition, and as discussed previously, it is impossible to decide whether this is due to an instability of the model or to numerical noise. This suggests that the instability found in BC1D is likely to be non-linear.

References

Côté, J., Béland, M. & Staniforth, A. 1983 , Stability of vertical discretizations schemes for semi-implicit primitive equation models: theory and applications, *Mon. Wea. Rev.* **111**, 1189–1207.

Gravel, S., Staniforth, A. & Côté, J. 1993 , A stability analysis of a family of baroclinic semi-Lagrangian forecast models, *Mon. Wea. Rev.* **121**, 815–824.

Staniforth, A., White, A., Wood, N., Thuburn, J., Zerroukat, M. & Cordero, E. 2002 , Unified Model Documentation Paper *No.*15 The Joy of U.M. 5.3 – model formulation.

Thuburn, J., Wood, N. & Staniforth, A. 2002 , Normal modes of deep atmospheres. II: $f - F-$plane geometry, *Q. J. R. Meteorol. Soc.* **128**, to appear.

APPENDIX A

Eigen analysis of a "layer-by-layer" vertical discretisation

A.1 Continuous equations

A.1.1 Continuous vertical-slice equations

The continuous set of governing equations, written in Cartesian $x-z$ coordinates, in the absence of orography ($z=0$ defines the lower boundary) and forcing ($S^u = S^v = S^w = S^\theta \equiv 0$), for a dry atmosphere ($\theta_v = \theta$, $\rho_y = \rho$) on an F-plane (an $f-F$ plane located at the equator), and neglecting perturbations in the y direction ($\partial/\partial y \equiv 0$), is:

$$\frac{Du}{Dt} = -c_{pd}\theta\frac{\partial \Pi}{\partial x} - Fw, \tag{A.1}$$

$$\frac{Dv}{Dt} = 0, \tag{A.2}$$

$$\frac{Dw}{Dt} = -g - c_{pd}\theta\frac{\partial \Pi}{\partial z} + Fu, \tag{A.3}$$

$$\frac{D\theta}{Dt} = 0, \tag{A.4}$$

$$\frac{D\rho}{Dt} = -\rho\left(\frac{\partial u}{\partial x} + \frac{\partial w}{\partial z}\right), \tag{A.5}$$

$$\Pi^{\frac{\kappa_d - 1}{\kappa_d}}\rho\theta = \frac{p_0}{\kappa_d c_{pd}}, \tag{A.6}$$

where $D/Dt \equiv \partial/\partial t + u\partial/\partial x + w\partial/\partial z$, $\Pi \equiv (p/p_0)^{\kappa_d}$, $\kappa_d \equiv R_d/c_{pd}$, and $F \equiv (2\Omega\cos\phi)|_{\phi=0} = 2\Omega$.

It is instructive to first examine the layer averaging/ differencing discretisation in the context of a much simpler linear column model to identify any obvious problems, so the continuous equation set is further simplified in preparation for this.

A.1.2 Continuous column equations (with $F \equiv 0$)

Setting $F \equiv 0$ and neglecting variations in the x direction ($\partial/\partial x \equiv 0$) the continuous set of governing equations (A.1) - (A.6) reduce to

$$\frac{Du}{Dt} = 0, \tag{A.7}$$

$$\frac{Dv}{Dt} = 0, \tag{A.8}$$

$$\frac{Dw}{Dt} = -g - c_{pd}\theta\frac{\partial\Pi}{\partial z}, \tag{A.9}$$

$$\frac{D\theta}{Dt} = 0, \tag{A.10}$$

$$\frac{D\rho}{Dt} = -\rho\frac{\partial w}{\partial z}, \tag{A.11}$$

$$\Pi^{\frac{\kappa_d-1}{\kappa_d}}\rho\theta = \frac{p_0}{\kappa_d c_{pd}}, \tag{A.12}$$

subject to

$$w|_{z=z_0\equiv 0} = w|_{z=z_N} = 0, \tag{A.13}$$

where $D/Dt \equiv \partial/\partial t + w\partial/\partial z$, $\Pi \equiv (p/p_0)^{\kappa_d}$, and $\kappa_d \equiv R_d/c_{pd}$.

A.1.3 Linearised column equations ($F \equiv 0$)

Linearising the se equations about a basic state atmosphere defined by

$$c_{pd}\theta_s\frac{\partial\Pi_s}{\partial z} = -g, \tag{A.14}$$

$$\Pi_s^{\frac{\kappa_d-1}{\kappa_d}}\rho_s\theta_s = \frac{p_0}{\kappa_d c_{pd}}. \tag{A.15}$$

and expanding variables as

$$u(z,t) = u'(z,t), \tag{A.16}$$

$$v(z,t) = v'(z,t), \tag{A.17}$$

$$w(z,t) = w'(z,t), \tag{A.18}$$

$$\theta(z,t) = \theta_s(z) + \theta'(z,t), \tag{A.19}$$

$$\rho(z,t) = \rho_s(z) + \rho'(z,t), \tag{A.20}$$

$$\Pi(z,t) = \Pi_s(z) + \Pi'(z,t), \tag{A.21}$$

leads to the linearised equation set

$$\frac{\partial w}{\partial t} = -c_{pd}\theta_s\frac{\partial\Pi}{\partial z} - c_{pd}\frac{d\Pi_s}{dz}\theta, \tag{A.22}$$

$$\frac{\partial\theta}{\partial t} = -\frac{d\theta_s}{dz}w, \tag{A.23}$$

$$\frac{\partial\rho}{\partial t} = -\frac{\partial(\rho_s w)}{\partial z}, \tag{A.24}$$

$$\left(\frac{1-\kappa_d}{\kappa_d}\right)\frac{\Pi}{\Pi_s} = \frac{\rho}{\rho_s} + \frac{\theta}{\theta_s}, \tag{A.25}$$

where primes have been dropped for convenience.

A.1.4 Linearised column equations ($F \equiv 0$, θ_s, ρ_s, Π_s constant)

Assume that the basic state atmosphere is also isentropic and very shallow, i.e $z_N/H \ll 1$ where the atmospheric scale height $H = RT/g$. Then not only is θ_s constant, but so are ρ_s and Π_s. Thus the linear equation set (A.22) - (A.25) can be further simplified to

$$\frac{\partial w}{\partial t} = -c_{pd}\theta_s \frac{\partial \Pi}{\partial z}, \tag{A.26}$$

$$\frac{\partial \theta}{\partial t} = 0, \tag{A.27}$$

$$\frac{\partial \rho}{\partial t} = -\rho_s \frac{\partial w}{\partial z}, \tag{A.28}$$

$$\left(\frac{1-\kappa_d}{\kappa_d}\right)\frac{\Pi}{\Pi_s} = \frac{\rho}{\rho_s} + \frac{\theta}{\theta_s}. \tag{A.29}$$

A.1.5 Analytic solution when $F \equiv 0$, θ_s, ρ_s, Π_s all constant

This constant-coefficient equation set is particularly simple since it is analytically equivalent to $\theta = \theta(z)$ ($\theta(z)$ can be arbitrarily set to zero without loss of generality since it only appears in the analysis when differentiated with respect to t), and the two simple harmonic problems

$$\frac{\partial^2 w}{\partial t^2} = c_{pd}\left(\frac{\kappa_d}{1-\kappa_d}\right)\theta_s \Pi_s \frac{\partial^2 w}{\partial z^2} = c_s^2 \frac{\partial^2 w}{\partial z^2}, \tag{A.30}$$

subject to (A.13), and

$$\frac{\partial^2 \Pi}{\partial t^2} = c_{pd}\left(\frac{\kappa_d}{1-\kappa_d}\right)\theta_s \Pi_s \frac{\partial^2 \Pi}{\partial z^2} = c_s^2 \frac{\partial^2 \Pi}{\partial z^2}, \tag{A.31}$$

subject to

$$\left.\frac{\partial \Pi}{\partial z}\right|_{z=z_0\equiv 0} = \left.\frac{\partial \Pi}{\partial z}\right|_{z=z_T} = 0, \tag{A.32}$$

where

$$c_s^2 \equiv \frac{R_d T_s}{1-\kappa_d}, \tag{A.33}$$

is the adiabatic sound speed.

The solutions of (A.30) - (A.31) subject to (A.32) - (A.33) are

$$w = \sum_{m=1}^{\infty} \sin\left(\frac{m\pi z}{z_T}\right)\left[w_m^0 \cos\left(\frac{m\pi c_s t}{z_T}\right) + \frac{c_{pd}\theta_s}{c_s}\Pi_m^0 \sin\left(\frac{m\pi c_s t}{z_T}\right)\right], \tag{A.34}$$

$$\Pi = \sum_{m=0}^{\infty} \cos\left(\frac{m\pi z}{z_T}\right)\left[\Pi_m^0 \cos\left(\frac{m\pi c_s t}{z_T}\right) - \frac{c_s}{c_{pd}\theta_s} w_m^0 \sin\left(\frac{m\pi c_s t}{z_T}\right)\right], \tag{A.35}$$

where w_m^0 and Π_m^0 are the Fourier components of the initial conditions, where it is assumed that both w and Π are specified functions at $t = 0$.

A.2 Discrete equations

A.2.1 Discretisation of linearised column model equations ($F \equiv 0$, θ_s, ρ_s, Π_s constant)

The "layer-by-layer" vertical discretisation of these equations is accomplished by discretising equations in which vertical derivatives appear (i.e. (A.26) and (A.28)) by evaluating terms over a layer using vertical differences and averages. Remaining equations are evaluated level-by-level. The object is to vertically difference equations in as compact a manner as possible in order to improve the numerical dispersion properties. The danger is that the discretisation may be problematic for the smallest vertical scale.

The "layer-by-layer" vertical discretisation applied to the linearised column model equations, when $F \equiv 0$, θ_s, ρ_s, Π_s are all constant, reduces to:

Vertical momentum

$$w^{n+1}\Big|_{z_0 \equiv 0} = 0, \tag{A.36}$$

$$\overline{w^{n+1}}^{z} + \alpha_4 c_{pd} \Delta t \theta_s \delta_z \Pi^{n+1} = \overline{w^n}^{z} - (1-\alpha_4)\, c_{pd} \Delta t \theta_s \delta_z \Pi^n, \tag{A.37}$$

at layers $k = 1/2,\ 3/2,\ ...,\ N - 1/2$, and

$$w^{n+1}\Big|_{z_N} = 0. \tag{A.38}$$

Thermodynamic at levels $k = 0,\ 1,\ ...,\ N$

$$\theta^{n+1} \;=\; \theta^n = 0. \tag{A.39}$$

Continuity for layers $k = 1/2,\ 3/2,\ ...,\ N - 1/2$

$$\overline{\rho^{n+1}}^{z} + \alpha_2 \Delta t \rho_s \delta_z \left(w^{n+1}\right) = \overline{\rho^n}^{z} - (1-\alpha_2)\, \Delta t \rho_s \delta_z \left(w^n\right), \tag{A.40}$$

Linearised gas law at levels $k = 0,\ 1,\ ...,\ N$

$$\left(\frac{1-\kappa_d}{\kappa_d}\right) \frac{\Pi^{n+1}}{\Pi_s} \;-\; \frac{\rho^{n+1}}{\rho_s} = 0. \tag{A.41}$$

A.2.2 The equations rewritten in matrix form

Using (A.41) to eliminate ρ in favour of Π in (A.36) - (A.40) leads to

$$A \begin{bmatrix} \underline{\Pi}^{n+1} \\ \underline{w}^{n+1} \end{bmatrix} = B \begin{bmatrix} \underline{\Pi}^{n} \\ \underline{w}^{n} \end{bmatrix}, \tag{A.42}$$

where

$$A = \begin{bmatrix} P & \alpha_2 \Delta t \left(\frac{\kappa_d}{1-\kappa_d}\right) \Pi_s D \\ \alpha_4 \Delta t c_{pd} \theta_s E & Q \end{bmatrix}, \tag{A.43}$$

$$B = \begin{bmatrix} P & -(1-\alpha_2) \Delta t \left(\frac{\kappa_d}{1-\kappa_d}\right) \Pi_s D \\ -(1-\alpha_4) \Delta t c_{pd} \theta_s E & Q_0 \end{bmatrix}, \tag{A.44}$$

$$P = \begin{bmatrix} \frac{1}{2} & \frac{1}{2} & 0 & \cdot & 0 \\ 0 & \frac{1}{2} & \frac{1}{2} & 0 & \cdot \\ \cdot & \cdot & \ddots & \ddots & \cdot \\ 0 & \cdot & 0 & \frac{1}{2} & \frac{1}{2} \end{bmatrix}, \tag{A.45}$$

$$Q = \begin{bmatrix} 1 & 0 & \cdot & 0 & 0 \\ \frac{1}{2} & \frac{1}{2} & 0 & \cdot & 0 \\ 0 & \frac{1}{2} & \frac{1}{2} & 0 & 0 \\ \cdot & \cdot & \ddots & \ddots & \cdot \\ 0 & \cdot & 0 & \frac{1}{2} & \frac{1}{2} \\ 0 & 0 & \cdot & 0 & 1 \end{bmatrix}, Q_0 = \begin{bmatrix} 0 & 0 & \cdot & 0 & 0 \\ \frac{1}{2} & \frac{1}{2} & 0 & \cdot & 0 \\ 0 & \frac{1}{2} & \frac{1}{2} & 0 & 0 \\ \cdot & \cdot & \ddots & \ddots & \cdot \\ 0 & \cdot & 0 & \frac{1}{2} & \frac{1}{2} \\ 0 & 0 & \cdot & 0 & 0 \end{bmatrix}, \tag{A.46}$$

$$D = \begin{bmatrix} -\left(\frac{1}{\Delta z}\right)\Big|_{z_{\frac{1}{2}}} & \left(\frac{1}{\Delta z}\right)\Big|_{z_{\frac{1}{2}}} & 0 & 0 & 0 \\ 0 & -\left(\frac{1}{\Delta z}\right)\Big|_{z_{\frac{3}{2}}} & \left(\frac{1}{\Delta z}\right)\Big|_{z_{\frac{3}{2}}} & 0 & 0 \\ 0 & 0 & \cdot & \cdot & 0 \\ 0 & 0 & 0 & -\left(\frac{1}{\Delta z}\right)\Big|_{z_{N-\frac{1}{2}}} & \left(\frac{1}{\Delta z}\right)\Big|_{z_{N-\frac{1}{2}}} \end{bmatrix}, \tag{A.47}$$

$$E = \begin{bmatrix} 0 & 0 & 0 & 0 & 0 \\ -\left(\frac{1}{\Delta z}\right)\Big|_{z_{\frac{1}{2}}} & \left(\frac{1}{\Delta z}\right)\Big|_{z_{\frac{1}{2}}} & 0 & 0 & 0 \\ 0 & \cdot & \cdot & 0 & 0 \\ 0 & 0 & -\left(\frac{1}{\Delta z}\right)\Big|_{z_{k-\frac{1}{2}}} & \left(\frac{1}{\Delta z}\right)\Big|_{z_{k-\frac{1}{2}}} & 0 \\ 0 & 0 & 0 & \cdot & \cdot \\ 0 & 0 & 0 & 0 & 0 \end{bmatrix}. \tag{A.48}$$

The matrix structure of A is

$$\begin{bmatrix} N \times (N+1) & N \times (N+1) \\ (N+2) \times (N+1) & (N+2) \times (N+1) \end{bmatrix},$$

and $\underline{\Pi} = [\Pi_0, \Pi_1, ..., \Pi_N]^T$, $\underline{w} = [w_0, w_1, ..., w_N]^T$ are vectors of dimension $(N+1)$.

A.3 Eigen analysis when the grid is uniform

In general, one would now proceed to perform a discrete eigen analysis of $A^{-1}B\underline{x} = \lambda\underline{x}$ using standard eigen-analysis software. However, when the grid is uniform, i.e. when

$$\Delta z_{1/2} = \Delta z_{3/2} = ... = \Delta z_{N-1/2} = \Delta z = z_T/N, \tag{A.49}$$

it is relatively straightforward to perform the analysis analytically. This is now done.

By inspection it is seen that the eigenfunctions (all but two, more on this later) can be obtained by expanding Π and w respectively as half-wave discrete Fourier cosine and sine series. Thus the m'th pair of eigenfunctions have the form

$$\begin{aligned} \underline{x}_m &= [\Pi_m, w_m]^T \\ &= \left[\Pi_m^{\pm}\left(1, \cos\frac{m\pi}{N}, \cdots, \cos\frac{(N-1)\,m\pi}{N}, \cos m\pi\right), w_m^{\pm}\left(0, \sin\frac{m\pi}{N}, \cdots, \sin\frac{(N-1)\,m\pi}{N}, 0\right)\right]^T, \\ & \quad m = 0, 1, \cdots, N. \end{aligned} \tag{A.50}$$

where $\Pi_m^{\pm}$ and $w_m^{\pm}$ are constant coefficients to be determined (the two signs anticipate downward and upward propagating modes). Note however that the $m = 0$ "pair" is degenerate and is actually a single mode such that Π is everywhere constant and w is identically zero everywhere. Similarly the $m = N$ "pair" is also degenerate and is a single mode such that Π has a grid-scale structure $[+1, -1, +1, -1, ...]$ and w is identically zero everywhere.

Now using (A.42) - (A.48) yields

$$A\underline{x}_m = \begin{bmatrix} \left(\gamma_m\Pi_m^{\pm} + \alpha_2\beta_m\frac{c_s^2}{c_{pd}\theta_s}w_m^{\pm}\right)\left(\cos\frac{m\pi}{2N}, \cos\frac{3m\pi}{2N}, \cdots, \cos\frac{(2N-1)m\pi}{2N}\right)^T \\ \left(\gamma_m w_m^{\pm} - \alpha_4\beta_m c_{pd}\theta_s\Pi_m^{\pm}\right)\left(0, \sin\frac{m\pi}{2N}, \sin\frac{3m\pi}{2N}, \cdots, \sin\frac{(2N-1)m\pi}{2N}, 0\right)^T \end{bmatrix}, \tag{A.51}$$

and

$$B\underline{x}_m = \begin{bmatrix} \left(\gamma_m\Pi_m^{\pm} - (1-\alpha_2)\,\beta_m\frac{c_s^2}{c_{pd}\theta_s}w_m^{\pm}\right)\left(\cos\frac{m\pi}{2N}, \cos\frac{3m\pi}{2N}, \cdots, \cos\frac{(2N-1)m\pi}{2N}\right)^T \\ \left(\gamma_m w_m^{\pm} + (1-\alpha_4)\,\beta_m c_{pd}\theta_s\Pi_m^{\pm}\right)\left(0, \sin\frac{m\pi}{2N}, \sin\frac{3m\pi}{2N}, \cdots, \sin\frac{(2N-1)m\pi}{2N}, 0\right)^T \end{bmatrix}, \tag{A.52}$$

where

$$\beta_m = \frac{\sin\frac{m\pi}{2N}}{\Delta z/2}\Delta t,\ \gamma_m = \cos\frac{m\pi}{2N}, \tag{A.53}$$

and

$$c_s^2 = \frac{R_d T_s}{1-\kappa_d}, \tag{A.54}$$

is the adiabatic sound speed.

So

$$\begin{aligned}
0 &= \lambda_m A\underline{x}_m - B\underline{x}_m \\
&= \left[\lambda_m\left(\gamma_m\Pi_m^{\pm} + \alpha_2\beta_m\frac{c_s^2}{c_{pd}\theta_s}w_m^{\pm}\right) - \left(\gamma_m\Pi_m^{\pm} - (1-\alpha_2)\,\beta_m\frac{c_s^2}{c_{pd}\theta_s}w_m^{\pm}\right)\right]\begin{bmatrix}\cos\frac{m\pi}{2N}\\ \cos\frac{3m\pi}{2N}\\ \vdots\\ \cos\frac{(2N-3)m\pi}{2N}\\ \cos\frac{(2N-1)m\pi}{2N}\end{bmatrix} \\
&\quad + \left[\lambda_m\left(\gamma_m w_m^{\pm} - \alpha_4\beta_m c_{pd}\theta_s\Pi_m^{\pm}\right) - \left(\gamma_m w_m^{\pm} + (1-\alpha_4)\,\beta_m c_{pd}\theta_s\Pi_m^{\pm}\right)\right]\begin{bmatrix}0\\ \sin\frac{m\pi}{2N}\\ \sin\frac{3m\pi}{2N}\\ \vdots\\ \sin\frac{(2N-1)m\pi}{2N}\\ 0\end{bmatrix}.
\end{aligned} \tag{A.55}$$

Thus

$$(\lambda_m - 1)\,\gamma_m\Pi_m^{\pm} + [\alpha_2\lambda_m + (1-\alpha_2)]\,\beta_m\frac{c_s^2}{c_{pd}\theta_s}w_m^{\pm} = 0, \tag{A.56}$$

$$-[\alpha_4\lambda_m + (1-\alpha_4)]\,\beta_m c_{pd}\theta_s\Pi_m^{\pm} + (\lambda_m - 1)\,\gamma_m w_m^{\pm} = 0. \tag{A.57}$$

For (A.56) - (A.57) to have non-trivial solutions for $\Pi_m^{\pm}$ and $w_m^{\pm}$ requires the determinant to be zero, i.e.

$$(\lambda_m - 1)^2\,\gamma_m^2 = -[\alpha_2\lambda_m + (1-\alpha_2)]\,[\alpha_4\lambda_m + (1-\alpha_4)]\,\beta_m^2 c_s^2. \tag{A.58}$$

Solving (A.58) for λ_m with general values of α_2 and α_4 is a job for the computer. However if $\alpha_2 = \alpha_4 = \alpha$ (this is recommended and has traditionally been so in the New Dynamics with α being set to unity) then (A.58) has solutions

$$\lambda_m = \frac{1 \pm i\,(1-\alpha)\,\xi_m c_s}{1 \mp i\alpha\xi_m c_s} = \frac{1 - \alpha\,(1-\alpha)\,\xi_m^2 c_s^2 \pm i\xi_m c_s}{1 + \alpha^2\xi_m^2 c_s^2}, \tag{A.59}$$

where

$$\xi_m \equiv \frac{\beta_m}{\gamma_m} = \frac{\tan\frac{m\pi}{2N}}{\Delta z/2}\Delta t. \tag{A.60}$$

Thus

$$|\lambda_m|^2 = \frac{1+(1-\alpha)^2\xi_m^2 c_s^2}{1+\alpha^2\xi_m^2 c_s^2}, \tag{A.61}$$

and the scheme will be stable (i.e. $|\lambda_m|^2 \leq 1$) provided $\alpha \geq 1/2$, with neutral stability ($|\lambda_m| = 1$) obtaining when $\alpha = 1/2$.

For the first of the two degenerate modes, for which $m = 0$, (A.61) is valid and $\lambda_0 = 1$. This mode, for which Π is everywhere constant and w is identically zero everywhere, is the same as for the Charney-Phillips staggering of variables except with a staggered sampling.

For the second one, for which $m = N$, (A.61) is invalid since ξ_N is unbounded due to division by $\gamma_N \equiv 0$. Returning to (A.56) - (A.57) with $\alpha = \alpha_2 = \alpha_4$ gives $\lambda_N = -(1-\alpha)/\alpha$. This mode is not present in the Charney-Phillips staggering of variables. With α set to one (the usual choice made in the New Dynamics discretisation using the Charney-Phillips staggering) this mode is perfectly exorcised. However when α is set to $1/2$, this mode will alternate sign on alternative timesteps with no damping. **This is a possible disadvantage of the "layer-by-layer" vertical discretisation since this mode has a grid-scale structure** $[+1,-1,+1,-1,...]^T$ **for** Π **with** $w \equiv 0$ **and might not respond well to forcing.**

Setting $\lambda_m \equiv \exp(i\omega\Delta t) \equiv \exp[i(\omega_R + i\omega_I)\Delta t] = \exp(-\omega_I\Delta t)\exp(i\omega_R\Delta t)$ in (A.59) and using (A.60) - (A.61) yields

$$\tan(\omega_R\Delta t) = \pm\frac{\xi_m c_s}{1-\alpha(1-\alpha)\xi_m^2 c_s^2} = \pm\frac{\left(\frac{\tan\frac{m\pi}{2N}}{\Delta z/2}\right)c_s\Delta t}{1-\alpha(1-\alpha)\left(\frac{\tan\frac{m\pi}{2N}}{\Delta z/2}\right)^2 c_s^2\Delta t^2}, \tag{A.62}$$

$$|\lambda_m|^2 = \exp(-2\omega_I\Delta t) = \frac{1+(1-\alpha)^2\xi_m^2 c_s^2}{1+\alpha^2\xi_m^2 c_s^2}. \tag{A.63}$$

Dividing (A.62) by Δt and taking the limits $\Delta t \to 0$ and $\Delta z \to 0$ in both the resulting equation and in (A.63) then gives

$$\lim_{\Delta t,\Delta z\to 0}\omega_R \;\to\; \frac{m\pi c_s}{z_T}, \tag{A.64}$$

$$\lim_{\Delta t,\Delta z\to 0}\omega_I \;\to\; 0, \tag{A.65}$$

and so

$$\lim_{\Delta t,\Delta z\to 0}\omega \equiv \lim_{\Delta t,\Delta z\to 0}(\omega_R + i\omega_I) \to \frac{m\pi c_s}{z_T}, \tag{A.66}$$

i.e. ω converges to the exact result - cf. (A.34) - (A.35).

Substituting (A.59) into (A.56) or (A.57) yields the relationship (when $\alpha_2 = \alpha_4 = \alpha$) between the coefficients:

$$\Pi_m^{\pm} = \pm i \frac{c_s}{c_{pd}\theta_s} w_m^{\pm}. \tag{A.67}$$

Thus far $2N$ independent eigenmodes have been identified, viz. pairs of modes for $m = 1, 2, ..., N-1$, and the two single modes $m = 0$ and $m = N$. Since A and B are square matrices of dimension $2(N+1)$, two further modes are expected.

These are both in the null space of B, i.e. they both have $\lambda = 0$ as eigenvalue. For the special case $\alpha_2 = \alpha_4 = \alpha = 1$ their eigenstructures are $[(+1, -1, +1, -1, ...), \pm(+1, -1, +1, -1, ...)]^T$. More generally, their eigenstructures can be obtained by arbitrarily setting $\Pi|_{z_0} = 1$ and $w|_{z_0} = \pm 1$ and solving $B[\Pi, w]^T = 0$. These modes are associated with the boundary conditions $w = 0$ at $z = 0, z_T$, and are a consequence of having explicitly included these in the definition of the eigen problem, even though they could have been decoupled from it (this would then have reduced the dimension of the A and B matrices from $2(N+1)$ to $2N$ and led to the $2N$ eigen modes defined by (A.50)).